SIZE EFFECTS AND DEFORMATION MECHANISMS IN NANOSCALE METALLIC MULTILAYERED COMPOSITES

By
Firas Akasheh

A dissertation in partial fulfillment of the requirements for the degree of

DOCTOR OF PHILOSOPHY

WASHINGTON STATE UNIVERSITY

School of Mechanical and Materials Engineering

May 2007

To the Faculty of Washington State University:

The members of the Committee appointed to examine the dissertation of Firas Akasheh find it satisfactory and recommend that it be accepted.

_____

Chair

_____

_____

ACKNOWLEDGEMENTS

First, I would like to express my deep gratitude to my major advisor Dr. Hussein M. Zbib for his unwithering support and encouragement during my studies especially during critical times. I would also like to thank Dr. David Field and Dr. V. S. Manoranjan for agreeing to serve on my committee and for their advice and support. I owe special thanks and deep appreciation to Dr. John P. Hirth for his time and insight and for providing valuable feedback my work and paper manuscripts. I would also like to acknowledge the technical collaboration with Dr. Amit Misra and Dr. Richard G. Hoagland at Los Alamos National Laboratory (LANL) and the financial support provided by the DOE, Office of Basic Sciences program on nanoscale multilayered structures through LANL.

My experience at the School of Mechanical and Materials Engineering was wonderful and enriching and this is attributed to its faculty and staff and fellow graduate students. I mention the kind advice of Dr. S. D. Antolovich, Dr. Sinisia Mesarovic, Dr. David Bahr, and my Masters advisor Dr. Amit Bandyopadhayay. I am grateful for many enjoyable moments and intellectual discussions with current and former graduate lab mates including Sreekanth Akarapu, Ionnis Masterakos, Shafique Khan, and Mutasem Shehadeh. Many thanks also go for the kind and professional computation support of Michael Shook and Giag Pham, as well as the administrative support of Gayle Landeen, Janet Danforth, Annette Cavalieri, Margie Kimball and Mary Simonson.

Last but not least, I am grateful for my family and a long list of great friends who are the blessing of my life. Without them the journey would not have been possible and no words can express my gratitude and appreciation. So I will just say: THANK YOU ALL.

SIZE EFFECTS AND DEFORMATION MECHANISMS IN NANOSCALE METALLIC MULTILAYERED COMPOSITES

ABSTRACT

By Firas Akasheh, Ph.D

Washington State University

May 2007

Chair: Hussein M. Zbib

In this work, size effects and deformation mechanisms in nanoscale metallic multilayered (NMM) composites were studied. Existing models for the prediction of the dependence of strength of NMM composites on the individual layer thickness do not capture the experimentally observed dependence. Dislocation interactions have been suggested as a significant contributor to this discrepancy. Due to the complexity and multiplicity of dislocation interaction in real systems, the study started by examining the hardening effect and implications on the dislocation structure of two known-to-be significant dislocation interactions in NMM composites. The first is the interaction between a threading dislocation and orthogonally intersection interfacial dislocations. Dislocation dynamics (DD) analysis was employed and it was found that the strongest interaction occurs when the interacting dislocations are collinear and involves annihilation reactions and the formation of 90^{o} dislocation bends at the interfaces, as commonly observed in experiments. The strength predictions indicate a strengthen

increase of about 50%; however, they do not follow the experimentally observed trend. The second interaction to study was that between a threading dislocation and parallel interfacial dislocations. A semi-analytical energetic approach was employed and it was found that parallel interactions can lead to softening effect, as well as hardening effect depending on the relative sign of the Burgers vector of the threading and the parallel dislocations. It was also found that when the Burgers vectors are collinear, the interaction is stronger. A comparison with the measured strength of real multilayered system shows that accounting for parallel interactions improves the strength predictions for an isolated glide dislocation, however that does not offer answers regarding the observed strength saturation when the individual layer thickness in the few nanometer range. Finally, large-scale DD simulations of NMM composites were performed. Such simulations naturally accounts for all the possible and complex interactions in a real system. The strength predictions of such simulations are in better qualitative agreement with experimental trends than any of the unit process. Nevertheless, more work is needed to validate the results by investigating different relaxation models to accomplish the initial dislocations structure used in subsequent loading. The simulations were also valuable in identifying dislocation mechanisms which can take place during the deformation.

TABLE OF CONTENTS

LIST OF FIGURES

LIST OF TABLES

Chapter One: Introduction

1.1 Background

1.1.1 Size effects in metals

Accurate models for predicting the elastic-plastic response of crystalline materials are crucial for the design and development of materials that can perform more efficiently and reliably under service conditions. The classical approach to modeling the mechanical response of metals has been phenomenological in nature. Based on macroscopic observations, theories were developed and translated into models describing the deformation behavior, e.g. Tresca and von-Mises yield criteria for metals. The fact that such an approach worked well for bulk materials and components (bulk meaning millimeter scale and above) does not change its inherent deficiency of ignoring the physical mechanisms involved in the deformation and not taking into account the details of the microstructure of the material. Those deficiencies, however, become obvious when such models are used to predict the experimentally measured response of materials at the microscale and smaller. For example, experiments on the bending of micro beams [1] showed that both the yield and flow stress increase as the beam size decreases. Similar experiments on torsion of microsized wires [2] and nanoindentation [3] showed the same trend. This effect, which came to be known as the "size effect", became a major focus of the materials and mechanics research aiming at understanding the origin of such discrepancy and ways to account for it.

The origin of size effect can be traced back to the presence of internal defects and inhomogeneties at the microstructure level of the material. Chief among such internal defects are dislocations, line defects whose motion and interactions are well known to be

the main factor governing deformation in crystalline materials. Besides making plastic deformation easier compared to defect-free crystals, dislocations exhibit long-range stress fields. This introduces non-local effects, which implies that the material behavior at a certain material point depends not only on the local state but also on the state at neighboring material points. Besides their interactions among themselves and other crystal defects, dislocations contribute to non-local effects through their interaction with surfaces and interfaces in the material. When the material is in the bulk scale, the range of influence of such effects is small compared to the overall size, making their effect insignificant. Furthermore, when the material scale is large, the statistical nature of dislocation distributions result in the averaging out of the stress fields from all dislocations. However, as the material scale enters the micrometer regime, the details of the distribution of dislocations and their discrete nature do not average out and, hence, net dislocation densities with non-vanishing Burgers vector become increasingly significant in determining the mechanical response leading to the observed size effects.

As a first step towards modeling size effects in crystals, the framework of classical crystal plasticity was proposed [4, 5]. This framework is an improvement over classical plasticity because it recognizes that plasticity in crystals is the result of motion of dislocations and hence incorporates the kinematics and kinetics of such motion. The fact that the macroscopic plastic strain in crystals is the result of the collective motion of large numbers of dislocations on a finite number of slip systems, each identified by a specific atomic plane and slip direction (slip system) depending on the crystal structure, is inherent to the theory. In this framework, the plastic strain increment $\dot{\varepsilon}^p$ is expressed as the tensorial sum of slip on specific slip systems,

$$\dot{\varepsilon}^p = \sum_{\beta} \dot{\gamma}^{(\beta)} \left(\hat{s}^{(\beta)} \otimes \hat{n}^{(\beta)} \right)_{sym} \quad \text{.....(1.1)}$$

where β is the slip system index, $\dot{\gamma}^{(\beta)}$ is the increment of slip on system β, $\hat{s}^{(\beta)}$ is the unit slip direction, and $\hat{n}^{(\beta)}$ is the slip plane normal. In the case of small deformation rate-independent crystal plasticity, Schmid law states that yield begins on a slip system when the resolved shear stress on the slip plane in the slip direction, τ^{β}, reaches a critical value, τ_{cr}^{β}, the current strength of the slip system. τ_{cr}^{β} is a function of the plastic strain and is typically described by a hardening law of the form,

$$\dot{\tau}_{cr}^{\beta} = \sum_{\alpha} h^{\beta\alpha} \dot{\gamma}^{\alpha} \quad \text{.....(1.2)}$$

where $h^{\beta\alpha}$ are the hardening moduli which relate the rate of increase of the strength of slip system β due to slip on system α. At the macroscale, the stress is related to the strain by Hooke's law,

$$\dot{\sigma} = C\left(\dot{\varepsilon} - \dot{\varepsilon}^p\right) \quad \text{.....(1.3)}$$

where C is the fourth order elastic tensor of the material. Finally to determine the increments of slip on the different slip systems, $\dot{\gamma}^{\beta}$, loading/unloading criteria similar to those in classical plasticity are used.

1.1.2 Modeling size effects in metals

1.1.2.1 Gradient crystal plasticity approach

Although the classical crystal plasticity framework does account for the physical deformation mechanism in crystals, it still fails to capture size effects because it does not account for the non-local effects due to non-vanishing long-range internal stress fields. In

terms of the dislocation structure, such fields can be physically associated with the net content of dislocations referred to as geometrically necessary dislocations (GND), which in turn can be associated with the gradients in strain (the dislocation content which statistically cancel out is called statistically stored dislocations and, to a first approximation, do not contribute to long-range effect). This concept, introduced by Nye and Ashby [6, 7], became the basis of the development of what is known as strain gradient crystal plasticity theory which can predict size effect.

Among the pioneering works in this area, Aifantis [8] and Zbib and Aifantis [9, 10] modified the flow stress of the classical crystal plasticity to include a dependence on the shear strain gradients, in addition to the shear strain. Fleck *et al*. [2] developed an asymmetric stress Crosserat-type gradient plasticity theory which successfully captured size effect in wire torsion experiments. Fleck and Hutchinson [11] expanded the formulation of the classical *J2* theory to accommodate more than one material length scale. Other gradient theories were developed which are based on the explicit introduction of GND density and length scales associated with it. Shizawa and Zbib [12], Gurtin [13], and Mesarovic [14], introduced the GND density tensor, the Nye's tensor, into the free energy expression along with a configurational stress as its work conjugate. Other researchers invoked crystallographic dislocations densities as internal variables with their own evolution laws, *e.g*., Arsenlis *et al*. [15], Yefimov *et al*. [16], Groma [17], Zaiser and Hochrainer [18], and El-Azab [19]. Some researchers introduced the GND density into the flow strength expression τ_{cr}^{β}, while others introduced it into the hardening law, *e.g*., Acharya [20] and Ohashi [21]. For example, the hardening

coefficients matrix $h^{\beta\alpha}$, Eq. (1.2), in the original size-independent form of the later model [21] are given as,

$$h^{\beta\alpha} = \frac{0.5\, a\, c\, \mu\, \Omega^{\beta\alpha}}{L^{(\alpha)}\sqrt{\rho_{ssd}^{(\alpha)}}}, \text{ with } L^{(\alpha)} = \frac{c^*}{\sqrt{\sum_{\alpha}\omega^{\alpha\beta}\rho_{ssd}^{(\beta)}}} \quad \text{.....(1.4a,b)}$$

where $L^{(\alpha)}$ is the mean free path of mobile dislocations, c^* is a constant on the order of 10-100 and $\omega^{\alpha\beta}$ is the weight matrix quantifying the contribution of dislocation density on system β to the mean free path length for system α. Based on the argument that the GND density leads to the shortening of the mean path length of dislocation motion, the following modified relation for the mean free path length was proposed,

$$L^{(\alpha)} = \frac{c^*}{\sqrt{\sum_{\beta}\omega^{\alpha\beta}\left(s\,.\,\rho_{ssd}^{(\beta)} + g\,.\,\rho_{gnd}^{(\beta)}\right)}} \quad \text{.....(1.5)}$$

where *s* and *g* are controlling coefficients with values ranging from 0-1. *g* is an example of the parameters introduced as part of this phenomenological approach, which has to be determined based on some fitting procedure to experimental results. This model has been used to address the plastic bending of microsized beams, see Appendix A. Bending is a classical problem where gradients in strain are inherent and studying such problem provides an introductory step towards a continuum approach to size effect prediction in NMM composites.

Each of the above approaches to gradient plasticity is motivated by different arguments and/or experimental evidence which can be controversial. The phenomenological nature of those theories leads to parameters whose physical meaning is not clear and whose values have to be determined by fitting model predictions to

experimental results. The conditions of such experiments are typically difficult to control so as to match the conditions under which the models are tested. The result of those drawbacks is that no general framework for gradient crystal plasticity is agreed upon. Differnet models show different degrees of success in adressing differnt problems.

1.1.2.2 Discrete dislocation dynamics (DD) approach

A recent significant develpoment in computational materials science which allows addressing plasticity problems in a more physical manner is DD analysis [22-27]. This framework was introduced in the early 1990s motivated by the improvement in the power and availability of computers and parallel processing algorithims. In this framework, dislocation motion and interactions are treated explicitly according to the well establsihed theory of dislocations. Dislocations move and evolve as they do in real systems and thus, size effects are naturally captured with minimal phenomenological assumptions. In three-dimansional DD, dislocations are modeled as curved lines and are identified by their Burgers vectors and line lense. According to the theory of dilsocations, the equation of motion of a dislocation segment is written as,

$$m_s \dot{\upsilon}_s + \frac{1}{M_s}\upsilon = F_s \tag{1.6}$$

which expresses the relation between the velocity of the dislocation segment of effective mass m_s, moving in a viscous medium with a drag coefficient of $1/M_s$ under the effect of a net force F_s on the segment. Depending on the problem, F_s can have several contributions including the Peierls stress (lattice friction), forces due to the long-range stress fields of other dislocations and obstacles in the medium, self-force on a dislocation, forces due to externally applied loads, image forces due to free surfaces and interfaces separating inhomogeneous domains, and forces due to thermally activated processes,

$$F_s = F_{Peierls} + F_{dislocation} + F_{self} + F_{external} + F_{obstacle} + F_{image} + F_{osmotic} + F_{thermal} \tag{1.7}$$

To track the evolution of the dislocation structure, the equation of motion is integrated using an implicit algorithm with a backward integration scheme,

$$v^{t+\delta t}\left(1+\frac{\Delta t}{m_s M_s}\right)^{t+\delta t} = v^t + \frac{\Delta t}{m_s} F^{t+\delta t} \tag{1.8}$$

This scheme is unconditionally stable for any time step δt. The time step in DD is determined by shortest flight distance for short-range interactions and based on the largest dislocation node speed. As for the spatial discretization, the dislocation curves are disrectized into linear segments bounded by dislocation nodes. Typical finite element formulation for linear elements with matrix lumping is used to determine the velocity distribution over dislocation lines,

$$\begin{aligned} &[M]\{\dot{V}\}+[C]\{V\}=\{F\} \\ &where\ [M]=m_s\int[N][N]^T dl,\ [C]=\frac{1}{M_s}\int[N][N]^T dl,\ [F]=m_s\int[N]F_s dl \end{aligned} \tag{1.9}$$

The increment of the plastic strain can be explicitly calculated from the area swept by the dislocation segments using the following relation,

$$\dot{\varepsilon}^p = \sum_{s=1}^{N_s} \frac{l_s \upsilon_s}{2V}\left(n_s \otimes b_s + b_s \otimes n_s\right) \tag{1.10}$$

where N_s is the total number of dislocation segments, l_s is the segment length, v_s is the segment glide velocity, b_s is the segment Burgers vector, n_s is the normal to the slip plane of the segment, and V is the volume of the *RVE*. This explicit calculation of the plastic strain eliminates the need for phenomenological relations of gradient plasticity and all the drawbacks associated with them. Similarly, no phenomenological relations are needed for the back stress. In real systems, dislocations collide with each other while in motion and,

based on the relative orientation of their Burgers vectors and line senses, can result in reactions which modify the dislocation structure and result in significant effects on the overall behavior. The DD framework accounts for such short-range interactions through constitutive rules inferred from experimental observations or molecular dynamics sinulations. Such interactions include annihilation, jog formation, junction formation, and dipole formation [28]. Finally, DD analysis can be coupled with contimuun scale finite element analysis expanding the scope of problems that can be treated. This multiscale coupling allows the rigorous treatment of dilsocation interactions with free surfaces and interfaces [24, 29].

Since its inception in the early 90s, DD analysis made major advancement and was successfully used to address problems related to microstructure-property relationships in small-scale plasticity. Shear banding and dislocation patterning are two important phenomena which were successfully predicted by DD analysis [30, 31]. The effect of size and distribution on the strength of metal matrix composites [32, 33] and hardening due to second phase inclusion during cyclic loading [34] were also analyzed using DD. Several authors simulated dislocation structure during nanoindentation, e.g. [29]. The effect of free surfaces on the yield strength was studied in [35]. The analysis of the stress fields and the relaxed structure of finite planar dilsocation boundaries of tilt and twist types were studied by Khan *et al*. [36]. Other interesting problems like the dynamic response of cyrstals to impact loading [37] and the study of deformation in irradiated materials [38, 39] were successfully anayzed as well.

In this thesis, DD analysis will be used to address s new problem of technological and scientific significance: plasticity in nanoscale multilayered dilsocation composites. Following is a brief introduction to the significance and issues related to these materials.

1.1.3 Nanoscale multilayered Metallic (NMM) composites

Nanoscale metallic multilayered (NMM) composites represent an important class of advanced engineering materials which have a great promise for multifunctional high performance that can be tailored for different applications. Traditionally, NMM composites are made of bimetallic systems produced by sputtering or electrodeposition. Careful experiments by several groups have clearly demonstrated that such materials exhibit ultrahigh strength, reaching 1/3 to 1/2 of the theoretical strength of any of the constituent materials [40], high ductility [41], and morphological stability under high temperatures [42] and after large deformation[41]. Enhanced fatigue resistance, order of magnitude higher than the values typically reported for the bulk form, were also reported [43, 44] as well as improved irradiation damage resistance [45]. However, the basic understanding of the behavior of those materials is lagging and not yet at a level that allows them to be harnessed and designed for engineering applications. For example the strong dependence of the strength of NMM composites on their characteristic size, identified by the individual layer thickness, is not well understood. While such dependence can be interpreted by the Hall-Petch effect (dislocation pileups) in the micrometer scale range, the known primary plasticity mechanism at the nanoscale, dislocation threading (also known as Orowan bowing), does not provide a satisfactory explanation. One reason for such discrepancy lies in the fact that threading dislocations strongly interact with other dislocations at the interfaces. Such interactions can modify the stress needed to propagate a threading dislocation. Furthermore, they can result in

new dislocation structures which in turn can affect the threading stress and lead to new interactions. Other factors include the interaction between interfaces and dislocations, image forces due to elastic modulus mismatch between the two constituent metals of the composite, anisotropic effects, and the chemical forces due to stacking fault energies. The combined complexity and interactions among all of the above-mentioned factors explains the deficiency in the theoretical understanding of the response of NMM composites.

1.2 Objective and Approach

The objective of this work is to understand the effect of dislocation interactions on the size effect in NMM composites. Two primary deformation mechanisms expected to be significant in goverening the response of NMM composites are studied: intersection of a threading dislocation with orthogonal pre-deposited interfacial dislocations, and the interaction of a threading dislocation with parallel pre-deposited interfacial dislocations. In doing so, an attempt is made to find out if either of these two significant processes, or both combined, can be used to model and understand the behavior of real composites. In both cases, the dependence of strength on the individual layer thickness of the composite is determined. Also the implications of those mechanisms on the dislocation structure and evolution in NMM compsites is outlined. Finally, large scale simulations of more realistic systems of dislocations in NMM composites is studied. In these simulations, all possible dislocation mechanisms and interactions occur naturally and interplay to determine the overall behavior. The dependence of strength on individual layer thickness in such simultaions is determined and qualitatively compared to the experimental results.

1.3 Dissertation Layout

The format of this thesis will be based on journal papers. This applies to Chapters Two and Three as well as Appendix A. In Chapter 2, the interaction between a threading dislocation and orthogonal dislocations is studied. The dependnce of the strengthening effect of this mechanism on the individual layer thickness is estimated using DD analysis. In Chapter 3, the interaction of a threading dislocation with parallel interfacial dislocations is examined. The effect of the layer thickness on the strength is calculated and the implications of the resulting trends on the nature of dislocation structure evolution is discussed. In Chapter 4, the large scale simulations methodology and results are presented. Finally, the conclusions from this work are made and directions of furure works and issues are suggested in Chapter 5. Appendix A presents multiscale approach for addressing size effects in crystals. This work addresses the classical problem of size effect in bending and is a first step towards a different future approach to study size effect in NMM composites, which will be a much more difficult problem to handle due the high density of interfaces, image forces and dislocations interface interactions.

Chapter Two: Dislocation dynamics analysis of dislocation intersections in nanoscale metallic multilayered composites

F. Akasheh*, H. M. Zbib*, J. P. Hirth**, R. G. Hoagland**, and A. Misra**
*School of Mechanical and Materials Engineering, Washington State University, Pullman, WA
** MST Division, Los Alamos National Laboratory, Los Alamos, NM

Abstract

In this work, dislocation dynamics (DD) analysis is used to investigate the strength of nanoscale metallic multilayered composites. Several possible interactions between threading (glide) dislocations and intersecting interfacial dislocations are considered and found to lead to strength predictions in better agreement with experimental trends and significantly higher than the predictions of the simplified confined layer plasticity model based on Orowan bowing of single dislocation in a rigid channel. The strongest interaction occurs when threading and intersecting interfacial dislocations have the same Burgers' vector and involves an annihilation reaction at their crossing points followed by the resumption of threading with a new dislocation configuration. The other possible dislocation intersections involve the formation of junctions, which are found to be more complex than simple models suggest. When the layer interfaces are modeled as impenetrable walls, as in existing analytical and some DD models, the predicted strengthening effect is weaker than that predicted by DD with more physical boundary conditions at the interfaces.

2.1 Introduction

Nanoscale metallic multilayered **(**NMM) composites represent an important class of advanced engineering materials due to their unusually high strength, several times larger than the rule-of-mixture prediction, and ductility among other favorable properties. Typically, NMM composites are made of bimetallic systems, built into alternating layers

of equal thickness, with individual layer thickness on the order of a few to tens of nanometers, by vapor or electro deposition. Careful experiments by several groups have clearly demonstrated that such materials exhibit a combination of superior mechanical properties: ultra high strength reaching 1/3 to ½ of the theoretical strength of any of the constituent materials [40], high ductility[46], morphological stability under high temperatures [42]and after large deformation[46], enhanced fatigue resistance[47], and improved irradiation damage resistance[45]. In this article, we focus our attention on understanding the deformation mechanisms and their contribution to the high strength of NMM composites.

Figure 2.1 shows the scale dependence of yield strength of multilayered structures. In *Regime I* (100's of nanometers and above) the strength can be well described by the Hall-Petch relation with the individual layer thickness acting as the characteristic length scale. Deformation in this regime is characterized by the formation of dislocation cell structure in the interior of the layers and dislocation pile-ups at the interfaces. In *Regime II*, the nanoscale range of interest to us here, the strength continues to increase as the layer thickness decreases; however, the dependence deviates from the Hall-Petch relation. Furthermore, no cell structure formation in the layer interior is observed upon deformation. Both observations indicate a fundamental difference in the active dislocation mechanisms at the two scales. While Frank-Read source operation leading to dislocation pile-ups is possible in the micrometer range, it becomes increasingly difficult as the layer thickness decreases, ultimately ceasing. Instead, glide of what is known as threading dislocations is believed to be the primary plasticity

mechanism at the nanoscale. Threading dislocations originate as faults in the atom arrangement during the deposition process and, once formed in one layer, replicate themselves in the next overlaid layer and so on. They are perfect glide dislocations, inhabiting typical glide planes and having Burgers' vectors of type a/2<110> in fcc, and stretch along the glide planes between the interfaces. When the stress in the layer is high enough, a threading dislocation glides on its slip plane depositing, in its wake, two dislocations, one at each interface, which results in the well-known hairpin configuration, Figure 2.2. This process is commonly referred as Orowan bowing and the stress required to propagate a threading dislocation in this confined fashion is commonly referred to as the *channeling stress*. As well established, the prediction of the channeling stress based on the Orowan bowing of single dislocation in a rigid channel model significantly underestimates the strength of NMM composites. In real systems, one expects that a threading dislocation will interact with other existing dislocations including threading dislocations and interfacial dislocation on parallel and/or intersection planes. In this work, we use DD analysis to investigate the contribution of the interaction between a threading dislocation and orthogonal interfacial dislocations to the increased strength measured in real systems.

Analytical models, for the onset of confined layer plasticity (CLP) by the glide of threading dislocations were developed by Frank and van der Merwe [48] and Matthews and Blakeslee [49]. Historically, these models were developed to predict the critical thickness at which interfacial dislocations are generated in heterogeneous epitaxial semiconductor films and layers. During the growth of coherent multilayered structures,

mismatch between the lattice parameters of the two materials results in a biaxial misfit stress in the layers and hence elastic energy stored in the structure, which increases linearly with thickness as the layer grows thicker. At a certain critical thickness it becomes energetically favorable for the system to relax part of the misfit strain by nucleating dislocations, thus trading elastic energy for defect energy. The same physical concept governs the determination of the channeling stress of a threading dislocation for a given layer thickness. From a mechanistic point of view[49], the idea is based on the balance between the force exerted by the misfit stress on the threading dislocation and the tension force in the created dislocation lines. For a certain critical layer thickness, h_c, the two forces become equal and the threading dislocation becomes unstable and propagates. By equating those forces, one finds the channeling stress dependence on layer thickness to be proportional to *ln(h)/h, h* being the layer thickness. The same concept can also be considered from an energetic point of view leading to the same result[50-52]. This simple model, however, underestimates the measured strength of NMM composites. Figure 2.3 is a compilation of the predictions of this classical model (the CLP model) for the channeling stress and experimentally measured strength of Cu/Ni cube-on-cube system with {100}interface orientation. The fact that both Cu and Ni are FCC metals and have low lattice parameter mismatch and a small difference in elastic properties, makes this system well-suited for comparison to simple starting-point models before further complexity associated with general real systems is included. As can be seen from the figure, the measured strength is higher with the gap increasing for increasing layer thicknesses. Suggested explanations for this discrepancy again came historically from observations regarding the relaxation process of misfit strain and the corresponding

critical thickness. The observation that the fraction of misfit strain relaxed by dislocations is much lower than that predicted for a given system and layer thickness indicates that significant impediment to dislocation propagation must exist in real systems. Among the proposed reasons for this impediment include dislocation-dislocation interactions leading to work hardening, barriers to dislocation nucleation, kinetic effects[53], Peierls friction stress [54], and step formation at surfaces and interfaces[55]. To complete the general picture drawn in Figure 2.3, the saturation and eventual dropping of the strengthening effect represent other important issues, which yet have to be understood. Theories put forward to explain the latter effects tie the point of saturation to the breakdown of the confining effect due to the interface acting as a barrier to dislocation crossing from one layer to the other[56].

The above-mentioned models for dislocation threading consider the introduction, in an otherwise defect-free medium, of a single dislocation dipole. In a real system, however, the threading of many dislocations in the form of orthogonal arrays will occur. Based on this observation, several authors developed energy expressions for stable dislocation arrays in multilayered systems as a function of layer thickness [57-63]. These approaches are more realistic-and resulted in enhanced predictions for the critical layer thickness for the onset of dislocation generation in multilayered structures. However, they assume simplified configurations for intersecting dislocations and perforce give approximate results. The same applies for the calculations made by Freund[64] and Nix[65] for the blocking effect an orthogonal interfacial dislocation and an array of them, respectively, has on a threading dislocation. The use of DD modeling gives an improved

analysis of local configurations and should give an improved relationship for the effect of layer thickness on strength.

In DD analysis actual dislocation structures with complex geometry are explicitly treated by the direct calculation of the Peach-Koehler force exerted on a dislocation by all existing stress fields, including those of the dislocations themselves, followed by the advancement and updating of dislocation positions using a physical mobility law. Other long-range effects from different boundary conditions can also be accounted for through the multiscale finite element (FE) and DD coupling. To the extent to which the short reaction rules used are physical, DD analysis can also capture dislocation-dislocation interactions including junction formation, annihilation, and cross slip; all of which are critical to any realistic predictions. When large systems consisting of many dislocations, applied loads, and various boundary conditions are dealt with, DD coupled with FE can handle this complexity simultaneously. For complete details on the DD analysis and its coupling with FE, the reader is referred to [66, 67] which provide a comprehensive overview of the topic.

Published DD analyses of nanoscale multilayers are limited. Pant *et al.* [68] studied dislocation interactions in layers with impenetrable walls and found that the blocking effect an intersecting interfacial dislocation has on a threading dislocation is weak, contrary to the predictions of simple analytical models [56, 64, 65]. Considering all four possibilities of orthogonal encounters between interfacial dislocations and a threading dislocation in (001) and (111) Cu films, they observed interactions that were either junction formation (2 cases) or annihilation (one case) while the fourth case,

involving the interaction between the (1-11)[011] threading dislocation and the (111) [0-11] interfacial dislocation, did not result in a junction (nor annihilation). Furthermore, junction formation was found to depend on layer thickness: the thinner the film, the greater the channeling stress, which in turn leads to the interfacial dislocations being pushed so strongly against the impenetrable interfaces to the point where they can no longer move locally and reorient themselves so as to engage in short-range reactions. The maximum increase in the channeling strength for an 800 nm thick layer was found to be about 20% for the no junction case, 10% for the junction formation case with the effect being stronger for thicker layers, while for the annihilation case the strengthening effect was 16%. In another effort, DD analysis of the blocking effect of a single fixed (non-reacting) interfacial dislocation[69] found that the maximum strengthening effect above the unobstructed channeling stress was 15%, much less than the corresponding analytical result of 50% [64]. The suggested reason for this discrepancy was that in DD calculations, the threading dislocation can dynamically adjust its configuration so as to bypass the obstacle with minimum resistance. The same problem addressed in [69]was revisited (using DD) but with the interfacial dislocation free to move and react while being confined to its layer by a stress free neighboring layer[70]. The blocking effect was found to be even weaker than that found for the fixed dislocation case[69] because the interfacial dislocation could now be locally pushed into the stress-free layer, hence presenting less restriction on the threading dislocation. As reported, even if a small restoring stress is applied to the neighboring layer, the strengthening effect is never above 15%.

Hence, a few DD analyses with a limited number of dislocations [68-70] have indicated that the predicted strengthening can differ markedly from the simple analytical results. In this work, we use a more extensive DD analysis to examine the strengthening effect due to the interaction between threading dislocations and intersecting interfacial dislocations. First, we obtain DD predictions for the channeling stress in a rigid channel, and compare them to the results of the classical CLP model as well as with a complete energetic model, which was developed for validation purposes. Using flexible boundary conditions for layer interfaces, we then investigate the reactions resulting from the intersection of different combinations of threading and interfacial dislocations and their strengthening effects. Climb, as a possible relaxation mechanism, is not considered in this analysis.

2.2 Problem setup in DD

Figure 2.4 shows the problem setup and crystallography. A 3-layered Cu system is used to idealize confined layer slip in a coherent multilayer system with small lattice parameter mismatch and moderate elastic properties difference, as in a {001} Cu/Ni cube-on-cube system. Table 2.1 lists the physical properties of Cu used in the model. The initial configuration consists of an a/2<011> threading dislocation residing on a (111) slip plane in the middle layer, as well as a long orthogonal a/2<011> interfacial dislocation dipole residing on the (-111) plane. This interfacial dipole can be thought of as resulting from an earlier threading event on a (-111) plane. In accordance with the fundamental principle of continuity of dislocations lines, two fixed semi-infinite dislocation lines, with the same line sense as that of the threading dislocation segment, are attached to both ends. Dislocations in the middle layer are driven by the application of biaxial tensile

stress of a desired magnitude in this layer. In the bounding layers, a biaxial compressive stress equal in magnitude to that applied in the middle layer is applied. As in coherent or semicoherent systems, the effect of this stress is to confine dislocations initially in the middle layer to that layer. With these flexible boundary conditions, interfacial dislocations are not overconstrained, as in the case of impenetrable boundaries, because, although confined to their layer, they can still move locally to adjust their configuration in response to the stress state. This in turn allows for the possibility of short-range interactions upon the encounter of the threading dislocation with the interfacial dislocations. Restricted by slip crystallography, four representative encounters between threading dislocations and intersecting interfacial dislocations are possible (see Figure 2.4).

Nanoscale composites, represent an unconventional application for DD analysis. While typical DD applications involve microscale specimens and dislocation segments on the order of 100 *b*, the layer thickness range of interest in our case can be as small as 25 *b* and up to 500 *b*. This requires the use of discrete segment lengths on the order of few *b*'s. The stress, of the order of several GPa, needed to drive dislocations confined to nanolayers requires the use of suitably small time steps. Both the spatial and temporal discretizations in this problem require optimization for stability and accuracy. An optimized mean segment length of 3.5 *b* was used in these simulations: however, the actual segment length is locally decided, based on the dislocation line curvature, by an adaptive meshing technique[66]. The choice of the time step is also automated based on dislocation velocities and the detected possibility of short-range interactions[66]. Table 2.2 lists the main numerical parameters used in the DD simulation. Originally, the core

was optimized as a numerical parameter to match the force calculations from an exact analytical model for a corresponding problem[71]. Here instead, the core size was fixed as 1 *b* and the average force per unit length on a given dislocation segment from its neighboring segment is calculated from the following equation, which is equivalent to an earlier expression for the case of an adjustable core size[71].

$$\left(\frac{F}{L}\right)_{avg} = \frac{\mu}{4\pi L} f_1(\theta, b)\left(\ln\left(\frac{L}{b}\right) + \beta\right) \tag{2.1}$$

where $(F/L)_{avg}$ is the average force per unit length acting on a dislocation segment of length L, μ is the shear modulus, $f_1(\theta,b)$ is a functional multiplier given in Ref.[72], p. 138, and β is an adjustable parameter that compensates for the energy contained in the core size. To validate our choice of parameters, a complete energetic model for the threading process in a rigid channel is developed and its results, as well as those of the classical CLP model, are compared to DD results. Here, "complete" means that the inherent assumptions to the CLP model, infinite dipole length and the layer thickness as the external cutoff radius in the logarithmic term in the energy expression, are relaxed. Appendix A describes the details of the model and the comparison results, which strongly validate the DD model for confidence in its results in more complex situations.

2.3 Results and discussion

The four representative cases for the intersection encounters between threading dislocations and glide interfacial dislocations are shown in Figure 2.4. Table 2.3 lists these interactions and their energetic favorability. Consistent with these trends, annihilation reaction is observed in the DD simulation for Case 1 at both the lower and upper interfaces where interfacial dislocations reside. For the threading dislocation to

overcome the obstacle (i.e., the interfacial dipole) and the threading process to continue, the annihilation process needs to occur twice. Figures 2.5a-d show this process and the corresponding dislocation configuration in the intermediate stages. As shown in Figure 2.6, which is a close-up of the annihilation reaction occurring within circled region in Figure 2.5b, the interaction involves a complex process of local realignment of the interfacial and threading dislocations to produce a configuration that is admissible to an annihilation reaction. This configuration consists of two antiparallel screw-oriented segments, each belonging to a different dislocation, and attracting each other to a common position along the line of intersection of the two slip planes. After this configuration is achieved, Figure 2.6c, the annihilation process occurs leaving behind two dislocation nodes, *i* and *j*, which can move only along the line of intersection of slip planes, Figure 2.6d. Notice that a 90^{o} dislocation bend structure has resulted from the joining of the trailing arm of the threading dislocation at the lower interface with that part of the interfacial dislocation at the lower interface which maintains the line sense of the aforementioned part of the threading dislocation, Figures 2.5b-d and 2.6d. This dislocation structure has been observed experimentally at the interfaces in NMM composites (e.g., see TEM images in [73]). The above observation that dislocations with initially repulsive interaction readjusting their configuration to reach a minimum energy configuration involving annihilation was also made by Madec *et. al* [74].

Table 2.4a details the incremental strengthening effect of the two annihilation reactions as a function of layer thickness. The third column in this table indicates the increase in stress, above that of the unobstructed threading case listed in column 2, necessary to push the threading dislocation against the long-range stress field of the

interfacial dislocation dipole, as close as possible to it, yet not close enough to over come the repulsive force and interact. In the simulation, this stress was noted after allowing the simulation to run long enough at that stress without observing the first annihilation reaction. The additional stress needed to push the threading dislocation beyond the first interfacial dislocation by inducing the annihilation reaction, fourth column in Table 2.4a, is the needed activation energy to reorient the dislocation segments for annihilation. If the stress is not increased further, the new dislocation configuration, Figure 2.5b, remains unchanged. To push the dislocation ahead from this position, another increase in stress is needed. Although a small portion of the original threading configuration is lost upon the first annihilation interaction, the new connection to the interfacial dislocation has a high curvature, resulting in higher line tension and leading to higher resistance to further threading. Another contribution to this hardening effect is that, as in the first reaction, energy needs to be spent to perform the realignment necessary for the reaction to take place. The same behavior is observed for the case of a single a/2<011> interfacial dislocation acting as the obstacle to threading. Obviously, only one annihilation reaction occurs. Table 2.4b breaks down the strengthening effect due to each of the three stages of the bypass process for this case: (a) bowing out of the threading dislocation to closely approach the interfacial dislocation just before the reaction is induced, column 3, (b) annihilation reaction leaving behind a configuration similar to that in Figure 2.5b (except for the absence of the interfacial dislocation at the upper interface), column 4, and (c) the final stage of completely overcoming the obstacle and the resumption of the threading process, column 5. If the stress value shown in column 4 of Table 2.4b is applied without further increase, the threading dislocation will only perform the annihilation and get stuck

at that point. Similarly if only the stress level shown in column 3 is applied and no more, the threading dislocation will be arrested close to the interfacial dislocation and will not advance any further. A comparison of the strengthening effect due to a single and a dipole a/2<001> interfacial dislocation obstacle for any corresponding bypassing stages, Tables 2.4a and b, indicates that the presence of the second interfacial dislocation in the dipole contributes to a higher resistance at all stages. Furthermore, the strengthening effect due to this interaction (dislocations with collinear Burgers vectors on intersecting slip planes) was found to be the strongest among other possible interactions. The same conclusion was made from large-scale DD simulations of forest interactions in FCC crystals [74].

Figure 2.7 summarizes the DD predictions, based on the 3-layer model, for the channeling stress in the absence and presence of a/2<01-1> single and dipole interfacial dislocations intersecting the path of a threading dislocation with the same Burgers vector. When an interfacial dislocation(s) exits, the channeling stress, *i.e.* the minimum stress needed for the threading dislocation to completely overcome the obstacle and continue past it, has the values reported in column 5 in Tables 2.4a and b. Also shown on the same plot are the experimental results for the strength of Cu/Ni multilayered system previously shown in Figure 2.3. Thus, including the interactions of a threading dislocation with orthogonal interfacial dislocations, as expected to happen frequently in a real system, does bring the baseline DD predictions (threading without obstacle) closer to the experimental measurements for layer thicknesses of 30 nm and above. However, the 3-layer model overestimates the strength below this range, as does the CLP model. This indicates that orthogonal intersections between threading dislocations and interfacial

dislocations cannot be considered as the single mechanism to account for the discrepancy between the experiment and the model. Obviously other mechanisms such as interface crossing, which are softening in nature, play an important role in the 30 nm and below range. This conclusion supports a similar general one made by Pant [68]on the existence of different mechanisms at different length scales. Also other mechanisms could be important with larger misfits, and with different crystal structures for the two types of layers.

For the other cases of intersections where a junction forms upon interaction, the threading process ceases, as long as no other conditions, e.g. load reversal, arise to unzip the junction and free the threading dislocation. DD analyses reporting on junction formation under different boundary conditions from the ones used here indicate that the strength is weaker and annihilation remains the stronger reaction[68]. Other mechanisms, such as cross-slip, as well as long-range effects in systems with many dislocations play an important role in determining strength. Those issues are the subject of a forthcoming article in which results from massive DD analyses will be reported [75].

Finally, we examined the effect of the assumption of rigid channel walls on the threading process. DD analysis for the interaction of an a/2[01-1](111) threading dislocation with a/2[01-1](-111) single and dipole interfacial dislocations as well as with Lomer-type interfacial dislocation was performed under the assumption of rigid channel walls with pinned dislocation. The first two cases correspond to those studied using the 3-layer model and whose results are presented in Tables 2.4a and b and in Figure2.7. Figure 2.8 shows a sequence of DD snapshots of the bypassing process of the threading dislocation in two cases: (a) over a Lomer-type interfacial dislocation, and (b) through an

interfacial dislocation dipole representing the two arms deposited in the wake of a threading dislocation. A third case, bypassing over an a/2<011> type interfacial dislocation, was also performed and the sequence was found to be similar to that of the Lomer-type case; thus, it is not included here for brevity. As can be deduced from the figure, there is a sequence of complex, dynamically changing configurations for the threading dislocation during the bypassing process and the notion of a critical effective thickness through which the threading dislocation passes[64] is not well-defined. Another difference between the rigid channel model with pinned interfacial dislocations and the flexible boundary results is in the predictions of the strengthening effect. Figure 2.9 shows DD predictions, for the case of the rigid channel model with pinned interfacial dislocation, for the channeling stress in the absence and presence of a/2<01-1> single and dipole interfacial dislocations intersecting the path of a threading dislocation with the same Burgers vector (same cases used to generate Figure 2.7). Also shown in the figure are the Cu/Ni measured strength values[56] and the strengthening effect due to a Lomer-type interfacial reaction. As can be seen by comparing Figures 2.7 and 2.9, which are plotted using the same scale for the ease of comparison, the strength predictions of rigid channel with pinned interfacial dislocations underestimate the strength of NMM composites when compared to the more realistic 3-layer model predictions and more so when compared to the experimental results.

2.4 Conclusions

- The use of flexible dislocations (which allows for short-range interactions) and flexible channel walls (where dislocations are confined by coherency stress) leads

to an improved agreement between predicted and experimentally measured strengths in nanoscale multilayered composites.

- Among the possible interactions between threading and orthogonal interfacial dislocations, the strongest contributor to hardening is that involving dislocations of same Burgers vector. For this case, the bypassing process entails annihilation reactions and leaves behind a 90^{o} bend dislocation structure. In the thickness range of 10-100 nm, the increased strength due to this interaction is about 1.5 times the reference (free threading with no obstacles present) strength.

Acknowledgments

This research is sponsored by the U.S. DOE, Office of Science, Office of Basic Energy Sciences.

Appendix: Energetic model for channeling strength

Figure 2.10 outlines the main features of an energetic model to estimate the channeling strength of a threading dislocation. The initial configuration consists of an infinite dislocation line, here made of a finite segment 0 and two semi-infinite segments 4 and 5. As the side view shows, the dislocation resides on a {111}slip plane and the crystallographic setup corresponds to that in Figure 2.4. Segment 0 represents the part of the dislocation which will bow out into a hairpin confined to the layer of thickness h under the effect of the applied stress. The semi-infinite segments are a necessity to maintain the dislocation continuity. A stress is applied to the layer with τ representing its resolved shear component in the slip plane along the Burgers vector. Under the effect of this applied stress, the threading dislocation advances, segment 3, depositing two finite misfit dislocations of length l, segments 1 and 2. The change of the system configuration energy ΔW as follows,

$$\Delta W = W(l,h) = \begin{pmatrix} 2W_1 + W_3 + 2W_5 + W_{12} + W_{31} + W_{32} \\ + 2W_{35} + W_{15} + W_{42} + W_{52} + W_{14} + W_{45} \end{pmatrix} - \left(W_0 + 2W_5 + 2W_{05} + W_{45}\right)$$

…….(2.2)

W with a single subscript represents a self-energy while that with two subscripts represents the interaction energy between the two segments indicated by the two subscripts. All the expressions needed for self and interaction energies can be found in Ref. [72]. The final result for the ΔW expression is a function of h and l and, after some algebra, reduces to, (to avoid the infinite energies of the semi-infinites segments, the terms W_{35} and W_{05} should be considered simultaneously, series expansion performed on the combined expression, and second term in the expansion kept)

$$\Delta W = 2C_0 L \ln\left(\frac{L}{e\rho}\right) + C_1\left\{2\eta - 2\sqrt{l^2+\eta^2} + 2l\ln\left(\frac{\sqrt{l^2+\eta^2}+l}{\eta}\right)\right\}$$
$$+ C_{10}\left\{\sqrt{l^2+\eta^2} + \eta\ln\left(\frac{2\eta}{\sqrt{l^2+\eta^2}+\eta}\right) - l - \eta\right\} \quad \text{…….. (2.3)}$$

$$C_0 = \frac{\mu b^2}{4\pi}(\cos\beta)^2 + \frac{\mu b^2}{4\pi(1-\upsilon)}(\sin\beta)^2 \quad ;$$

$$C_1 = -\frac{\mu b^2}{4\pi}(\cos\beta)^2 - \frac{\mu b^2}{4\pi(1-\upsilon)}(\sin\beta)^2$$

$$C_{10} = \frac{\mu}{4\pi}(\sin\beta)^2 + \frac{\mu b^2}{4\pi(1-\upsilon)}(\cos\beta)^2 \quad \text{……...… (2.4)}$$

The equilibrium position of the threading dislocation corresponding to a certain applied stress can be determined by minimizing the free energy, $\Delta G = \Delta W - \tau b \eta l$, while the stable point beyond which the threading dislocation propagates indefinitely can be determined for a given layer thickness h from the condition $\frac{\partial^2 \Delta G}{\partial l^2} = 0$. Figure 2.11 shows the results of performing those calculations for the critical channeling stress as a function of layer thickness, expressed in terms of its resolved shear component, which satisfies both conditions. Physically, this stress corresponds to the stress needed to bow out the threading dislocation to the point were the hairpin configuration is not stable any more and the dislocation will propagate indefinitely. At any stress value below this critical stress the dislocation will bow out to a certain equilibrium length proportional to the applied stress. For comparison and validation purposes, the channeling stress prediction from the classical confined layer plasticity model (CLP) and the prediction of our DD model are shown in Figure 2.11. As can been seen from the figure, our DD model

produces excellent agreement with the analytical models. Furthermore, our energetic model and the CLP model match perfectly as far as the stress prediction is concerned in spite of the fact that the CLP model starts out by assuming semi-infinite arms connected to the threading dislocation and finding their dipole energy by taking the external cutoff radius in the logarithmic term of the energy expression to be equal to the layer thickness. Our energetic model remains more complete because it considers the exact configuration and includes all the interaction energies, and is physically based on minimizing the free energy of the system. This principle difference reflects in the fact that our energetic model predicts an equilibrium threading length for any applied stress below the critical stress, while the CLP model does not. In this regard, DD calculations support this finding of our energetic model predictions. Figure 2.12, shows the agreement between the DD model and our energetic model in this regard.

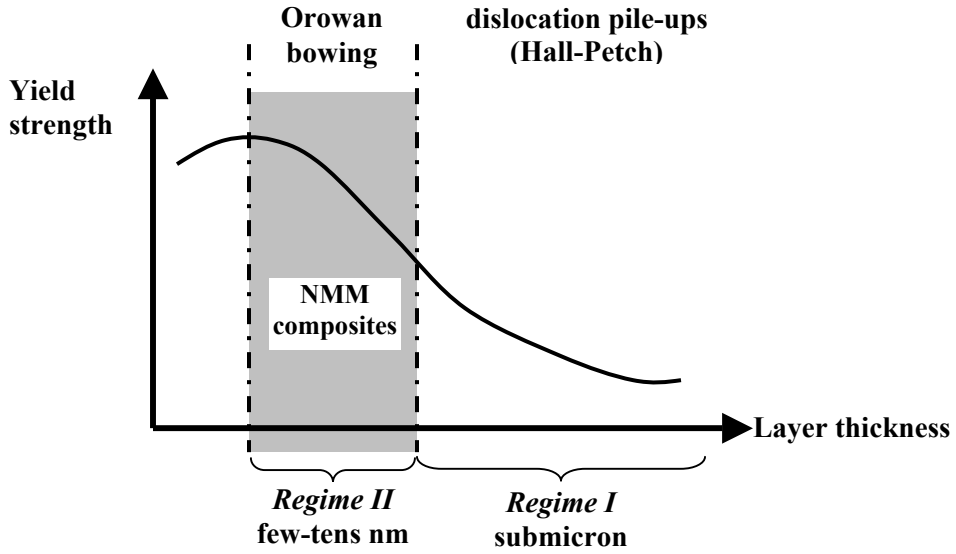

Figure 2.1 Schematic showing dependence of yield strength of multilayered structures on the individual layer thickness.

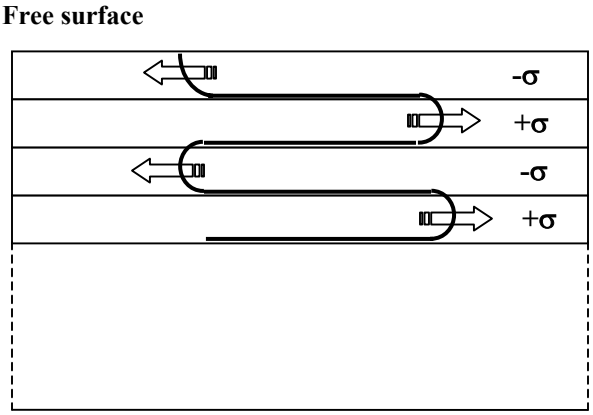

Figure 2.2 Schematic illustrating the glide of a threading dislocation in different layers.

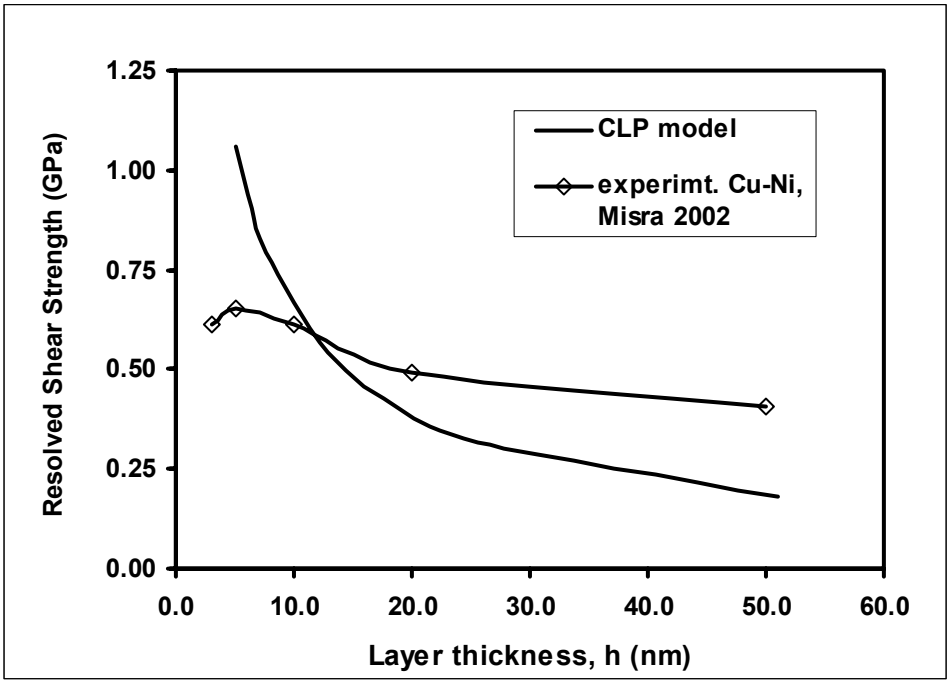

Figure 2.3 Comparison between the strength predictions of the classical confined layer plasticity model with experimental results for Cu/Ni system[56].

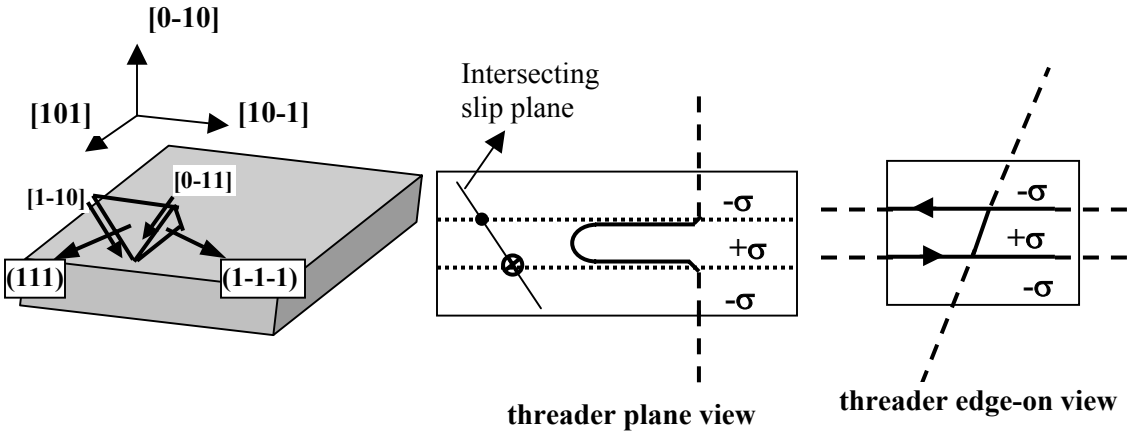

(a)

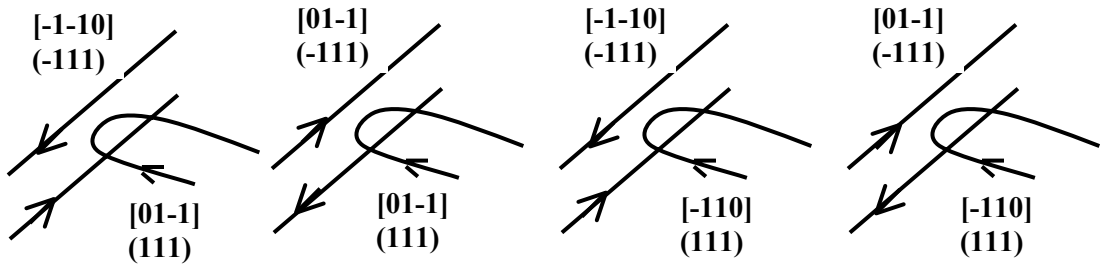

(b)

Figure 2.4 Problem setup, (a) crystallographic orientation of the layers idealized setup, (b) four encounters representing all possible intersections between threading dislocation and a/2<011> type interfacial dislocation dipoles.

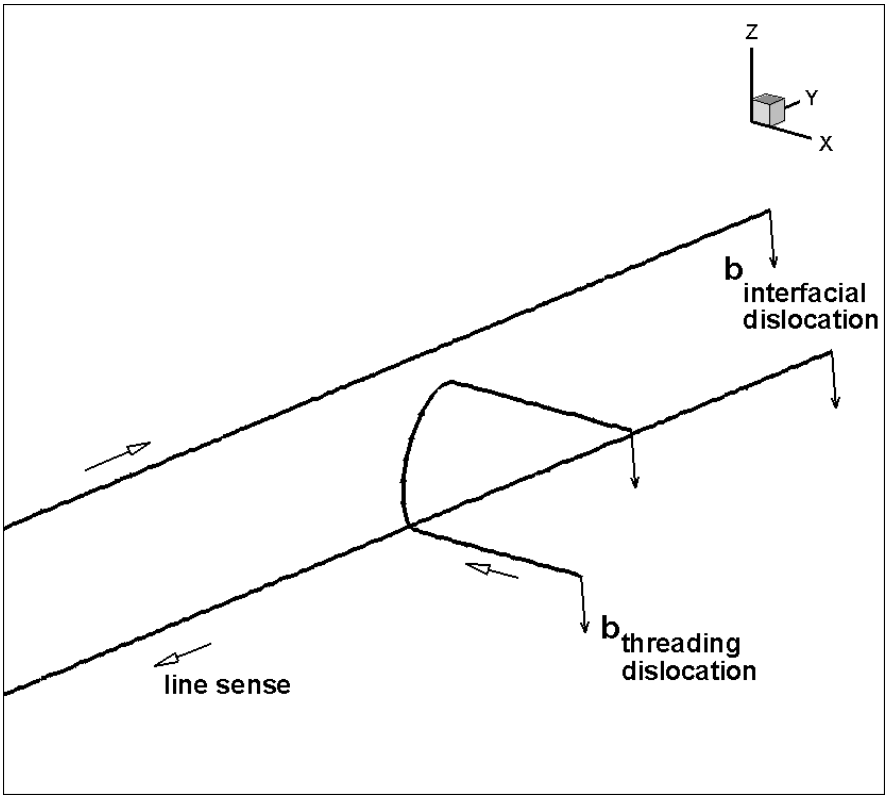
Z
Y
X
b
interfacial
dislocation
b
threading
dislocation
line sense

(a)

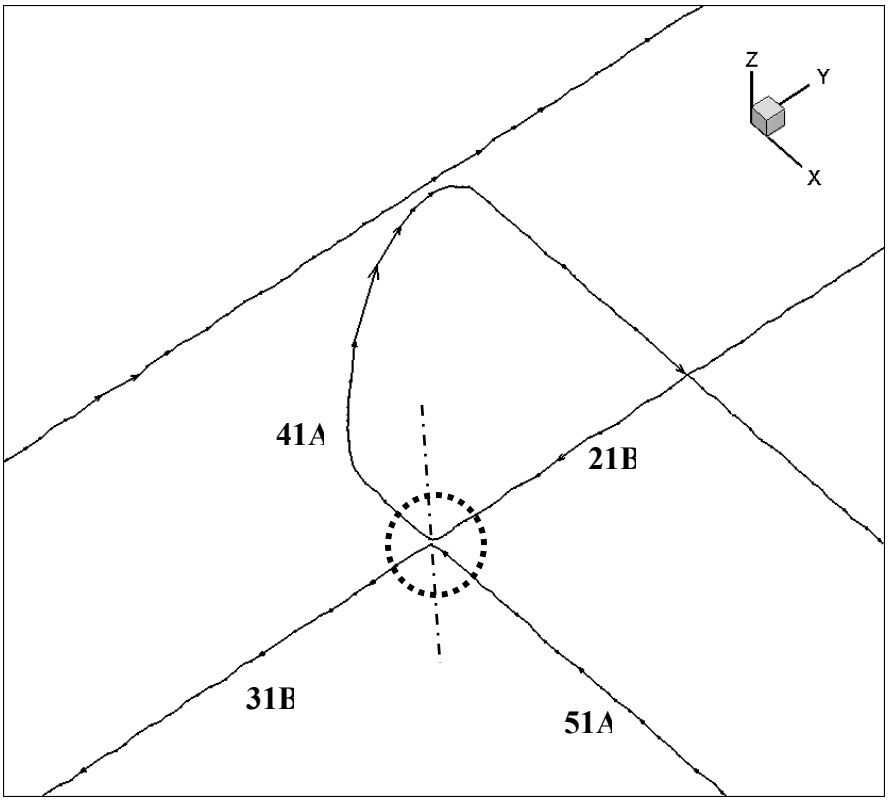
Z
Y
X
41A
21B
31B
51A

(b)

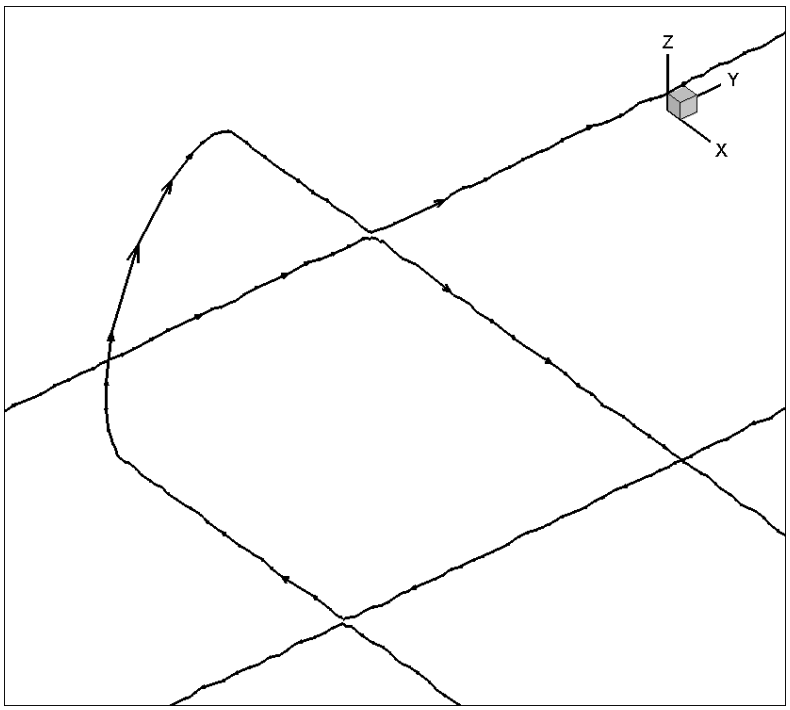

(c)

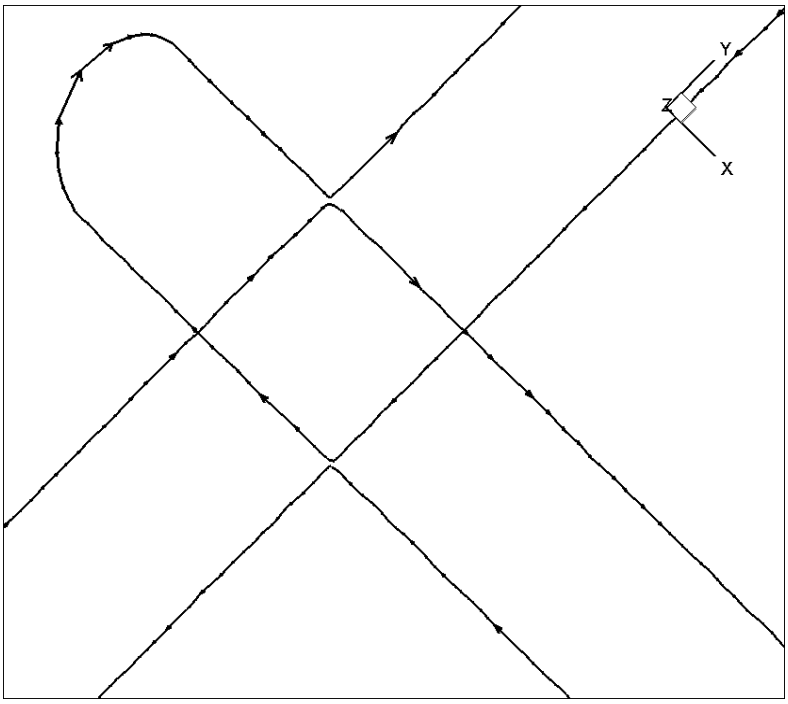

(d)

Figure 2.5 Stages of interaction between a/2[01-1](111) threading and a/2[01-1](-111) interfacial dislocation, (a) arrest of threading dislocation by the long-range stress field of the interfacial dislocation; stress needs to be increased to propagate further (b) intermediate configuration after first annihilation reaction at lower interface (circled region indicated region zoomed-in at in Figure 7), (c) final configuration after second annihilation at upper interface, (d) interface plane view of final dislocation configuration.

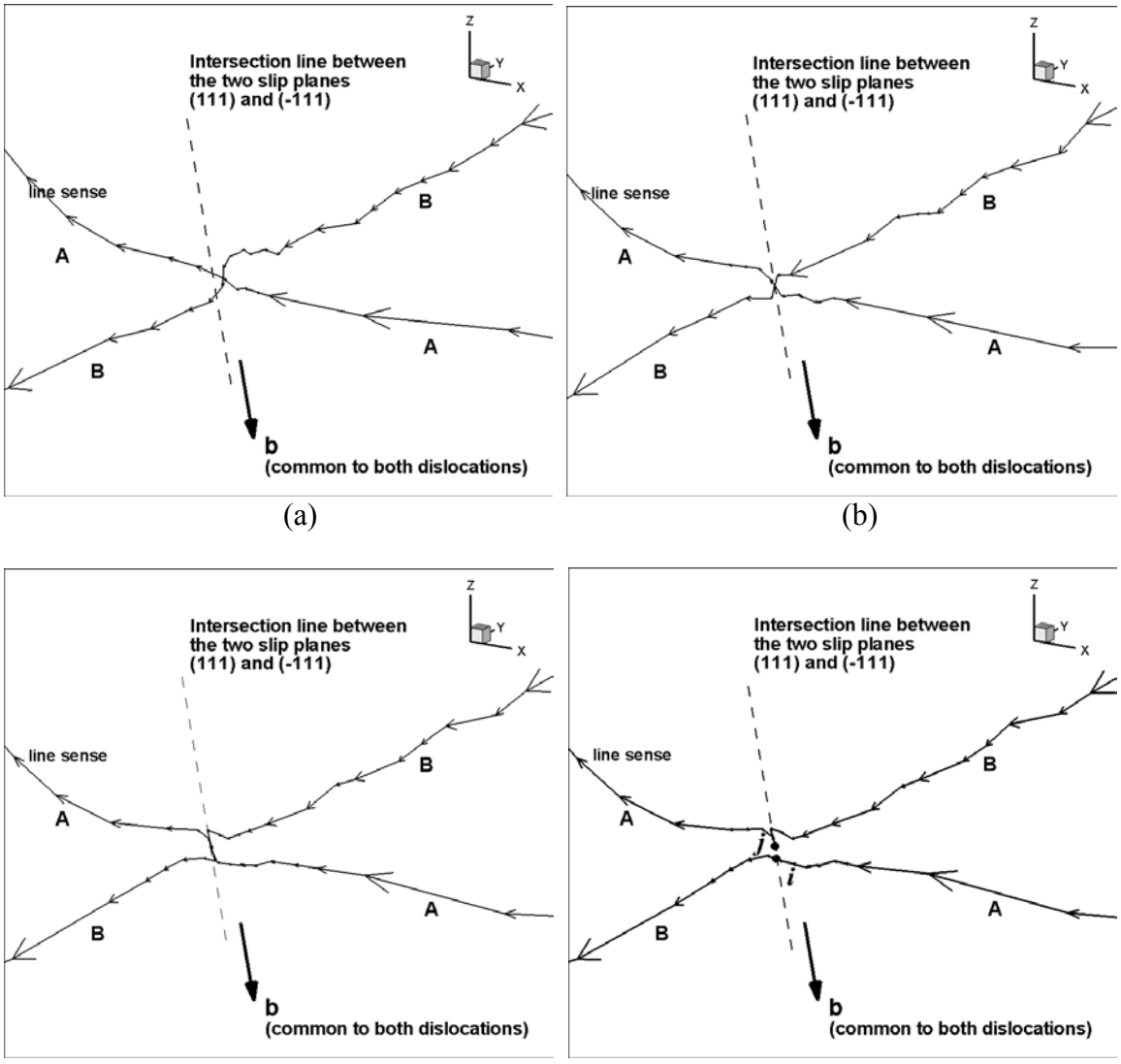

Figure 2.6 Sequence showing the details of the realignment process which the a/2[01-1](111) threading dislocation A and the a/2[01-1](-111) interfacial dislocation B undergo to admit the annihilation reaction.

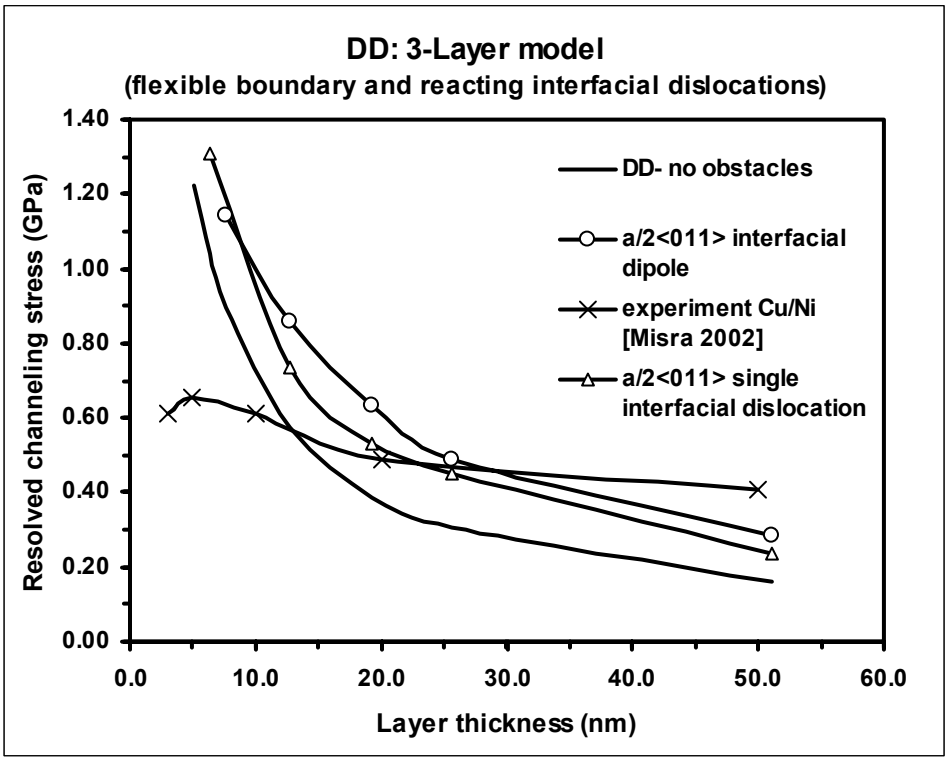

Figure 2.7 Comparison of measured strength of Cu/Ni bimetallic system with DD predictions using the3-layer idealized model (flexible confinement boundary conditions and reacting interfacial dislocations). The strengthening effect is due to annihilation reactions occurring between a threading dislocation and an intersecting interfacial dislocation of the same Burgers vector.

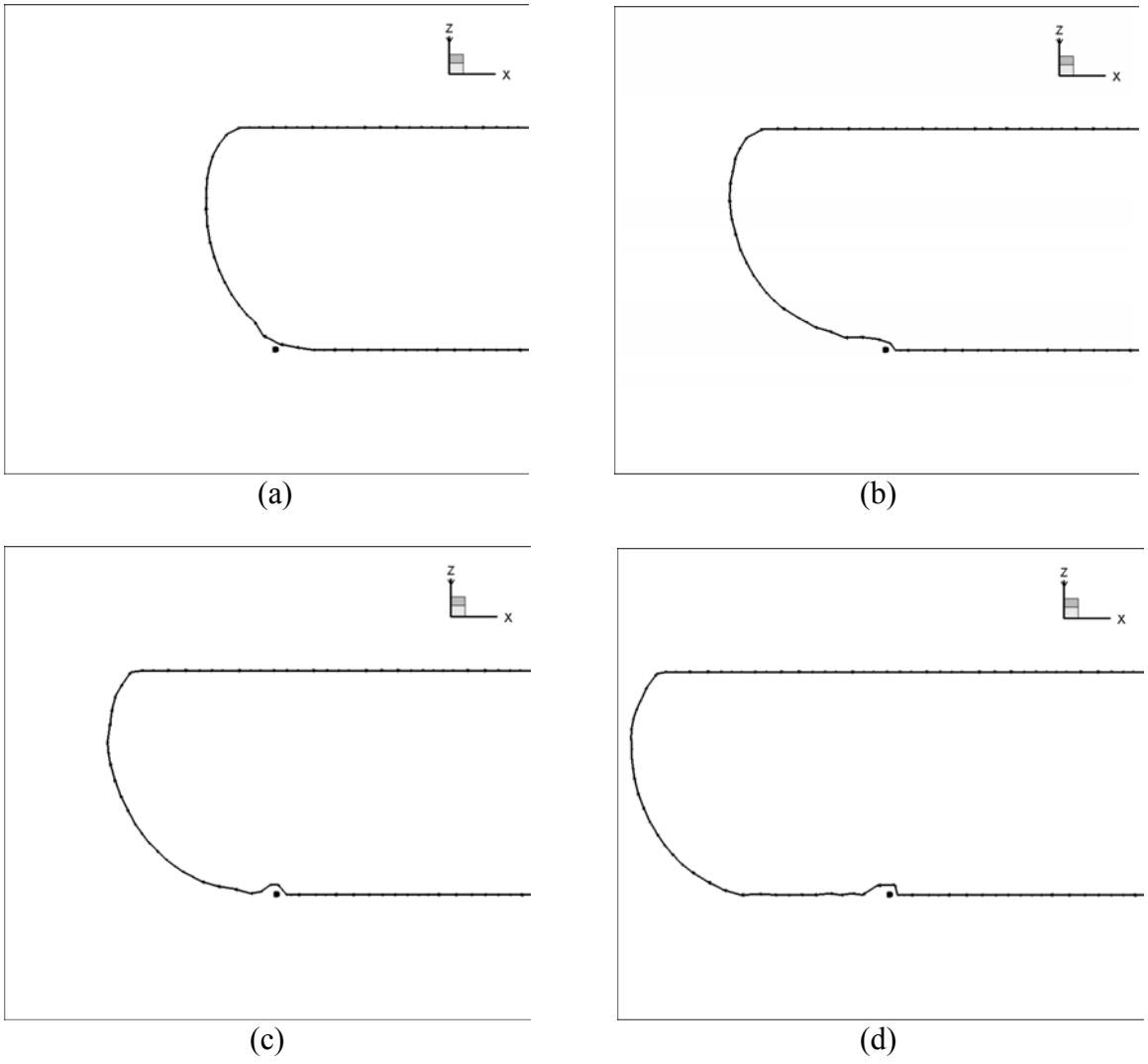

Figure 2.8a Slip plane (111) view of a sequence of simulation snapshots of the bypassing process of a/2 [01-1](111) threading dislocation over a Lomer-type interfacial dislocation with Burgers' vector a/2[10-1] (globally, parallel to the x-axis) in a 13 nm-thick layer under a stress of 1.7 GPa.

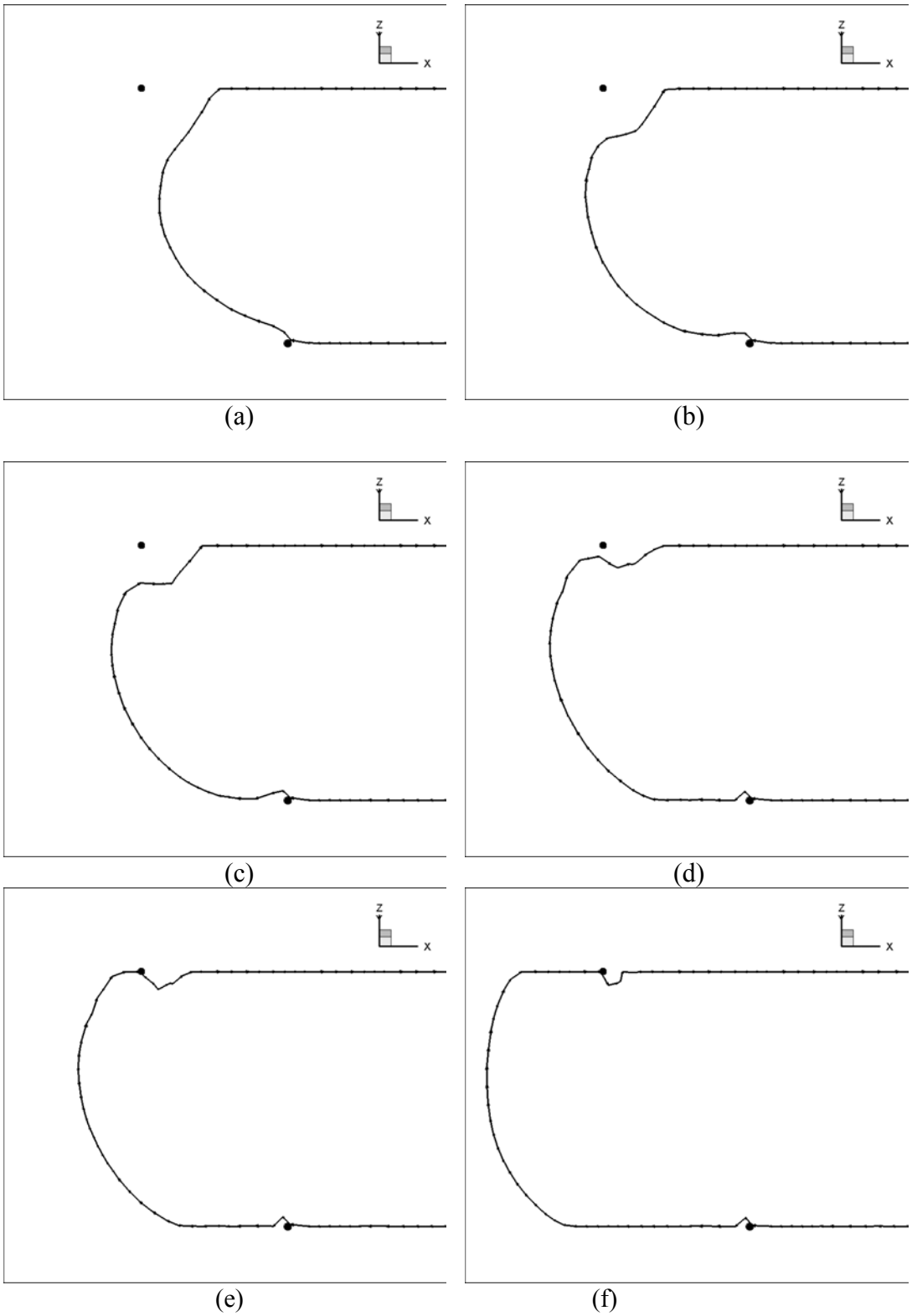

Figure 2.8b Slip plane (111) view of a sequence of simulation snapshots of the bypassing process of a/2 [01-1](111) threading dislocation over a/2[01-1](-111) interfacial dislocation dipole treated as pinned and non reacting in a 13 nm-thick layer under a stress of 2.1 GPa.

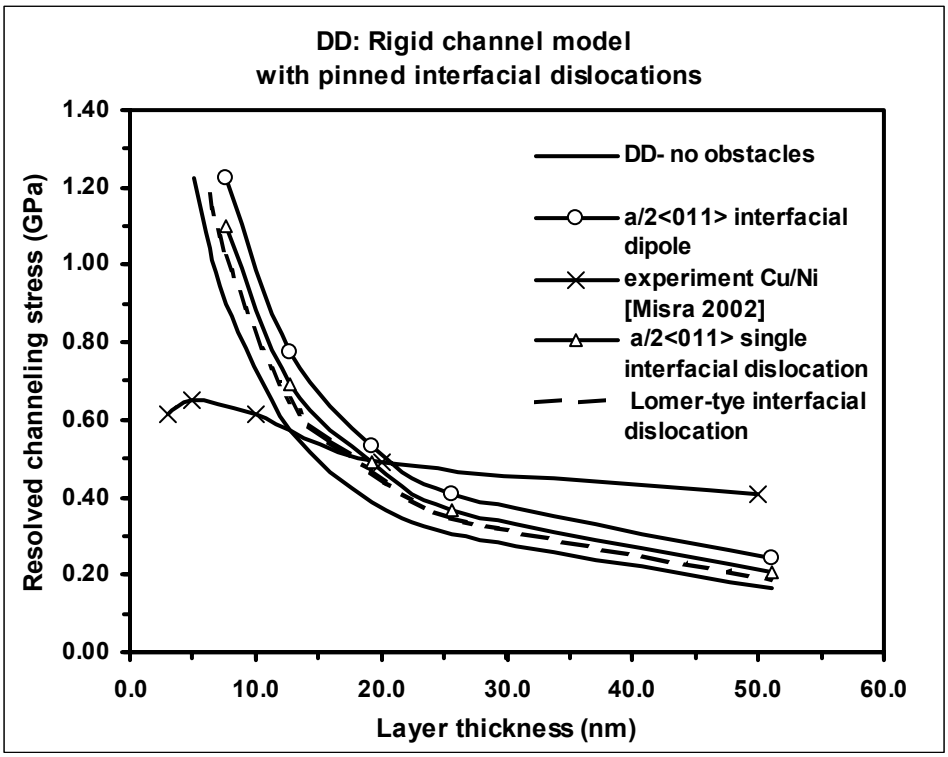

Figure 2.9. Comparison of measured strength of Cu/Ni bimetallic system with DD predictions using the rigid channel idealized model (impenetrable layer interfaces and pinned interfacial dislocations). The strengthening effect is due to annihilation reactions occurring between a threading dislocation and an intersecting interfacial dislocation of the same Burgers vector.

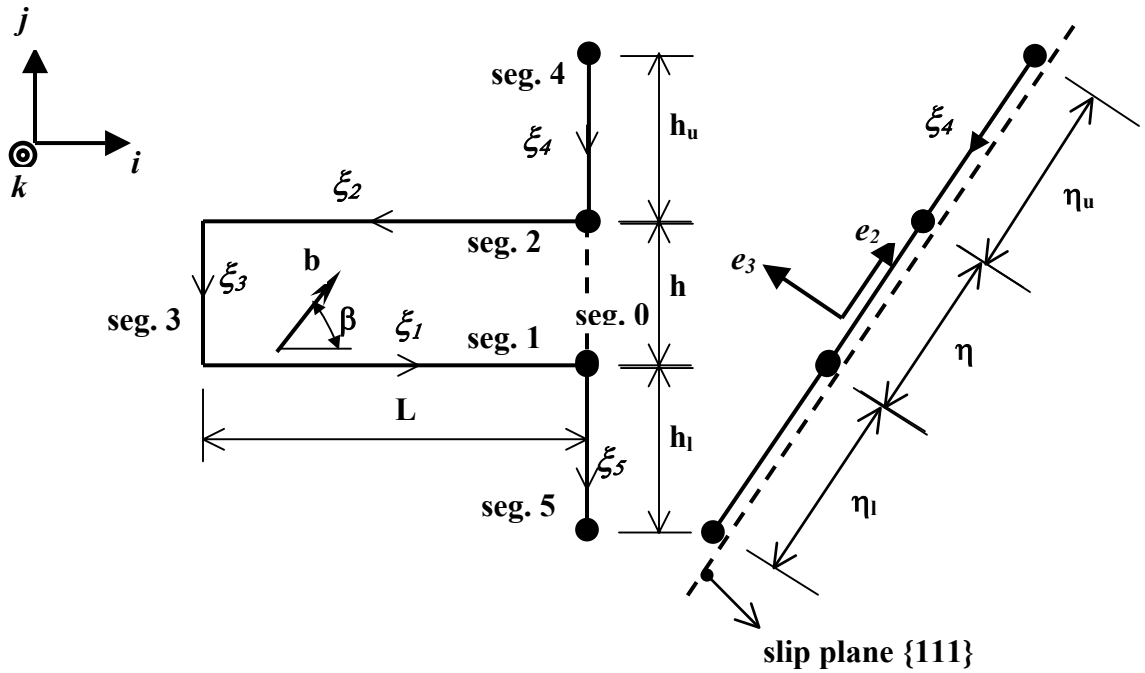

Figure 2.10. Dislocation configuration modeling the threading process in a confined layer.

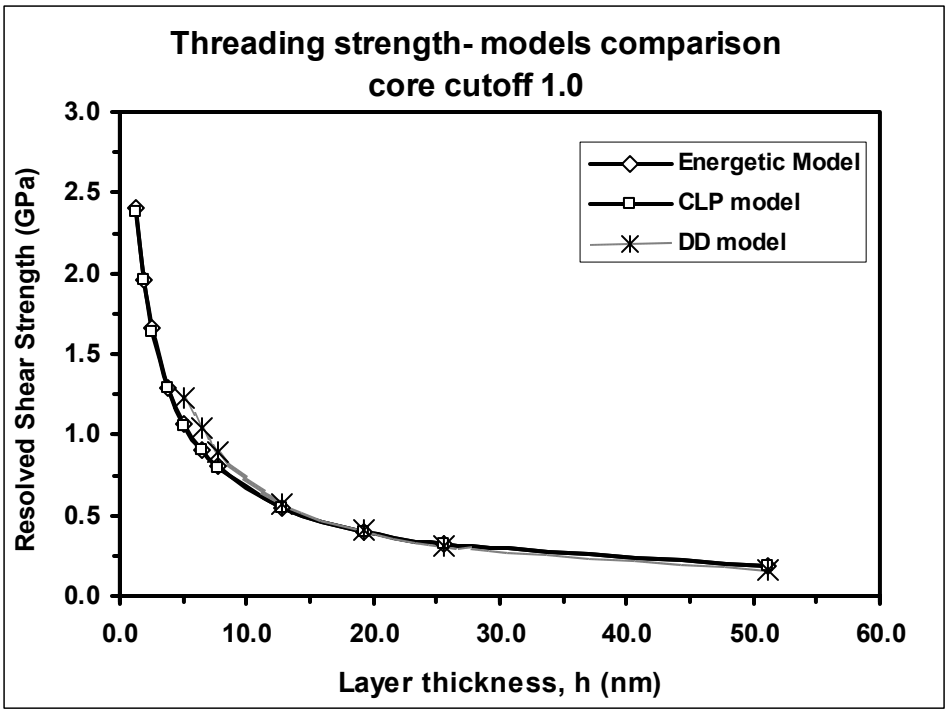

Figure 2.11. Critical stress for threading in a confined rigid channel of thickness $\boldsymbol{h}$, comparison of different models' predictions: classical confined layer plasticity (CLP) model, DD models, and our energetic model.

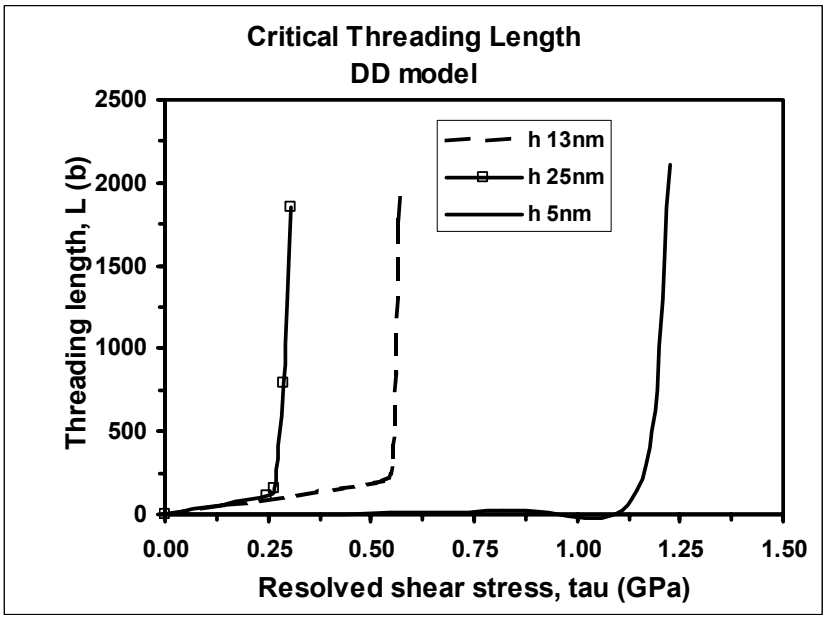

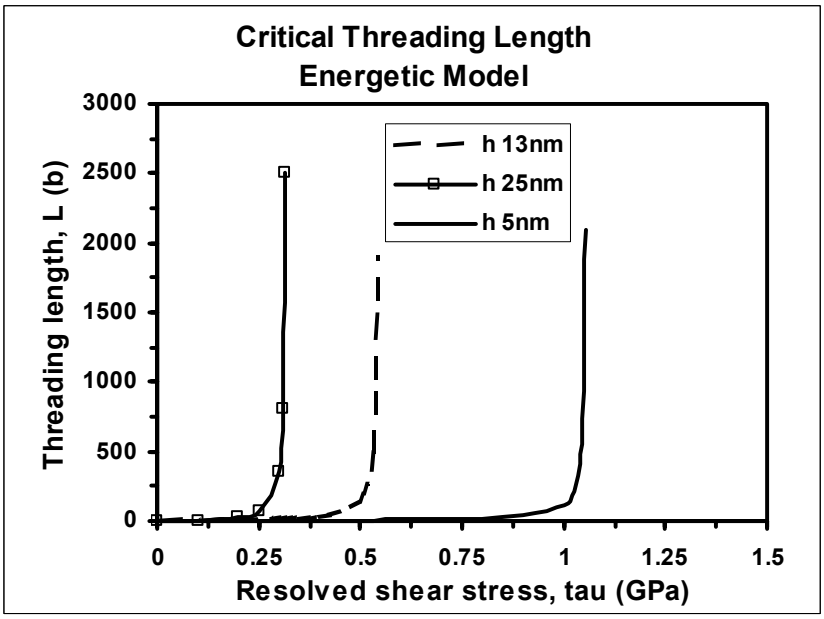

Figure 2.12. Threading length as a function of applied stress, comparison between DD model and our energetic model. The CLP model only predicts infinite threading once the applied stress reaches a critical value.

Density (Kg/m^3)	8980.0
Burgers vector magnitude (A^o)	2.556
Shear modulus (GPa)	38.46
Poisson's ratio	0.3
Core size (b: Burgers' vector magnitude)	1.0
Mobility (1/pa.s)	$1.0x10^4$

Table 2.1. Physical properties of Cu used in DD calculations.

Mean segment length (b)	3.5
Minimum segment length (b)	1.75
Maximum segment length (b)	5.25
β parameter (Equation 1)	0.5
Time step (s) (variable)	1.0×10^{-13}-3.0×10^{-13}

Table 2.2. Main numerical parameters used in DD calculations. Within the minimum and maximum segment length, the precise choice is made automatically based on adaptive meshing.

Case no.	Reactants		Reaction favorability		Expected reaction
	Threading dislocation	interfacial dislocation	parallel sense	anti-parallel sense	
1	a/2 [01-1]; (111)	a/2[01-1]; (-111)	neutral	favorable	Annihilation
2	a/2 [01-1]; (111)	a/2 [-1-10]; (-111)	favorable	unfavorable	Junction formation
3	a/2 [-110]; (111)	a/2 [01-1]; (-111)	unfavorable	favorable	Junction formation
4	a/2 [-110]; (111)	a/2 [-1-10]; (-111)	neutral	neutral	Junction formation

Table 2.3. Possible encounters between threading and a/2<011> type interfacial dislocations on intersecting planes and the corresponding reactions.

Layer thickness (nm)	Reference (no obstacle) strength τ_o * (GPa)	Stress to approach obstacle, just before reacting (τ/τ_o)	Stress to overcome first dislocation in the interfacial dislocation dipole (τ/τ_o)	Stress to overcome second dislocation and completely bypass the dipole (τ/τ_o)
6.4	1.04	1.06	1.10	1.13
12.8	0.57	1.14	1.21	1.51
19.2	0.41	1.20	1.29	1.59
25.6	0.31	1.32	1.45	1.58
51.1	0.16	1.25	1.50	1.66

Strength values are as resolved on the slip system.

Table 2.4a. Strengthening effect of annihilation reactions between a/2[01-1] (111) threading dislocation and a/2[01-1] (-111) interfacial dipole as a function of layer thickness.

Layer thickness (nm)	Reference (no obstacle) strength τ_o * (GPa)	Stress to approach obstacle, just before reacting (τ/τ_o)	Stress to overcome the interfacial dislocation by inducing annihilation reaction (τ/τ_o)	Stress to completely bypass the dipole and resume threading (τ/τ_o)
6.4	1.04	1.04	1.06	1.26
12.8	0.57	1.11	1.15	1.29
19.2	0.41	1.05	1.10	1.29
25.6	0.31	1.05	1.19	1.58
51.1	0.16	1.28	1.35	1.48

Strength values are as resolved on the slip system.

Table 2.4b. Strengthening effect of annihilation reactions between a/2[01-1] (111) threading dislocation and single a/2[01-1] (-111) single interfacial dislocation as a function of layer thickness.

Chapter Three: Interactions between glide dislocations and parallel interfacial dislocations in nanoscale strained layers

F. Akasheh*, H. M. Zbib*, J. P. Hirth**, R. G. Hoagland**, and A. Misra**
*School of Mechanical and Materials Engineering, Washington State University, Pullman, WA
** MST Division, Los Alamos National Laboratory, Los Alamos, NM

Abstract

Plastic deformation in nanoscale multilayered structures is thought to proceed by the successive propagation of single dislocation piles ups at the interfaces. Based on this view, we simulate the effect of pre-deposited interfacial dislocation on the stress (channeling stress) needed to propagate a new loop parallel to them. Single interfacial dislocations as well as finite parallel arrays are considered in the computation. When the gliding dislocation and the pre-deposited interfacial array have collinear Burgers vectors, the channeling stress increases monotonically as the density of dislocations in the array increases. In the case when their Burgers vectors are inclined at 60^{o}, a regime of perfect plasticity is observed which can be traced back to an instability in the flow stress arising from the interaction between the glide dislocation and a single interfacial dislocation dipole. This interaction leads to a tendency for dislocations of alternating Burgers vectors to propagate during deformation leading to non-uniform arrays. Inclusion of these parallel interactions in the analysis improves the strength predictions as compared with the measured strength of a Cu-Ni multilayered system in the regime where isolated glide dislocation motion controls flow, but does not help to explain the observed strength saturation when the individual layer thickness is in the few nanometer range.

3.1 Introduction

It is well known that the primary plasticity mechanism in nanoscale multilayered structures is the channeling of dislocation loops confined within individual layers resulting in the familiar hairpin dislocation configuration. In contrast to microscale layers, where multiple dislocation pileups at the interfaces are possible, only single dislocations are thought to be present in the case of nanoscale layers. Consequently, deformation under this condition proceeds by the successive propagation of single dislocation loops [76], Figure 1. This unique deformation pattern results in a more uniform dislocation distribution in nanoscale layers, which leads to improved ductility [41, 46, 77] and fatigue resistance [43, 44, 78, 79] because of the suppression of both strain localization and cell structure formation within the layers [80]. Furthermore, multilayered laminates exhibit both ultra high strength, reaching a factor of 1/3 to 1/2 of the theoretical strength of the constituents [40, 56], and morphological stability, even at high temperatures [42], making them uniquely multifunctional materials. Nevertheless, many aspects of deformation in these structures are not well understood. The nature of dislocation mechanisms and their interactions among each other and with interfaces, including nucleation, recovery, and interface crossing are not clear, let alone their implications to the overall strength and work hardening. A full understanding of the observed dependence of strength on individual layer thickness, particularly the saturation of the strengthening at thicknesses of few nanometers, remains elusive. In a previous article [81], we employed dislocation dynamics (DD) analysis to investigate how interactions between channeling dislocations and orthogonal pre-deposited interfacial dislocations affect the strength and dislocation structure in nanoscale multilayers. Here,

we examine the effect of pre-deposited parallel dislocations on the strength and the nature of dislocation evolution in nanoscale multilayers.

The framework for the calculation of the channeling stress of an isolated loop was presented by Matthews *et al*. [49, 54]. Their main interest was in the determination of the critical film thickness below which an epilayer is coherent with its substrate with no dislocation generation. The same analysis can be used to calculate the critical stress required to propagate a dislocation for a given layer thickness. The underlying concept involves the balance between the force from the applied stress, tending to propagate a threading dislocation along its glide plane, Figure 1, and the impeding forces arising from the line tension of the newly created dislocation and from lattice friction. This results in the $ln(h)/h$ dependence of the channeling stress on the layer thickness, h, better known as Orowan strengthening. An essentially equivalent energy argument leading to the same result has also been employed by several researchers [48, 51, 52]. The energy approach, nevertheless, is more versatile, allowing further refinement of the model. For example, other sources of resistance to dislocation propagation like surface steps [82, 83], interactions with intersecting interfacial dislocations [64, 65], and the effect of square networks of interfacial dislocation arrays [57, 58, 60, 62, 63] can be included readily in the analysis.

The interaction of threading dislocations with parallel pre-deposited interfacial dislocation arrays in strained layers was studied by several authors. In a two-dimensional setup, Weihnacht and Bruckner [84] used a force balance to estimate the critical stress required to propagate the gliding trailing arm of a threading dislocation to a film-substrate interface in the presence of several film-substrate pre-deposited parallel

dislocations. However, their model consisted of infinite dislocations in a two-dimensional arrangement and included only the segment of the threading dislocation parallel to the array. They showed that the critical stress increases linearly with the inverse of spacing. Furthermore, this slope is steeper when all dislocations in the array have the same Burgers vector as that of the threader, as compared to the case when they alternate between that Burgers vector and the other Burgers vector on the same slip plane inclined at 60^{o}. Pant et al. [68] used DD analysis to show that the glide of a threading dislocation parallel to a single pre-existing interfacial dislocation leads to hardening that increases as the spacing between the two dislocation decreases. Using an energetic approach, Embury and Hirth [76] calculated the stress needed to propagate a threading dislocation in an embedded layer having an infinite uniform array of interfacial dislocations. The authors showed that the channeling stress is inversely proportional to layer thickness h, compared to $ln(h)/h$ in the case of isolated threading. Following the analysis of Embury and Hirth [76], Kreidler and Anderson [85] analyzed the difference between "shear" and "stretch" channeling loops in single and multiple layers. They found that at large plastic strains, the behavior is significantly different in the two cases. In the shear case, strain softening was observed in the single embedded layer case but not in the multilayer case. In an extension to the later work, Anderson and Kriedler [86] studied the properties of channeling stress in close connection to the view that deformation in nanoscale layers proceeds by the successive propagation of single-loop pileups. For an existing array with uniform spacing λ, they calculated the stress needed to propagate the first loop to halve a pair in the array and the last loop to complete the array starting from one with 2λ spacing. In the shear case, the softening effect is manifested in the possibility of an avalanche of such

halving loops in the course of completion of the uniform array. Following a similar energetic approach as in [58, 76], Misra *et al*. [56] developed a more comprehensive model to predict the strength of multilayered metallic structures. The model assumes that macroscopic yield occurs when layer-confined single dislocation loops overcome the resistance to interface crossing offered by the stress field of the interfacial dislocation arrays. It also accounts for the residual coherency stress in the case of semicoherent multilayer systems and provides a good match to the measured strength of Cu-Ni multilayers. Also Atkinson and Jain [61, 62] presented an energetic approach where the layer energy is calculated by the explicit calculation of the interaction energy between the dislocations in the array as they are successively introduced into the system at random locations.

In the spirit of [56, 76, 85, 86], we employ an energetic approach in a three-dimensional arrangement to study the characteristics of the interaction between a threading dislocation and finite arrays of parallel interfacial dislocations in FCC strained layers. The actual mixed character of the interacting dislocations is considered without distinction of the stretch and shear contributions to the interactions [85, 86]. Also, the effect of the relative orientation of the Burgers vectors of the interacting dislocations on the strength and nature of evolution of dislocation structure is explored. In agreement with the theories and experimental observations regarding the early stages of deformation in nanoscale layers [49, 54, 76, 87, 88], see also Figure 1, we assume that the interfacial dislocations consist of dipoles, each representing the trailing "arms" deposited at the interfaces during a previous threading event. They are located at the intersection of {111} glide planes and the layer interfaces and are perfect glide dislocations.

3.2 Problem setup and method

Figure 2a shows the problem setup. A strained layer of thickness *h* having an FCC structure is bound by two impenetrable walls but otherwise lies in an infinite homogenous elastic medium. The x, y, and z- axes coincide with the $[10\bar{1}]$, $[101]$, and $[0\bar{1}0]$ crystallographic directions, respectively, with the interface normal parallel to the z-axis. This {100} interface orientation is common in epitaxial multilayered coherent FCC-FCC systems and is referred to as the cube-on-cube orientation. The multilayered Cu-Ni system is an example of such systems and is used a basis of comparison with the modeling results. Threading dislocations successively propagate parallel to each other on the $(\bar{1}\,\bar{1}\,1)$ slip plane in the y-direction under the effect of some applied load the same direction. A given dislocation will only propagate if it has either the $a/2[1\bar{1}0]$ or the $a/2[0\bar{1}\,\bar{1}]$ Burgers vector, which are inclined at 60^o to each other. A dislocation exhibiting the other possible Burgers vector on the same plane, $a/2[101]$, would not move under the described loading. The question is how a finite array of "long" pre-deposited parallel dislocation dipoles affect the stress needed to propagate the next fresh threading dislocation

An energetic approach based on the complete account of the mutual interactions between all dislocation segments is used to estimate the channeling stress. The model has been previously detailed in [81]. The initial configuration consists of a threading dislocation segment, having a Burgers vector $\boldsymbol{b}_{threader} = a/2[0\bar{1}\,\bar{1}]$ and extending between the layer walls along the glide plane. The length of this segment is extended in both directions by a semi-infinite segment to ensure dislocation continuity, Figure 2b. Also

included in the initial configuration is an array of infinitely long pre-deposited interfacial dipoles of Burgers vector $\boldsymbol{b}_{array}$, which can have one of the two possible Burgers vector on the plane mentioned above, Figure 2a. Under the effect of the layer strain, the portion of the threading dislocation in the layer starts to bow out as shown. The change of the energy of the system in the new configuration, $\boldsymbol{\Delta W}$, is evaluated as a function of the threading length, l_{th}. The expressions for the self energies of individual segments and the interaction energies between different segments can be found in reference [89]. For a certain layer thickness h, the applied resolved stress τ at which the threading dislocation becomes unstable can be determined from the minimization of the Gibbs free energy $\Delta G = \Delta W - \tau\, b\, \eta l_{th}$ along with the stability condition, $\frac{\partial^2 \Delta G}{\partial l_{th}^{\,2}} = 0$ .The energy is monitored as the system evolves to the unstable configuration.

3.3 Results and discussion

Typically, the estimation of the channeling stress in strained layers has been restricted to infinite arrays of interfacial dislocations with the threader and the array having the same Burgers vector. As a starting point, we revisit the same problem using our model along with more realistic dislocation arrangements in agreement with the physical view of how dislocations evolve in the early stages of deformation of nanoscale layers. We assume that plastic deformation has uniformly proceeded to a configuration where the dislocation spacing in the array is λ, and estimate the stress needed to propagate the next threading dislocation expected to occur at a position half way between neighboring dipoles, Figure 3. Thereafter, deformation proceeds at stress increments

corresponding to the successive introduction of threaders each halving the λ spaced dipoles finally arriving at a uniform array of spacing $\lambda/2$.

Figure 4 shows the convergence behavior of the calculated channeling stress as the breadth B of the array increases for a layer thickness h of $25b$, where b is the magnitude of the Burgers vector. The case where both the threader and the array have the same Burgers vector is shown in Figure 4a, while Figure 4b shows the corresponding result when they are inclined at 60^o. The stress is normalized by the saturation stress arrived at when B becomes sufficiently large so that the influence of any additional dislocations on the threading stress is negligible. This value is largest for the denser arrays and is approximately $300h$. The observation that the denser array case converges to the infinite array case slowly was also made by Atkinson and Jain [61, 62] in their calculations for the energy of strained layers with misfit dislocations of the same Burgers vector. The convergence characteristics are the same for the collinear and inclined Burgers vector cases although the convergence is faster in the collinear case for denser arrays. The difference in convergence rate vanishes for arrays of spacing $2h$ and larger.

Figure 5 shows the hardening effect caused by an infinite array (*i.e.* with B large enough to ensure saturation) of parallel interfacial dislocations of spacing λ and Burgers vector collinear with that of the threading dislocation. The spacing is normalized by the layer thickness. The hardening is associated with the increased energy of the system due to the introduction of new segments of dislocation lines whose net interaction energy is positive. To explore the scaling characteristics, the channeling stress τ (resolved stress) in Figure 5b is normalized by $\tau_o=\tau_o(h)$, the channeling stress of a single isolated threader for the same layer thickness. Figure 6 shows the actual values of τ_o as calculated using our

model for Cu with shear modulus of 38.46 GPa. Figure 5 demonstrates that interfacial dislocations can severely impede the glide of dislocation loops parallel to them and that this effect increases rapidly when the spacing of interfacial dislocations is less than two times the layer thickness. The other important observation is that the channeling stress does not scale with the layer thickness. This can be explained by the fact that, for a given layer thickness, the current configuration energy is a function of the threading length l_{th}, Figure 2b. The interaction energies among the leading segment and trailing arms and among both of them and the parallel dislocations do not scale with h. The scaling with the thickness would be true, however, in the case for the simple line tension model, that has no dependence on the threading length. The fact that the channeling stress is large for the smaller thicknesses is physically sensible as one expects that more work is needed to cause the threading segment to break away from the stronger interactions which hold it back when the thickness is smaller. DD calculations, e.g. [66], which are based on the explicit calculation of the Peach-Koehler force from the stress field of dislocations also support this result [81].

Similar to Figure 5, Figure 7 shows the dependence of the channeling stress on the spacing λ of the infinite array when the Burgers vectors of the threader and the array dipoles are inclined at 60^o to each other, Figure 2a. Two major differences can be deduced from a comparison with the collinear results in Figure 5. First, the stress needed to propagate the threader is much smaller in the case of inclined Burgers vectors than that for the collinear case, particularly when the array spacing is less than two times the layer thickness; there is almost a factor of two difference between the two cases. This can be easily understood since, although the edge components of the threader and array are the

same in both cases, yet the screw components are antiparallel in the inclined case while parallel in the collinear case. The attractive interaction between the screw components in the inclined case reduces the stress required to propagate the threader. The second notable difference is that the stress is almost constant in the range $2 < \lambda/h < 4$. This implies that, in the stage of plastic deformation corresponding to this range of array spacing, there would be an avalanche of dislocation motion that does not require any additional loading. This is effectively a form of unstable deformation.

To examine the origin of this behavior, we consider the simple system consisting of a threader and a single dislocation dipole separated by a distance *l*. The result is shown in Figures 8a and 8b for the two extreme layer thickness considered in this work, 25*b* and 200*b*. In both cases the effect of the parallel interfacial dipole on the channeling stress is characteristically different for the collinear and inclined cases. In the inclined case, the system exhibits a distinct unstable regime when $0.5<(l/h)<3$, roughly, where the channeling stress dips. This behavior can have important implications on the evolution of the dislocation structure. Since deformation in nanoscale strained layered proceeds by the successive propagation of single dislocation loops, once a dislocation of a certain Burgers vector has propagated, then it would be easiest for a dislocation having the 60^{o}-inclined Burgers vector to be the next one to propagate in the vicinity of the first glide event. One would then expect that deformation proceeds by the successive propagation of loops of alternating Burgers vectors. This expectation is not precise because it ignores the effect other neighboring interfacial dislocations have on the threader-single interfacial dipole interaction characteristics. Other relevant considerations include the probability of existence of the right dislocation (easiest to propagate) at the right location and the other

stochastic aspects of dislocation motion. Furthermore, in a real system, dislocations from different planes and/or layers can intersect at the layer interfaces and react to produce dislocations of different Burgers vector or annihilate, all of which complicate the simplified picture depicted above regarding the nature of evolution of dislocation structure. Nonetheless, the present result suggests that during plastic deformation a dislocation array with non-uniform spacing is more likely to evolve than a uniform one.

Another relevant conclusion regarding how close interfacial dislocations can come to each other may be made form Figure 8, for the isolated case, and from Figures 5a and 7a for the case where large arrays are present. Dislocations can be more closely spaced in thicker layers, also supported by experimental observations [90]. Furthermore, the minimum spacing between dislocations increases when there are other dislocations in the interface. Such a conclusion has implications to the type and potential for short-range interactions between interfacial dislocations. Such interaction have been hypothesized to occur and to be significant in influencing the overall deformation characteristics in nanoscale multilayers [80, 91]. More detailed examination of these issues is needed.

In Figure 9, we plot the stress normalized by the shear modulus μ of the material (here Cu with μ=38.46 GPa and b=2.556A^{o}) against the inverse of the spacing normalized by the Burgers vector magnitude d/b. The plot clearly shows the characteristics of the hardening behavior. The hardening is linear only at small spacing corresponding to large inelastic strains, *i.e.*, in the later stages of deformation. A similar observation was also made by Weihnacht and Bruckner [84] in their analysis of parallel interaction at film-substrate interface. However, their result does not show the divergence from nonlinearity in the early stage of deformation. In this stage when dislocation loops

are being propagated successively at large separations, the hardening is nonlinear as can be deduced from Figure 9.

Figure 10 summarizes the effect of parallel dislocation interactions on the channeling stress for both the collinear and inclined Burgers vectors cases. In both cases, parallel interactions can lead to either hardening or softening depending on the relative orientation of the Burgers vectors of the threading and the interface dislocations. In all cases the interactions are stronger when the Burgers vector are collinear. For the purpose of qualitative comparisons, Figure 10 also overlays the measured strength of Cu-Ni cube-on-cube with {100} interface multilayered structure [56]. Besides having the same crystallographic orientation as that used in our model, this particular system departs least from our idealized single layer model because the small difference in their elastic properties allows image the effects to be neglected. The comparison suggests that the behavior of a real system can be explained based on parallel interactions over a wide thickness range. Based on the results presented in this paper and from previous work [81] we propose the following constitutive relation for the macroscopic stress σ in nanoscale layers

$$\sigma(h,l) = c_1 \mu \frac{ln(h/b)}{h/b} + c_2 \mu \frac{b}{l}$$

where l is the dislocation spacing in the interface and c_1 and c_2 are constants on the order of 10^{-1} and where c_2 can be positive or negative. The first term on the right hand side of the equation represents a structure-induced layer thickness dependent hardening, while the second is strain hardening which, to a first approximation, is dependent only on the dislocation spacing. The statistical aspects of the dislocation content of the interface and their influence of the stress are all lumped together in c_2. As mentioned before, a more

detailed discussion on such factor has to be made in view of how the dislocation content evolves during the deformation and how the dislocations react at the interfaces.

Of course, the strength saturation effect observed in real multilayered systems in the few nanometer layer thickness regime cannot be explained by either the Orowan model or that including parallel interactions. Other dislocation mechanisms, particularly those involving dislocation-interface interactions, seem to control the behavior in that regime, where atomistic calculations are the most suitable methodology.

3.4 Conclusions

An energetic model based on the explicit determination of self and interaction energies between a threading dislocation and pre-deposited interfacial dislocations was used to study the characteristic of such interactions and their effect on the flow stress in strained nanoscale layers. The findings can be summarized as follows,

- Parallel dislocations interactions are stronger for smaller layer thicknesses.
- Parallel dislocation interactions are stronger when the threading dislocation and the pre-deposited interfacial dislocations have collinear Burgers vectors. This suggests that the successive propagation of loops on non-collinear Burgers vectors would be energetically favored over that of uniform Burgers vector.
- When the threading and array dislocations have inclined Burgers vectors, an unstable deformation regime exists.
- Parallel interactions can lead to either hardening or softening. None of these effects can independently explain the measured dependence of strength on layer thickness in multilayered structures. The statistical aspects of the dislocation

structure evolution during deformation, neglected in this study of regular arrays, needs to be considered.

Acknowledgments

F. Akasheh would like to acknowledge the financial support of Los Alamos National Laboratory- MST division, originally provided by the U.S. DOE, Office of Basic Energy Sciences.

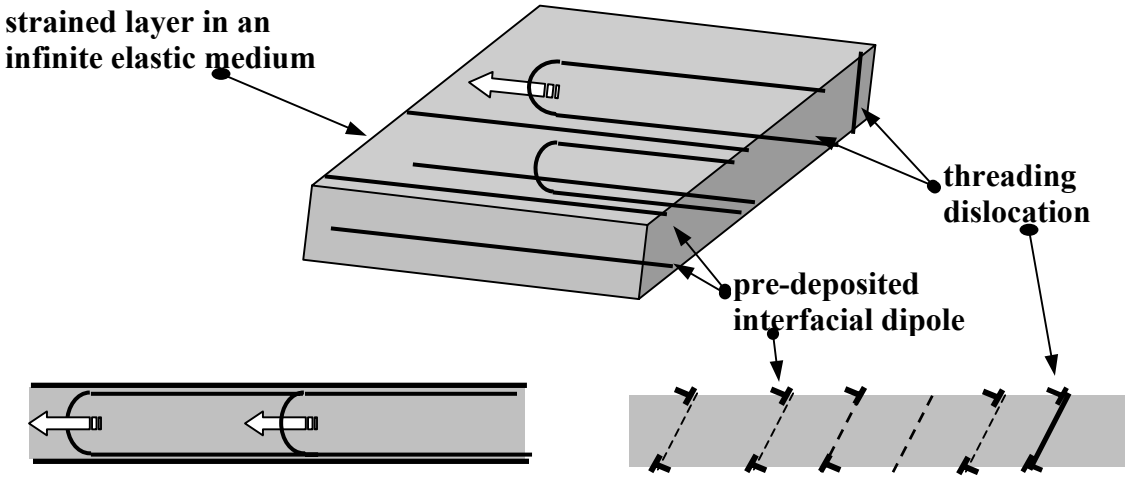

Figure 3.1. Single dislocation pile-ups in an embedded strained nanoscale layer. Deformation proceeds by the successive channeling of threading dislocations confined to the layer resulting in the hairpin configuration. In the process, the trailing "arms" are deposited at the intersection between the layer walls and the slip plane.

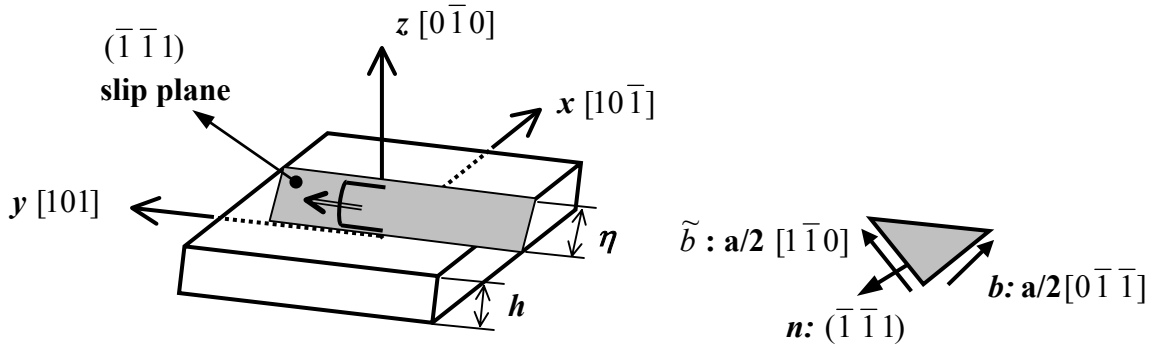

Figure 3.2a. Crystallographic setup of the problem: FCC strain layer in infinite elastic medium with parallel glide occurring on the $(\bar{1}\,\bar{1}\,1)$ slip plane.

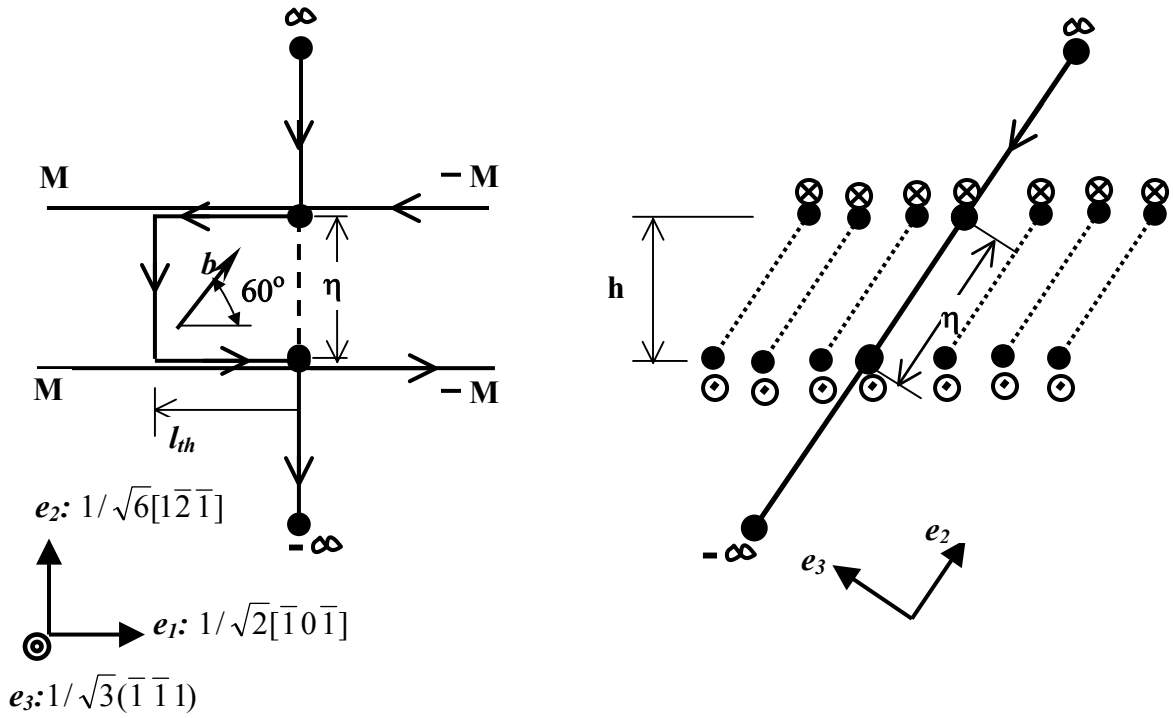

Slip plane view **Slip plane edge-on view**

Figure 3.2b. Elements of the energetic model used to estimate the channeling stress. The pre-deposited array of dipoles is finite and not necessarily.

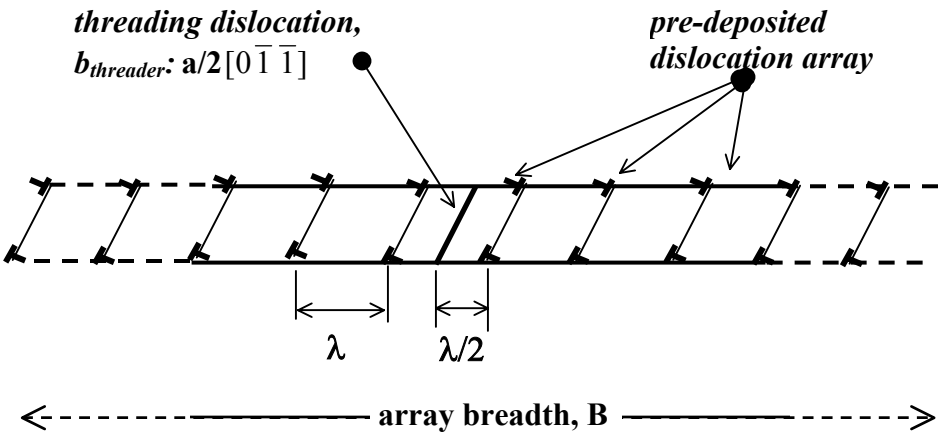

Figure 3.3. Edge-on view of the slip planes, a threading dislocation, and a uniform finite array of pre-deposited dipoles at the layer wall. The threading dislocation about to propagate is the first dislocation to halve the spacing. As the process continues, an array of spacing *λ/2* is generated. In all calculations $b_{threader}$ is fixed as a/2[0 $\bar{1}$ $\bar{1}$], while b_{array} can be $\mp b$ or $\mp \tilde{b}$, Figure 2a.

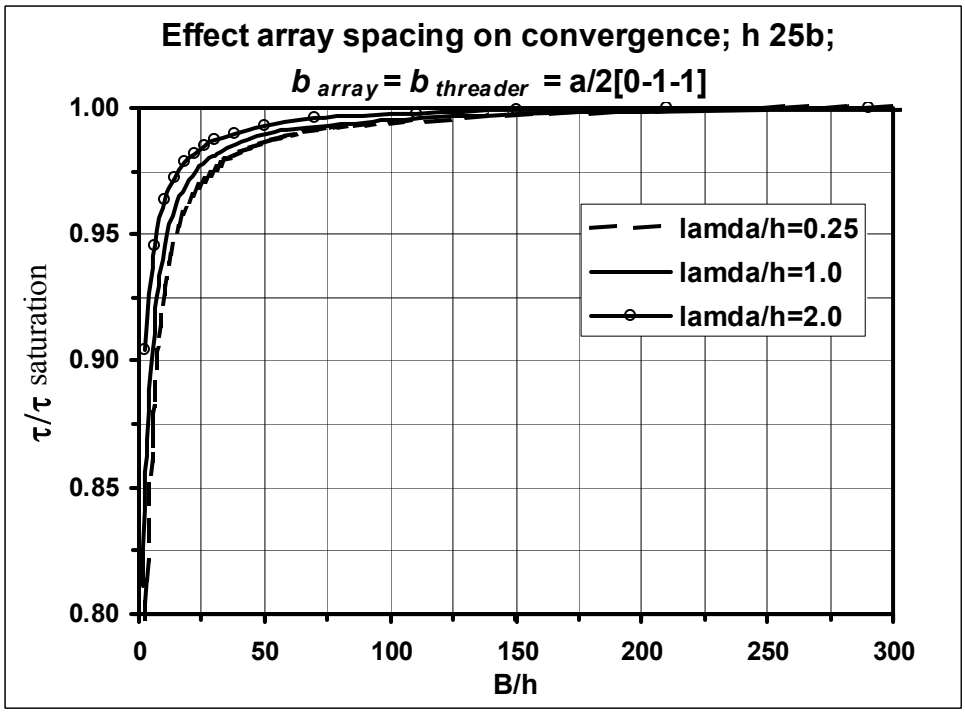

(a)

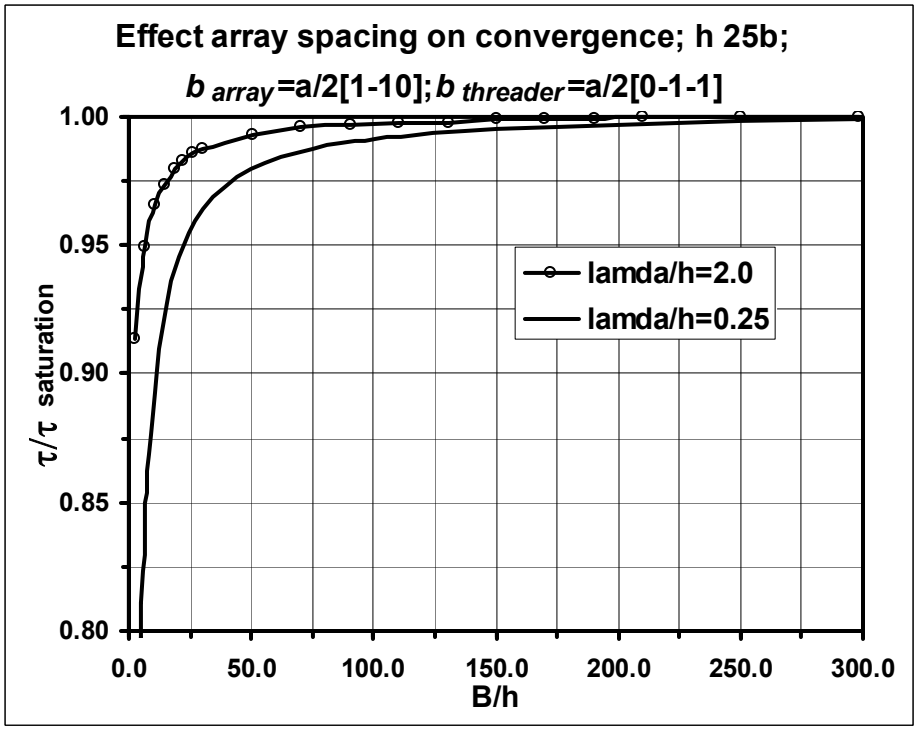

(b)

Figure 3.4, Convergence behavior of the channeling stress for a finite array of interfacial dipoles, (a) threading dislocation and array Burgers vectors both a/2$[0\bar{1}\bar{1}]$, (b) threading dislocation and array Burgers vector inclined at 60^{o}.

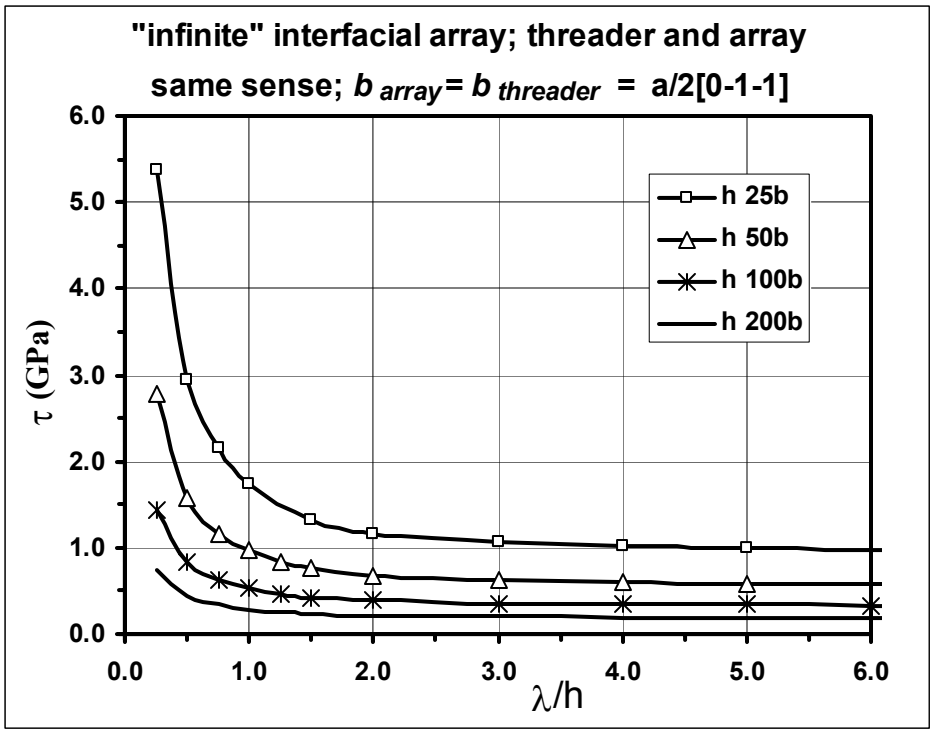

(a)

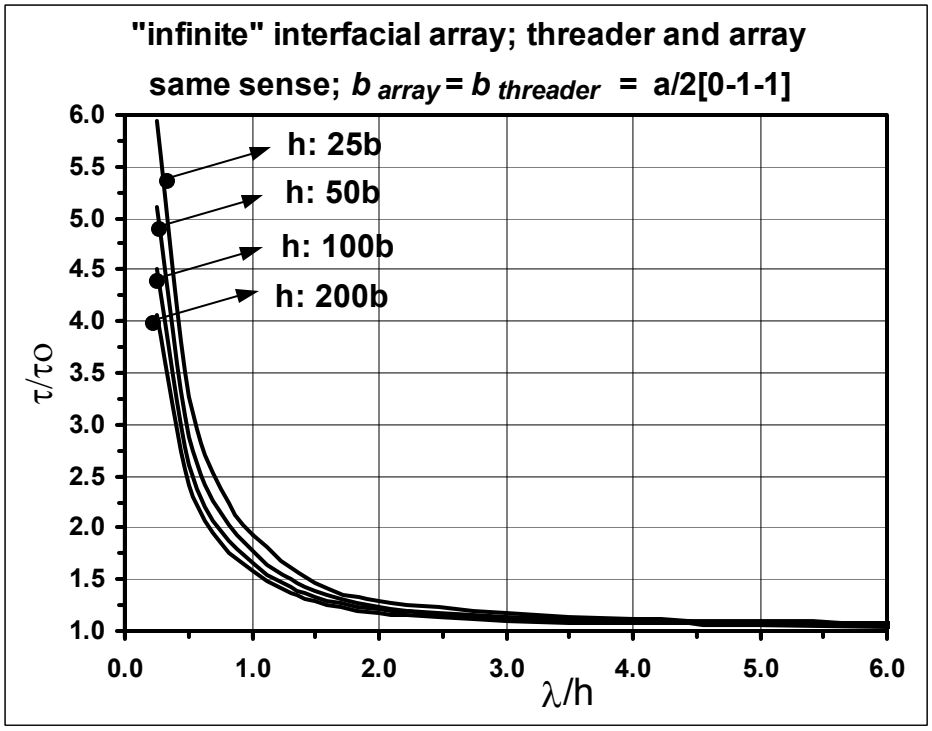

(b)

Figure 3.5, Hardening due to an infinite array of parallel interfacial dislocations with spacing λ and Burgers vector collinear with that of the threading dislocation, (a) absolute resolved shear stress, (b) stress normalized by τ_o, the channeling stress of the isolated threading dislocation $\tau_o(h)$, see Figure6.

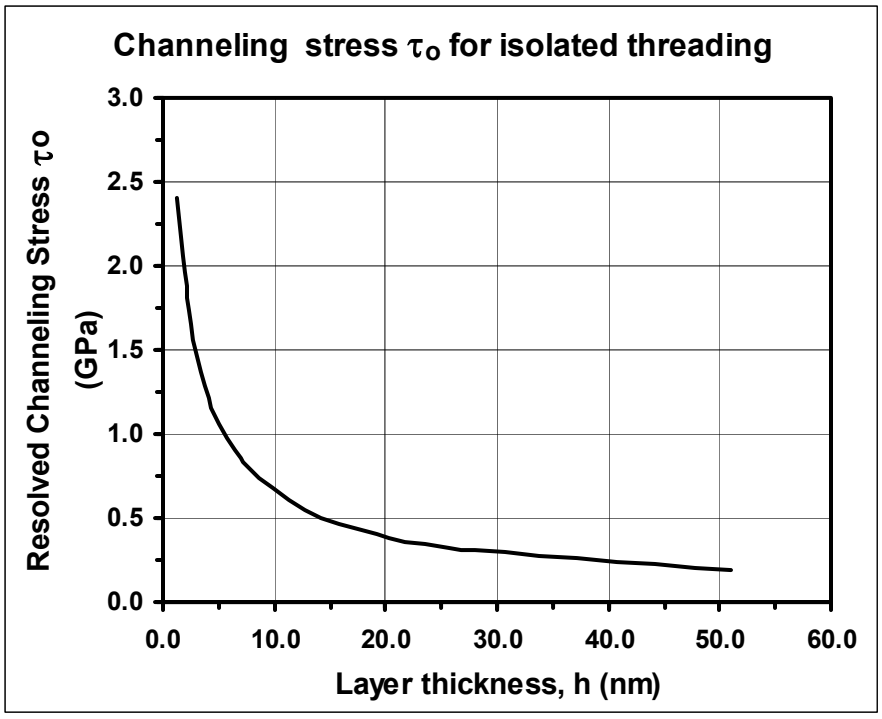

Figure 3.6, Resolved channeling stress τ_o of an isolated threading in a confined layer. The same energetic model based on explicit dislocation interaction energies, Figure 2b, was employed for these estimates.

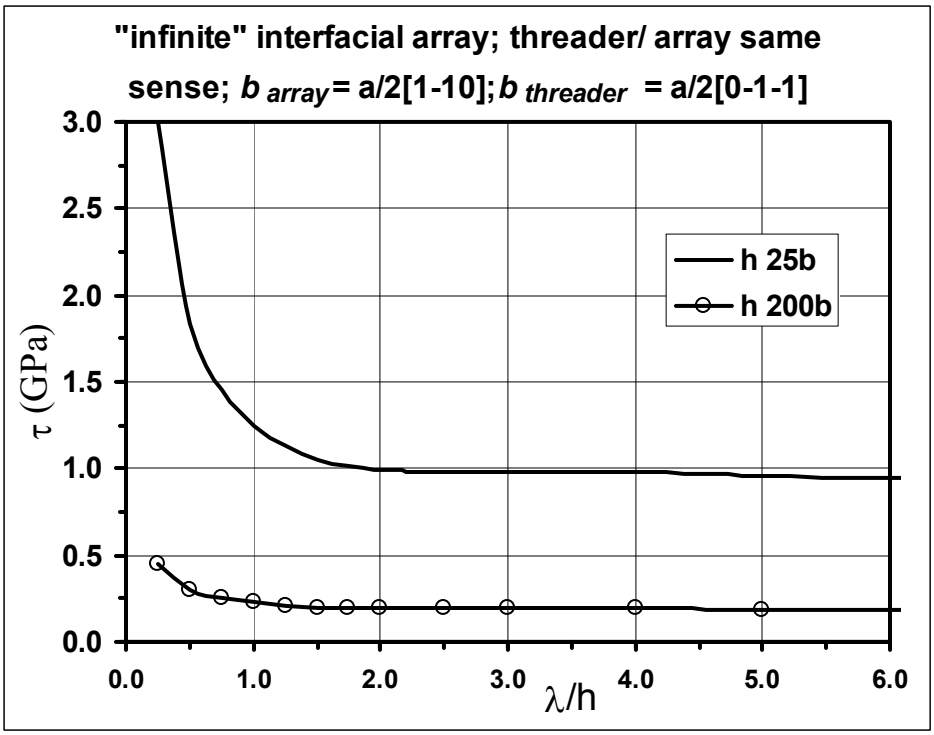

(a)

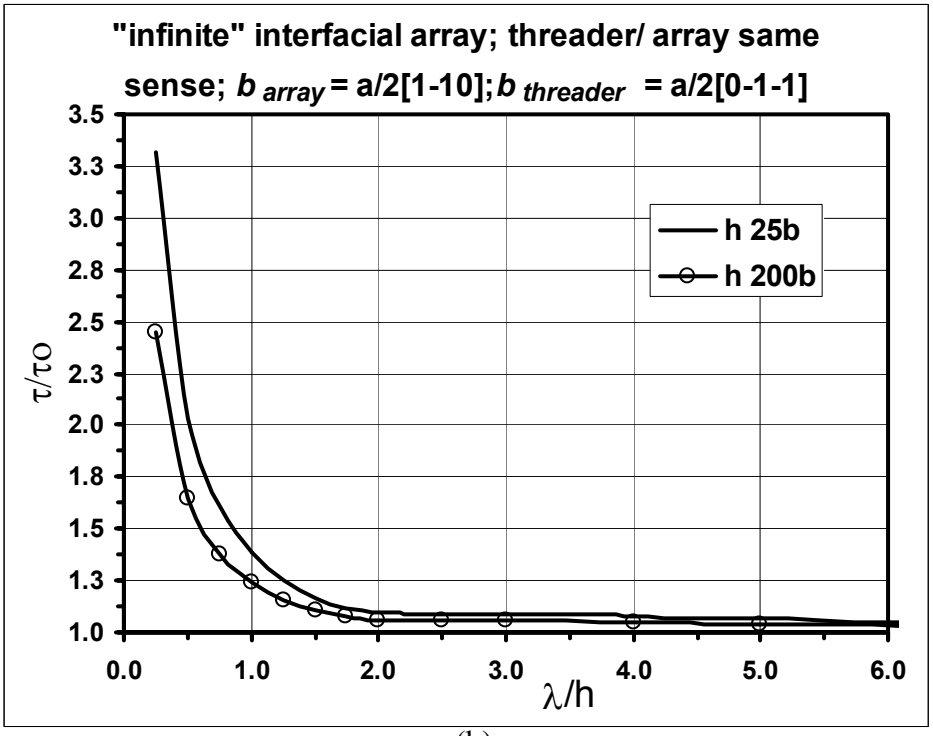

(b)

Figure 3.7, Hardening effect due to an infinite array of parallel interfacial dislocations with spacing λ and Burgers vector inclined at 60° to that of the threading dislocation, (a) absolute resolved shear stress, (b) stress normalized by τ_o, the channeling stress of the isolated threading dislocation $\tau_o(h)$, see Figure 6.

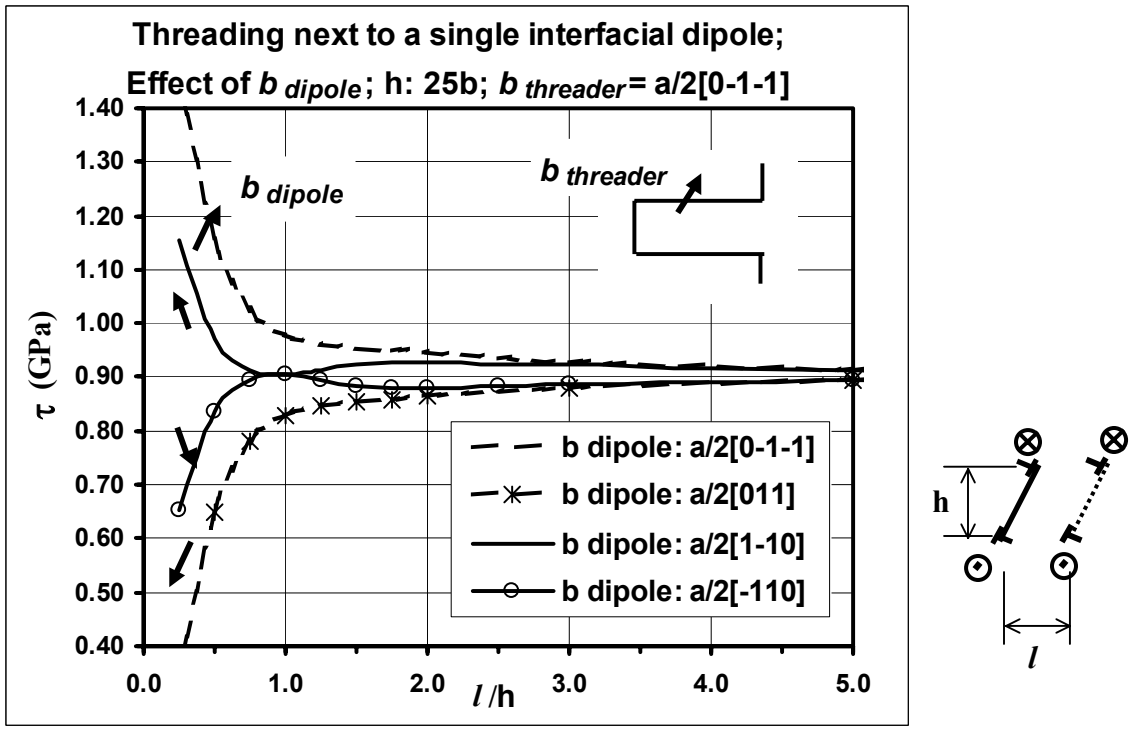

(a)

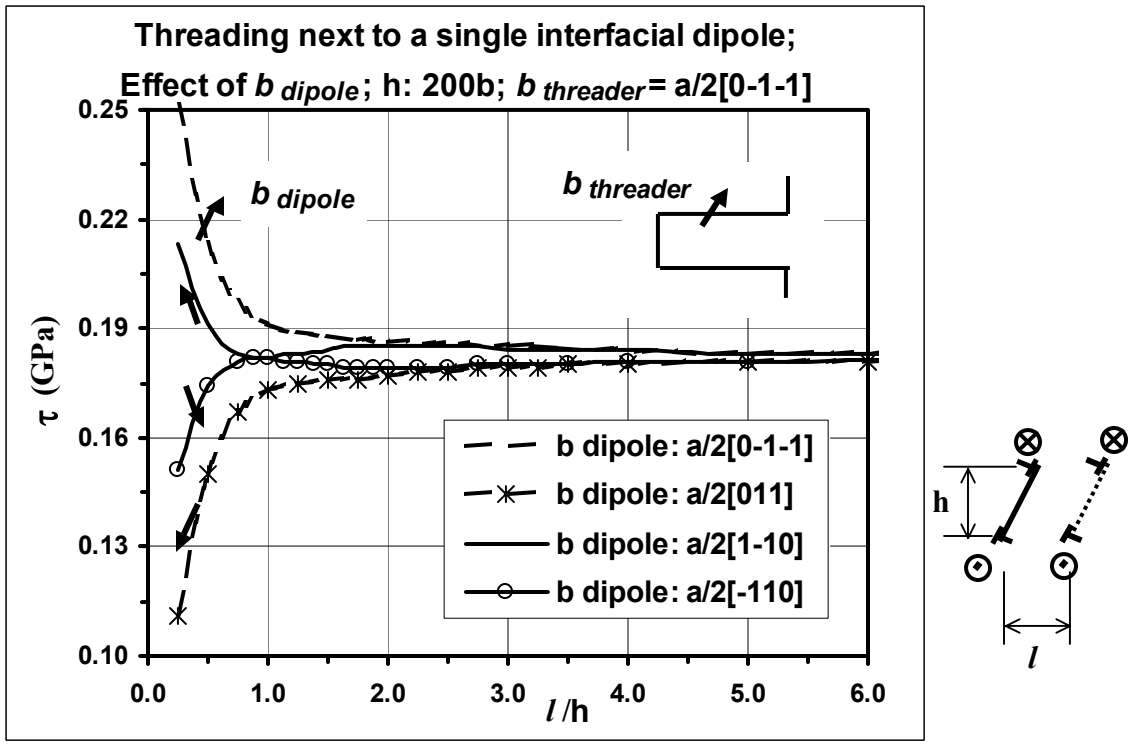

(b)

Figure 3.8, Hardening effect due to a single interfacial dislocation dipole located at distance d from the threading dislocation (a) h 25 b = 6.4nm in Cu (b: magnitude of Burgers vector) thick layer, (b) h= 200 b= 51nm.

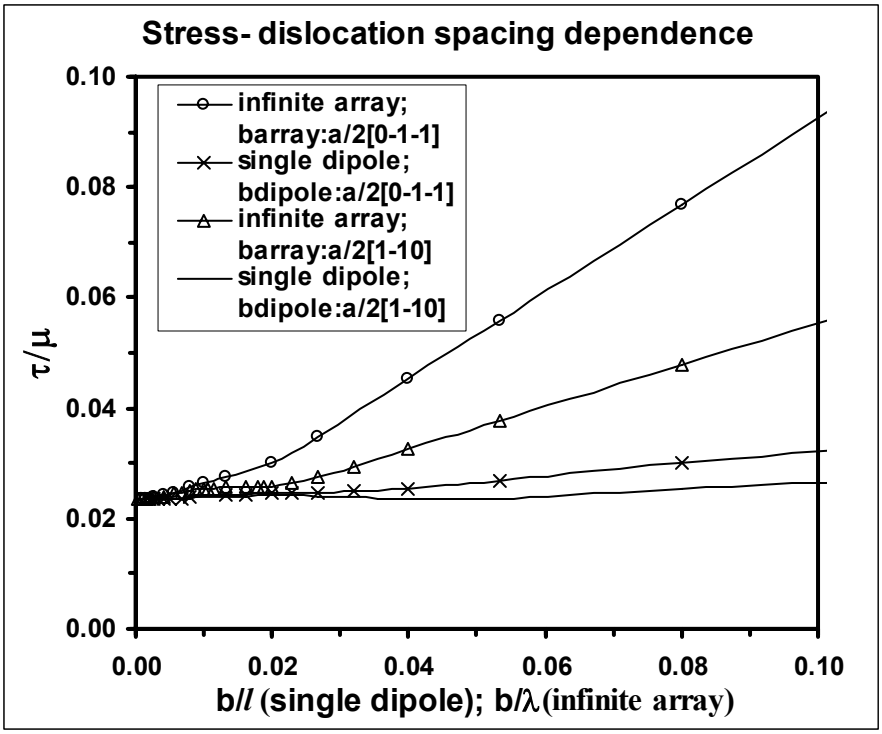

Figure 3.9, Stress strain response due to parallel dislocation interaction. Stress is normalized by the shear modulus μ (here equal to 38.46 GPa for Cu case)

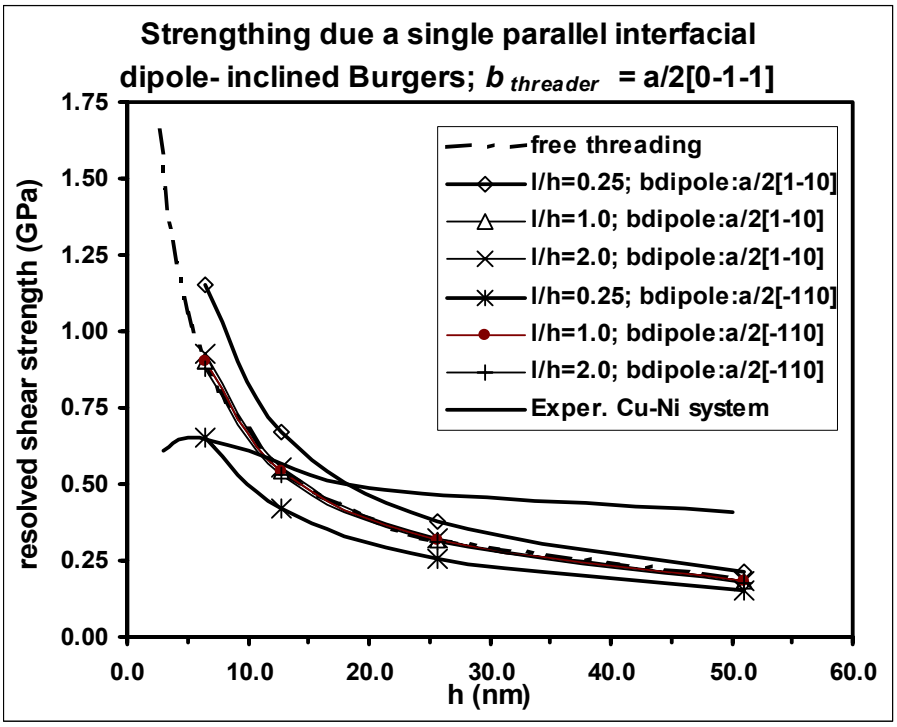

(a)

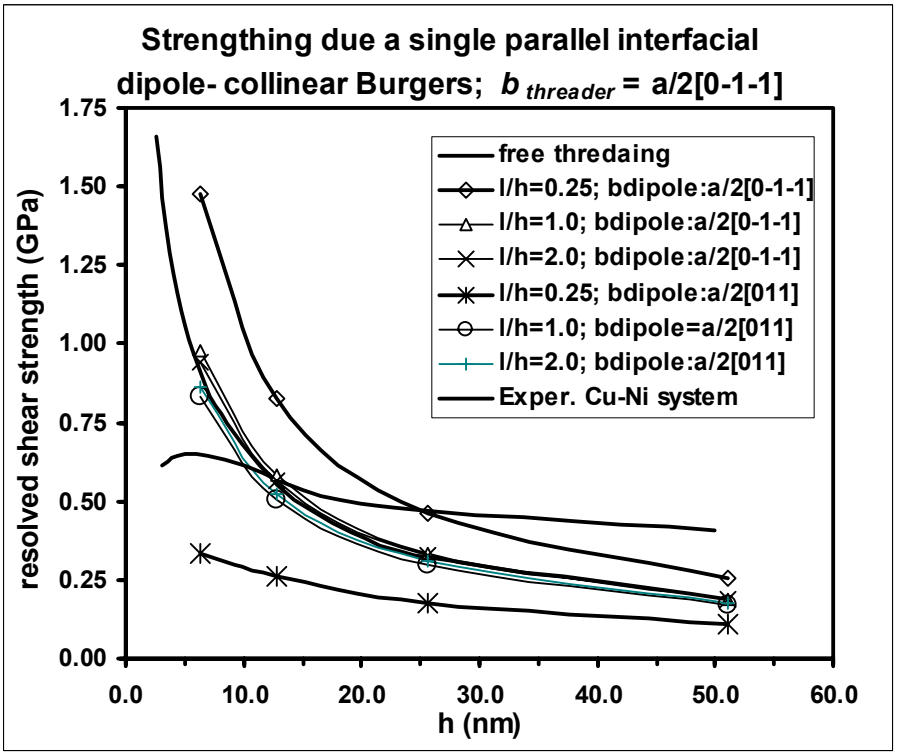

(b)

Figure 3.10. Effect of parallel dislocation interactions on the strength of stained layers as a function of layer thickness *h*, (a) inclined threader/array Burgers vectors, and (b) collinear threader/array Burgers vectors. Measured strength of cube-on-cube (100) Cu/Ni system is overlaid for qualitative comparison.

Chapter Four: Large scale simulations of deformation in nanoscale multilayered metallic (NMM) composites

4.1 Introduction

In a realistic multilayered system, the dislocation density can be on the order of 10^{15} $1/m^2$, which implies that a large number and a wide variety of dislocation interactions and collisions take place simultaneously and in a coupled manner. Besides the interactions between threading dislocations and pre-deposited orthogonal and parallel interfacial dislocations, other essential mechanisms like cross slip and short-range interactions like annihilation, jog, junction, and dipole formation can take place. Furthermore, the net stress field within the layers and at the interfaces will have a complex distribution further complicating the situation. This implies that the behavior of a certain dislocation mechanism when in isolation can be different from that in a realistic system. For example, DD simulations showed that, while in isolation from other dislocations in their vicinity, two threading dislocations gliding in opposite directions on parallel planes can form a dipole and block each other. However, a third threading dislocation approaching this dipole on a close parallel plane can "free" one of the dislocations in the existing dipole and form a new dipole [68]. From the above, it can be concluded that dislocation interactions and how they influence the plastic behavior are practically intractable and attempts to understand the macroscopic behavior of NMM composites based on one or few significant isolated unit dislocation processes may not be sufficient. Indeed this was demonstrated when orthogonal and parallel interactions, potentially thought of as representative of the overall behavior, where studied in Chapters 2 and 3. In both cases, the two mechanisms were able to bridge the gap between the theory and experiment only over certain range of layer thicknesses.

The above complexity of dislocation behavior in NMM composites can be handled using DD analysis. As eluded for in Chapter 1, DD analysis provides a physical framework where the motion and interaction of dislocation populations are explicitly treated. All dislocation interactions, both among themselves and with the complex stress field, are naturally captured and used to evolve the dislocation structure. Besides allowing better predictions for the strength of NMM composites, such simulations can also be valuable in examining the details of dislocation interactions and mechanisms occurring during the deformation. Such "*in-situ*" observations can provide answers regarding the origin of experimentally observed dislocation structures as well as the origin of dislocation multiplication and other macroscopic phenomena like the uniform reduction in reduction in thickness and texture preservation observed during the rolling of NMM composites [41]. Nevertheless, such simulations are computationally expensive and the extraction of information from large output data can be challenging.

Reports on large-scale simulations of nanoscale strained layers are limited in the literature. Schwarz *et al*. [92] used DD analysis to simulate the relaxation of SiGe films using a single layer with impenetrable walls having double the film thickness to approximately account for image effects. They found good agreement with experimental results regarding the residual strain after relaxation and the relaxed dislocation structure. Similar type of analysis was carried out by Schwarz to identify mechanisms for threading dislocation blockage in 2-8 μm thick layers [93]. It was found that local hardening interactions like jog, junction, and dipole formation played a significant role in limiting the extent of relaxation. It was also found that local over-relaxation is equally significant in impeding relaxation in strained layers and can help understand the discrepancy

between experimental observations and theory regarding the degree of relaxation of strained layers.

In this work, our primary objective is to predict the strength of NMM composites as a function of their individual layer thickness. The validity of such simulations rests on the proper choice of initial dislocation structure and the method used to generate it. In the next section, we layout the methodology used to obtain such initial dislocation structure and their subsequent loading. Then we present the problem setup followed by the results and their discussion and conclude with a summary.

4.2 Method and approach

As mentioned in Chapter 1, DD analysis is currently the only framework available to study the behavior of large systems of dislocation explicitly at the fundamental level. Here, we will employ DD to study the collective behavior of dislocation systems in NMM composites. An essential requirement for valid simulations is an initial dislocation structure which is representative of that in the real composite system. NMM composites are typically produced by vapor deposition and the origin of dislocations is believed to be threading dislocations. Threading dislocations are nucleated during the deposition process at random locations due to faults in atomic arrangement, see Section 2.1. In the case of *coherent* NMM composites, which is the focus of this study, the alternating layers experience tensile/compressive stresses due to the lattice parameter mismatch. This implies that a threading dislocation extending through the layers will glide in opposite directions in the alternating layers. This process is commonly known as the relaxation process because the glide of dislocation is driven by the minimization of the total energy of the system. When the stored elastic energy (from coherency strain) becomes high, it

becomes favorable to replace the strained structure with a dislocated structure of lower total energy. Thus, in obtaining the initial dislocation structure for our DD simulations, we mimic this process by first performing a "relaxation" simulation where random distributions of threading dislocations is subjected to the appropriate coherency stresses and allowed to move and interact until the process naturally ceases. This implies that a dislocation structure has resulted which is in equilibrium with the net stress field from coherency and the generated dislocation network. This relaxed configuration now serves as the initial configuration for the "loading" phase simulation. In this phase, the structure is loaded under constant strain rate conditions and the yield strength obtained.

4.3 Problem setup

Figure 4.1 shows the simulation setup. A representative volume element (*RVE*) consisting of four layers, each of thickness *h* and representing two sets of the periodic bimetal layered structure, is used. The two metals are assumed to have the same elastic properties and crystal structure but to differ in the lattice parameter. This mismatch results in the layers being subjected to tension/compression alternating biaxial stress state, which drives the dislocation threading process if *h* is larger than a certain critical thickness. In the case of Cu/Ni bimetal system, such stress amounts to 2.6 GPa [94]. The properties of the medium are those of copper with shear modulus of 38.46 GPa, Poisson's ratio of 0.3, density of 8980 Kg/m3, and Burgers vector magnitude of 2.556 A^o. Although this is an idealized model, the small lattice parameter mismatch and mild difference in elastic properties makes the model plausible for qualitative comparison with actual Cu/Ni systems. In such system, slip systems can be considered continuous across the interfaces

and image forces effects can be neglected for a first approximation [76]. Periodic boundary conditions are imposed in all directions. An initial random distribution of glide loops is created which amounts to threading dislocation density on the order of 10^{14} 1/m^2. The average dislocation line segment is 5*b*, where *b* is the magnitude of the Burgers vector. For the loading phase, the same crystallographic setup is used as in the relaxation phase. However, the initial dislocation structure becomes that produced at the end of the relaxation phase. Also the loading is performed through the application of a constant strain biaxial stretching along the *x*- and *y*-directions, as shown. A high strain rate on the order of 10^4 1/s is used to expedite the calculation.

4.4 Results and discussion

4.4.1 Relaxation phase

Figure 4.2 shows the dislocation density history for the relaxation process of a NMM composite with individual layer thickness *h* of 25.6 nm. As can be seen, the dislocation density increases with time as threading dislocations move and, in the process, deposit interfacial dislocation dipoles. The saturation of the density in the figure marks the end of the relaxation process when dislocation activity ceases and an equilibrium structure is arrived at. Figure 4.3 shows the resulting relaxed dislocation structure. As can be seen it consists of an orthogonal network of interfacial dislocations aligned with the loading axes. The side view shows a number of remnant threading dislocations which are blocked, while most of them disappeared due to annihilation events. The blocking can be attributed to the repulsive stress fields of the interfacial dislocation network and/or other threading dislocations acting to oppose the continued

threading process driven by the coherency stress. This final dislocation configuration will be the point of departure of the subsequent loading phase.

4.4.2 Loading phase

The objective of this phase of the simulation is to capture the dependence of the strength of NMM composites on the layer thickness. As concluded in Chapters 2 and 3, strength models individually based on any of the two significant dislocation unit processes, orthogonal and parallel interactions, where not sufficient to explain the observed dependence of strength on layer thickness in a satisfactory way. Figure 4.4 shows an example of an initial relaxed dislocation structure for a loading simulation for the case of 12.8 nm thick NMM composite. For that case, the side view shows that the layers were free from any remnant threading dislocations to act as subsequent multiplication sources. In the early stages of loading, the two layers which were originally under tensile coherency stresses (the top and third-from-top layers, Figure 4.4b) experience increased stress and are under elastic loading conditions due to the absence of dislocation activity. Meanwhile, the loading will act to decrease the residual compressive stresses in the layers originally subjected to compressive coherency stress during the relaxation phase (the second-from-top and bottom layers). This implies that those layers will start to deform plastically before the other two layers. This can be seen in Figure 4.5, which shows higher dislocation activity in the second and forth layers due to the collapse of dislocation loops. The other observation to make from the same figure is that threading dislocations now exist in the other two layers in spite of the fact that they were free of any threading dislocation at the beginning of the simulation. These threaders are the result of different multiplication events that take place at the interfaces. The details of one such event are depicted in Figure 4.6. All the dislocation segments shown

have the same Burgers vector, a/2[011] while their line senses are as shown. Segments FG, FH, ED and CD reside on the lower interface of the layer which was originally under compressive stress, while segment AB is on the upper interface. Apart from segments DE and FG, which lie on the (-11-1) plane, all segments lie on the orthogonally oriented plane (-1-11). As the residual stress in the layer decreases, the threading dislocation BC retracts on its glide plane. The corner point D of the bend acts as a pinning point for further retraction beyond it. Together with the repulsive effect of the segment FG, the retreating loop is forced into the configuration shown in Figure 4.6c, which leads to an annihilation reaction and leaves behind segment DF which has an opposite line sense. This results in this segment gliding into the neighboring elastically loaded layer and acting as a source. The avalanche of dislocation motion and multiplication in all layers marks the yield point of the composite. Figure 4.7 plots the yield strength captured from such simulations as a function of the individual layer thickness. Actual strength measurements of Cu/Ni maultilayered system are overlaid for qualitative comparison. As pointed out earlier, this system comes closest to our idealized model due to the small lattice parameter mismatch and the moderate difference in elastic moduli, making it suitable for comparison. As can be seen from the figure, the predicted strength is in better agreement with the experimentally measured strength particularly in the range of 25 nm and above. This less steep drop in strength as layer thickness increases comes closer to the trend due to the Hall-Petch pile-up strengthening mechanism. In fact, as observed from our simulations, multiple dislocation pileups at the interfaces become increasingly frequent in the case of layers with thickness above 25 nm and maybe one contributor to this better match with the measured strength trend. In the range of 12-25 nm, the strength

predictions of the large simulations are similar to the strength predictions due to unit orthogonal and parallel interactions presented in Chapters 2 and 3, respectively. The reason why the large simulations predict a lower strength in the case of the 6 nm thick layers than does the free threading model of an isolated dislocation lies in the residual stress field due to the dislocation structure which develops at the interface and acts to assist in threading dislocations' glide.

4.4.3 Observations on dislocation structure and mechanisms

Besides the extraction of the macroscopic yield strength of NMM composites, large scale simulations contain a wealth of information about dislocation mechanisms and interactions and the details of how they occur. To the extent that such simulations are realistic, they can be thought of as *in-situ* experiments where dislocation motion and interactions can be observed as they happen. This is important because only hypothesis about dislocation mechanisms in NMM composites can be made based on TEM observations of end- result dislocation structures. A number of important observations were made from our simulations by animating the evolution of the dislocation structure. One example is the case of nucleation from the interface during loading which was described in Section 4.4.2 in connection with Figure 4.6. Another mechanism observed in NMM structures during relaxation is multiplication by cross slip. This mechanism, which was observed in the case of individual layer thickness of 25 nm and above, involves a segment of the threading dislocation (the threading front) cross slipping into the orthogonally intersecting slip plane. This configuration acts as a Frank-Read type source on the new plane. Figure 4.8 shows an interface top view of a sequence of snapshots detailing the process as captured from our DD simulation. The two mechanisms mentioned above are just an example and not meant to be exhaustive. More analysis of

this type can lead to the identification of more important dislocation mechanisms and interactions, which in turn can help better understand and model the macroscopic behavior of NMM composites.

4.5 Conclusion

Large scale DD simulations proved valuable for advancing our understanding of the behavior of NMM composites. The strength predictions of such simulations are in better qualitative agreement with experimental trends and in any case better than unit mechanism predictions. Nevertheless, more work is needed to validate the results by investigating different relaxation models to accomplish the initial dislocations structure used in subsequent loading. The simulations were also valuable in identifying dislocation mechanisms which can take place during the deformation. Two such mechanisms, nucleation from the interfaces and multiplication by cross slip within the layers, were noted but more detailed investigation can lead to the identification of more mechanisms and interactions. The simulations also indicate that multiple dislocation pileups are possible in 25 nm and thicker layer but not in 12 nm and thinner layers.

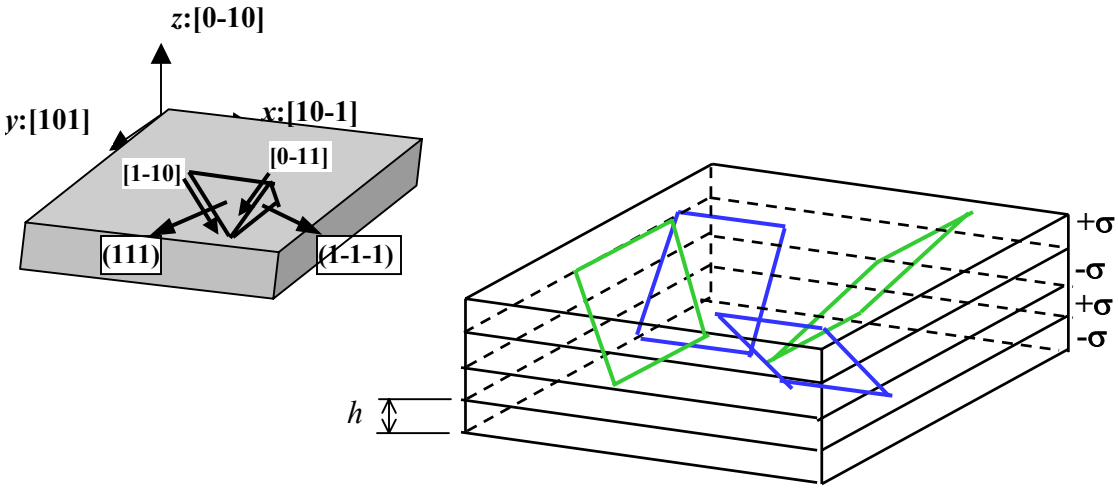

Figure 4.1, Setup for the large simulation of the relaxation process in NMM composites

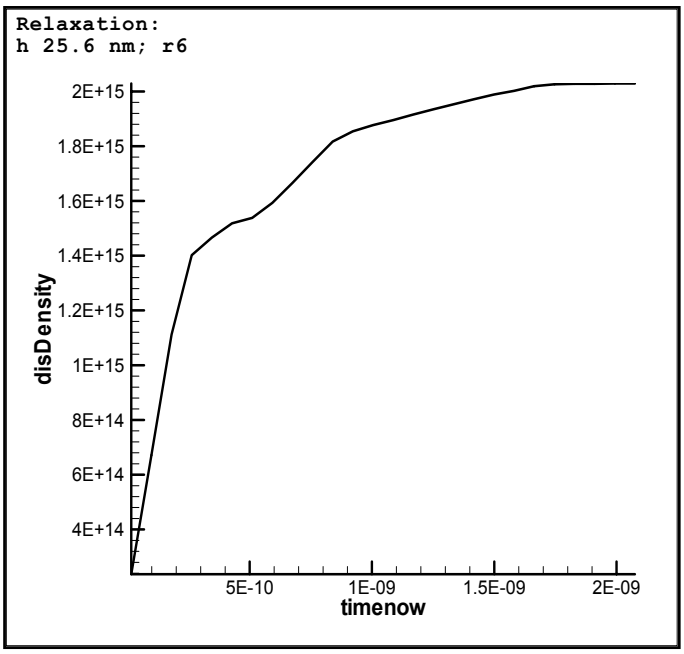

Figure 4.2, Dislocation density history during the relaxation phase of a NMM composite with individual layer thickness of 25.6 nm.

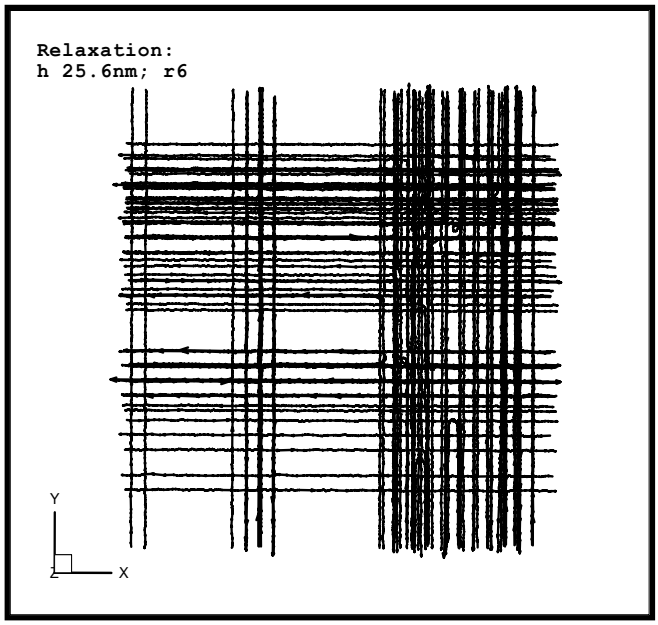

(a)

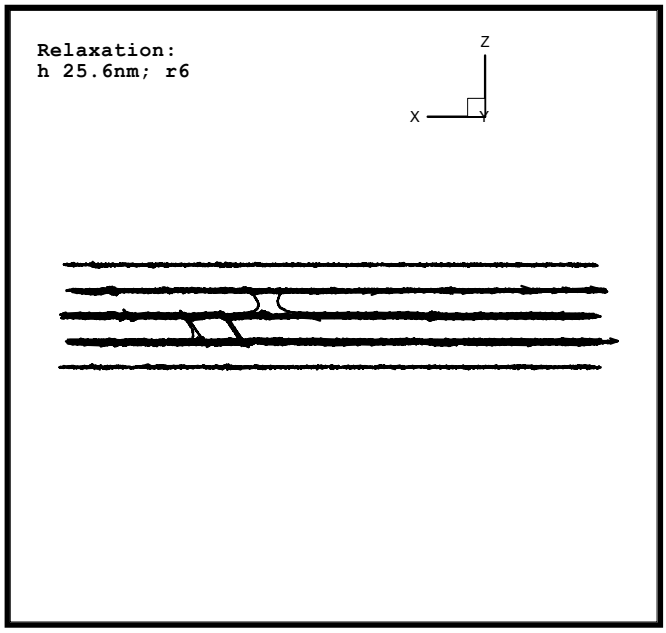

(b)

Figure 4.3, Relaxed structure of a NMM composite with individual layer thickness of 25.6 nm, (a) view normal to the interface, and (b) side view.

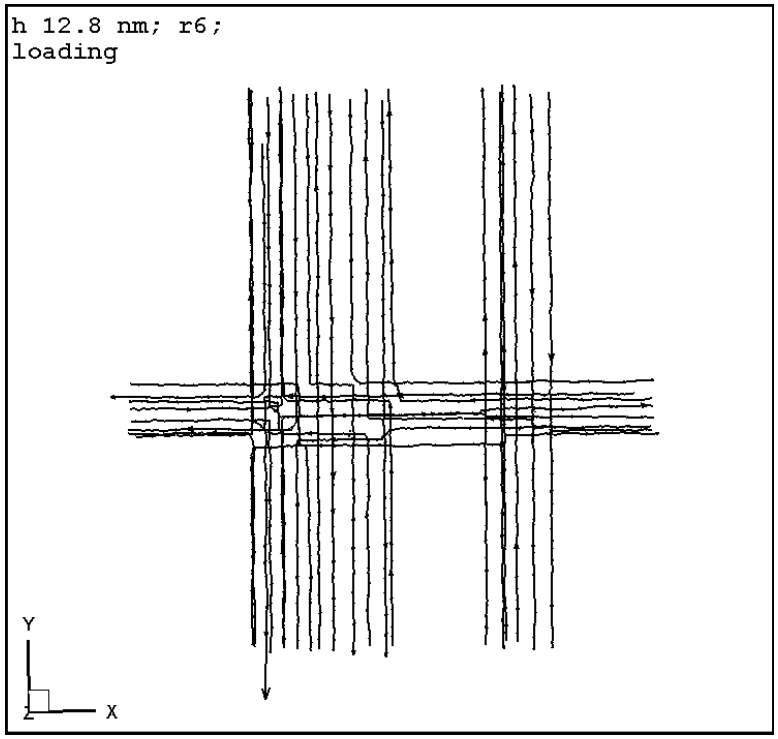

(a)

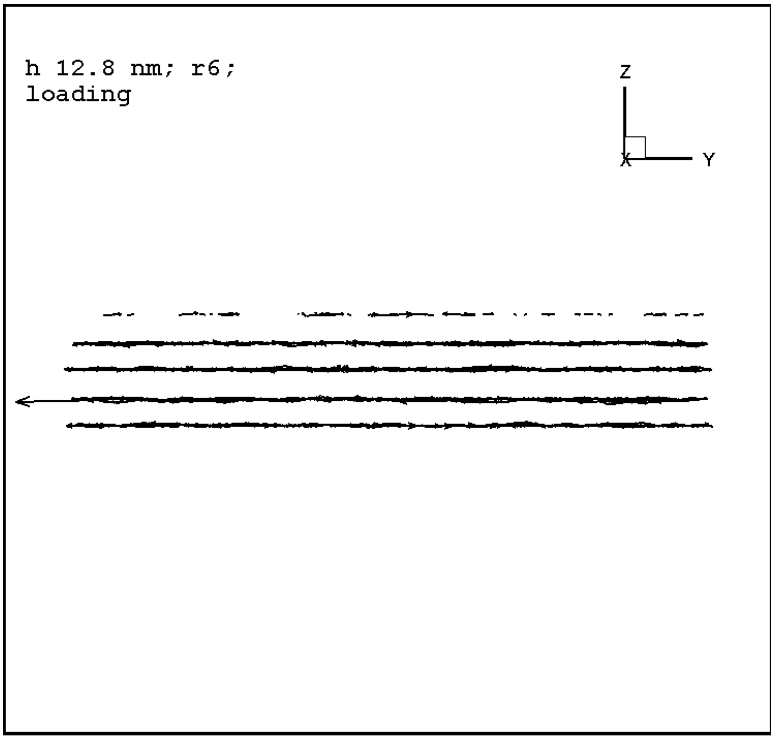

(b)

Figure 4.4 Initial (as-relaxed) dislocation structure of an NMM composite having 12.8 nm individual layer thickness, (a) interface view, (b) side view.

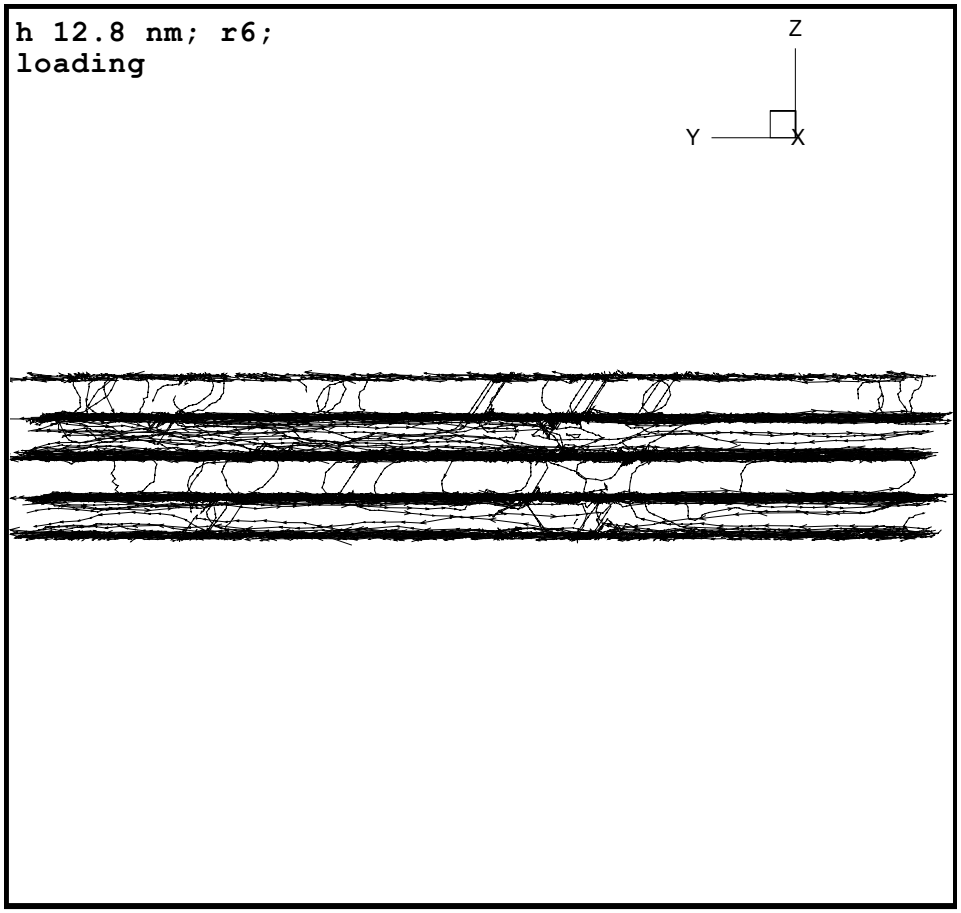

Figure 4.5 side view snapshot of the dislocation structure during loading for the same case shown in Figure 4.4.

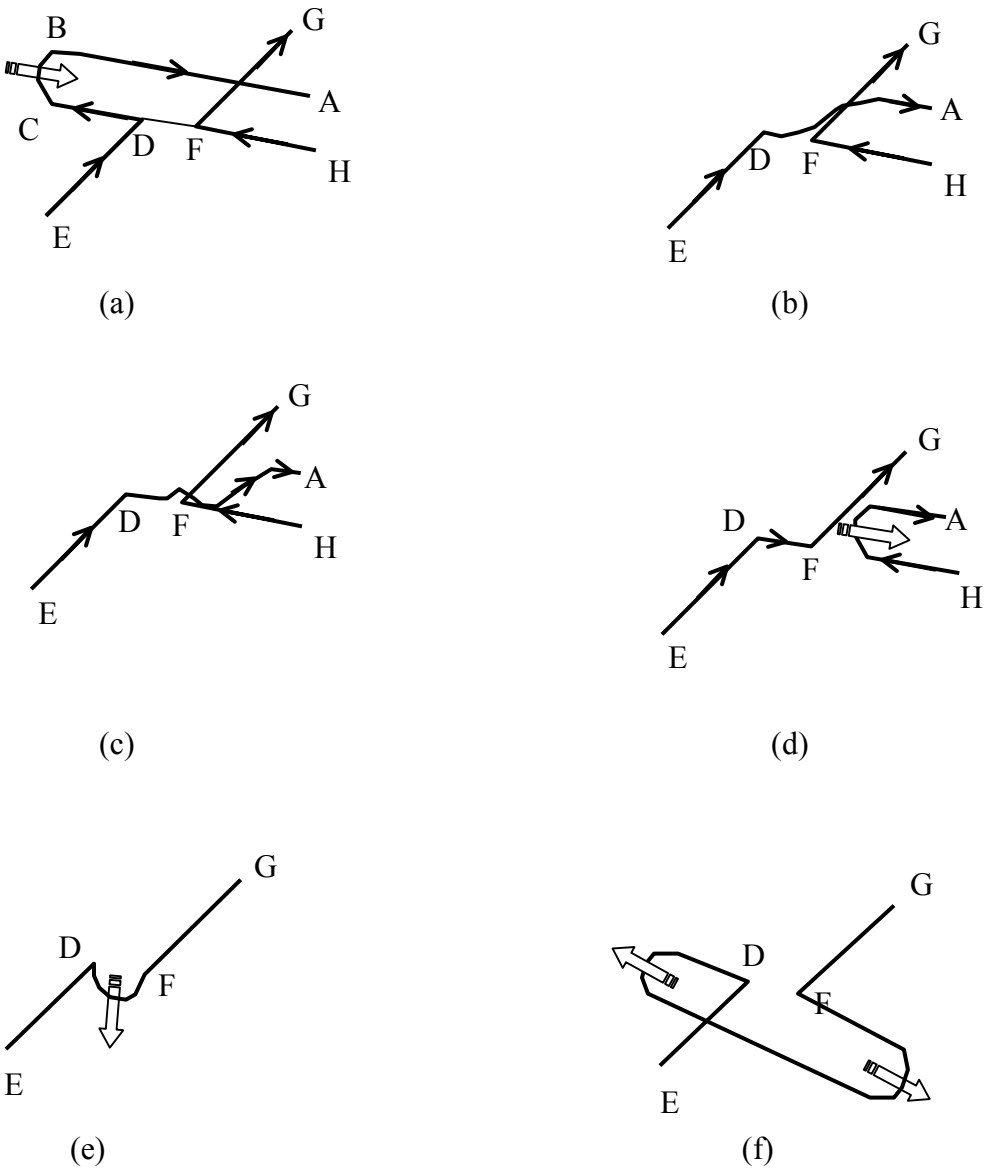

Figure 4.6, Example of a nucleation event from the interface into the neighboring layer. Nodes E, D, C, H, F, and G are the lower interface while nodes B and A are the upper interface.

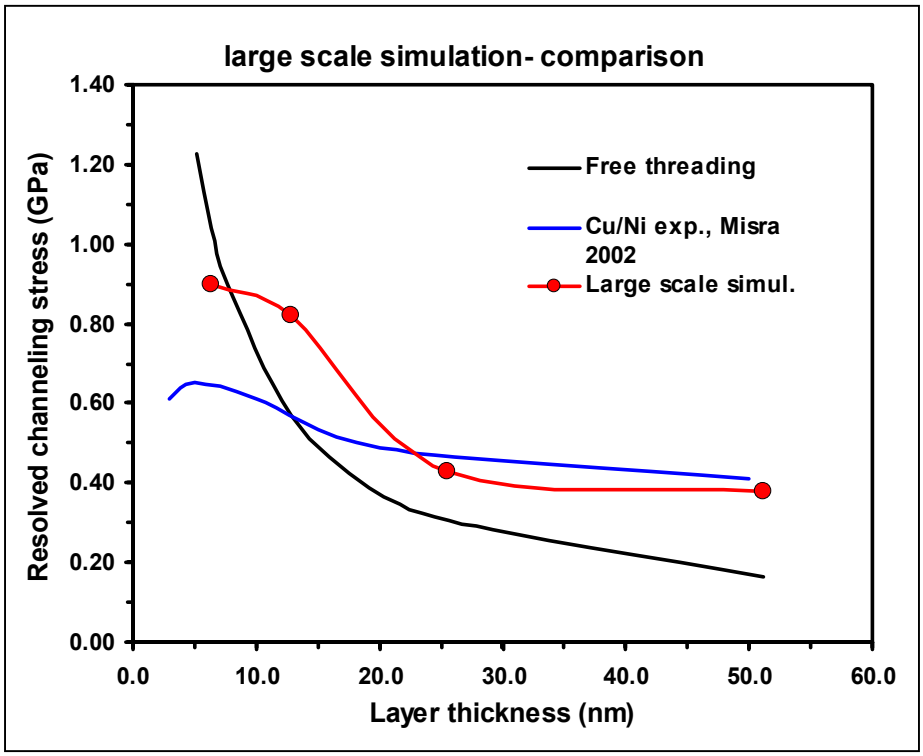

Figure 4.7, Strength predictions due to large scale simulations as qualitatively compared to those based on the free threading of a single dislocation model and those measured experimentally for Cu/Ni multilayered structures.

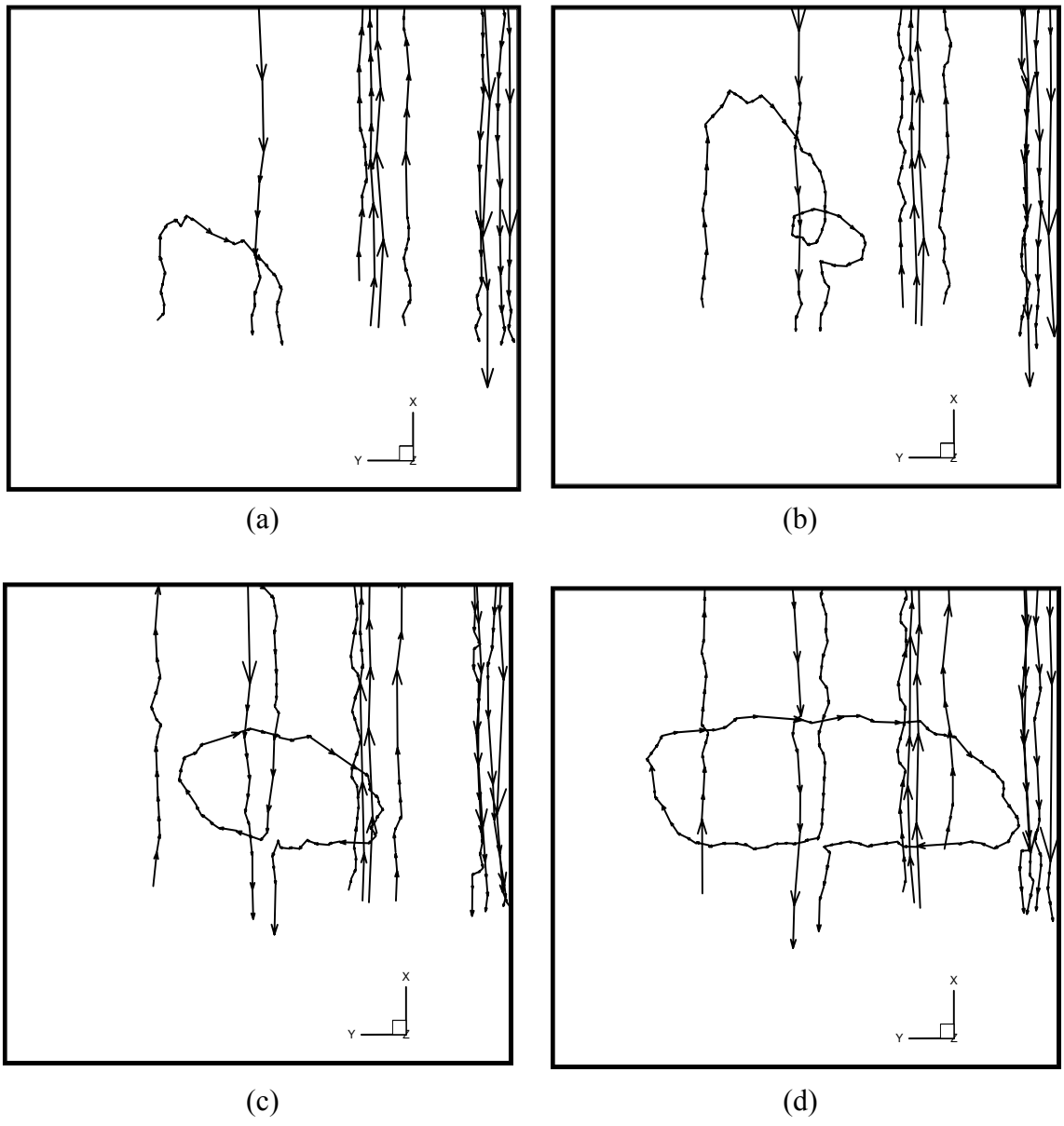

Figure 4.8, Simulation snapshots showing the sequence of events leading to multiplication by cross slip during the relaxation process of a NMM composite structure having individual layer thickness of 25 nm.

Chapter Five: Conclusion and future work

Size effects in NMM composites were investigated to understand the dependence of their strength on the individual layer thickness. Under the confinement conditions encountered in NMM composites, it is thought that the threading of dislocations confined to their respective layers is the primary deformation mechanism. Based on this process, however, strength predictions underestimate the experimentally measured strength. Among other reasons, this discrepancy can be attributed to dislocation interactions which naturally occur in a real system. Two important unit dislocation interactions of common occurrence in a real system were separately considered in an attempt to improve the predictions of the simple threading model (*i.e.* with no interactions). The first is the interaction between a threading dislocation and orthogonal intersecting interfacial dislocations. DD analysis was employed to study such an interaction due to the potential of short-range interactions taking place. It was found that the strongest of such interactions occurs when the two interacting dislocations have collinear Burgers vectors. The interaction involves an annihilation reaction at the intersection line of their glide planes and leaves two 90^{o} dislocation bends at the interfaces, a common dislocation structure observed in NMM composites. The interaction produces a hardening effect which improves the strength predictions but cannot fully explain the trend in measured dependence of strength on thickness in NMM composites. The second significant interaction studied is that between threading dislocations and parallel interfacial dislocations. A semi-analytical energetic model was used for these calculations. As in the previous case, the interaction is stronger when the Burgers vectors of the interacting dislocations are collinear. Parallel interactions can lead to either hardening or softening

depending on the Burgers vector directions, while the strength of such interaction depends on the statistics of the distribution of dislocations in the vicinity of the threading dislocation. More investigation is needed to determine the nature of such distributions and hence the overall strength. Nevertheless, the experimentally measured dependence of strength on thickness in NMM composites cannot be completely explained based solely on parallel interactions.

To better capture the macroscopic behavior of NMM composites, large-scale DD simulations of the collective behavior of dislocation systems were conducted. Such simulations naturally combine the complex effects of all possible dislocation interactions occurring simultaneously as the dislocation structure evolves under loading. An essential requirement for the validity of those simulations is a realistic initial dislocation structure. To this end, relaxation simulations mimicking the coherency strain relaxation process in actual systems are first conducted. In agreement with experimental evidence regarding the origin of dislocations in NMM composites, a random distribution of threading dislocations is subjected to the proper magnitude of coherency stresses, which alternates in sign in the alternating layers of the simulation cell. The end-result dislocation structure of this phase then serves as the initial structure for the loading phase, which is used to capture the yield strength of the composite. The resulting strength predictions better match the experimentally measured dependence of strength on layer thickness in Ni/Cu system. This particular system was chosen because it is compatible with our idealized model as explained in Chapter 3. Other useful information can also be extracted from the simulations. For example, a mechanism for dislocation multiplication due to cross slip and a mechanism for nucleation from the interface upon loading were observed. More

detailed examination can yield more insight about other dislocation mechanisms in NMM composites. The simulation also showed that multiple dislocation pileups do occur when the layer thickness is 25 nm and above.

As indicated above, the initial dislocation structure is critical in determining the validity of the large-scale simulations. Hence more work is needed to validate the relaxation model used above. Although is it well established that threading dislocations contribute to misfit relief in NMM composites, other contributions come from misfit dislocation nucleation and loop nucleation at interfaces. One immediate suggestion for future work is to examine a relaxation model that combines misfit dislocations as well as threading loops with the proper partitioning of the lattice parameter mismatch, *f*, between misfit and coherency,

$$f = \varepsilon + \delta \text{, with } f = \frac{a_s - a_f}{a_f} \quad \text{.....(5.1)}$$

where δ is the portion of *f* relieved by an orthogonal array of misfit dislocations having an average spacing λ, $\delta = b / \lambda$ and *b* is the Burgers vector of the misfit dislocation network. ε is the "left-over" lattice parameter misfit resulting in coherency stress, Figure 5.1. Another important factor to account for in future efforts is the effect of image forces due to the difference in elastic modulus of the two materials in the layered structures. Although such forces can be ignored for a first approximation in the Ni/Cu case, as suggested in literature, it is worthwhile quantifying such effect and to be able to account for it in other bimetal systems where the difference in modulus is more pronounced. Image forces repel dislocations in the softer layer away from the interface, leading to an

effective layer thickness that is smaller than the nominal thickness, which in turn may change the interaction characteristics at the interfaces.

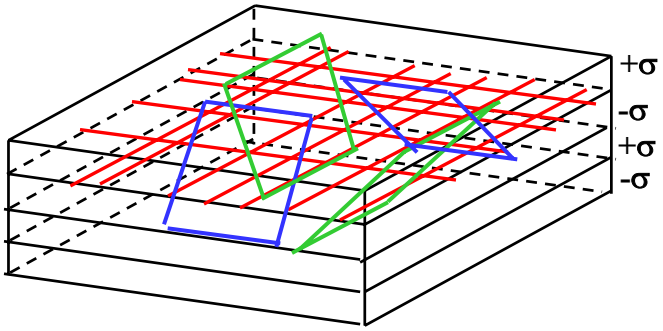

Figure 5.1, Initial configuration for a relaxation model based on both misfit and coherency strain.

Appendix A: Multiscale modeling of size effect in FCC crystals Discrete dislocation dynamics and dislocation-based gradient plasticity

F. Akasheh, H. M. Zbib*, and T. Ohashi[#]

School of Mechanical and Materials Engineering,
Washington State University, Pullman, WA
[#]Kitami Institute of Technology, Kitami, Japan

Abstract

A multiscale approach to modeling size effect in crystal plasticity is presented. At the microscale, discrete dislocation dynamics (DD) coupled with finite element (FE) analysis allows the rigorous treatment of a broad range of micro plasticity problems with minimal phenomenological assumptions. At the macroscale, a gradient crystal plasticity model, which incorporates scale-dependence by introducing the density of geometrically necessary dislocations (GNDs) in the expression of mean glide path length, is used. As a case study, bending of micro-sized single crystal beams is considered and the correspondence between the predictions of both models is made. In its current framework, the macroscale model did not capture the experimentally observed effect of specimen size on the initial yield stress. With this effect naturally captured in the corresponding DD analysis, the absence of a density-independent size effect in the expression for the strength of slip systems was concluded. In an independent work on the tensile loading of micrometer-sized polycrystals [95], a size effect, physically rooted in the size and location of a Frank-Read sources (FRS) relative to grain boundaries, was identified. This effect can be generalized in the context of dislocation-interfaces interactions, typically missing, to one extent or another, in current gradient crystal plasticity models and can, in principle, be used to understand the initial yield size-dependence in single crystal bending identified through DD analysis.

A.1 Introduction

Modeling the mechanical response of metallic structures with features on the order of tens of micrometers and below is growing to be more and more important from the technological point of view. As technology continues to drive the development of miniaturized devices exhibiting superior performance, more functional mechanical components on this scale need to be designed and their response adequately understood and predicted. Existing phenomenological models, good to predict the response of metals in large volumes ("bulk" range of millimeters and above), fail to make similar good predictions in the microscale range for several reasons. As components become smaller, details of the microstructure and the nature of interfaces (both external and internal) become increasingly significant in determining the mechanical response. Besides, crystalline materials are far from perfect and generally contain defects such as vacancies, interstitials, dislocations, incidental dislocations boundaries, grain boundaries, and cracks. Such defects introduce internal stress fields whose range of influence are on the microscale level and hence cannot be ignored when the sample size is on a similar order. Even if not for internal defects, the mere existence of external free surfaces naturally made up of higher energy atoms influences the mechanical response in an increasingly significant manner when surface-to-volume ratio becomes significant as in the case of miscroscale specimens. The above factors generally result in the microscale "smaller-stronger" trend seen in many experiments, including bending of thin beams [1], torsion of wires [2], and micro/nano indentation [3]. Attempts at providing a better understanding of the origin of this size effect and developing models that predict it have been the subject of much research efforts.

In spite of the complexity of the details of the microstructure and its effect on small scale, most of the physics of deformation at the microscale can be captured if dislocation motion and interactions are properly accounted for in any predictive model. The basis for this argument has been well founded in the early experimental and theoretical studies by pioneers like Taylor [96] and Frank and van der Merwe [48] who established that dislocation motion is the origin of plasticity in metals. Generally speaking, there have been two main approaches to dislocation-based modeling of the response of materials in small volumes. The first approach starts from the continuum level and attempts at including dislocation-based constitutive relations within existing classical frameworks of plasticity. The idea here, originally introduced by Nye [6] and further established by Ashby [7], is that size dependence is intimately connected to the non-local effects, which in turn can be related to the presence of slip gradients and their physical manifestation, GND densities. Among the pioneering works in this area, Aifantis [8] and Zbib and Aifantis[9, 10] proposed a "symmetric stress" strain gradient theory, where strain gradients were introduced in the flow stress relation of classical plasticity, and showed that size effects can indeed be rationalized through this approach. Justifications for this preposition included the reaction-diffusion model for dislocation motion used in the original work [8] and the Taylor expansion of the average strain over a material volume and retention of second-order terms [97], while Zbib drew on the inclusion-matrix model to justify the use of strain gradients and to provide rigorous evaluation and physical connection for the gradient coefficients used in the theory[98]. Fleck *et al*. developed an asymmetric stress Crosserat-type gradient plasticity theory and

successfully used it to capture their experiment observations of size effect in wire torsion[2]. Fleck and Hutchinson [11] expanded the formulation of the classical *J2* theory to accommodate more than one material length scale. GND-based plasticity theories, which are not fundamentally different from the strain gradient plasticity theories, represent another class of size-dependent theories. As mentioned above, the physically motivated GND densities can be linked to plastic strain gradients through geometric[7] and dislocation dynamics arguments[99]. Nevertheless, the exact method by which the effect of GNDs is incorporated in these theories is not generally agreed upon. While some researchers introduced it into the flow strength expression [2, 100], others incorporated it into the hardening law, *e.g*., Acharya [20], Ohashi [21]. Shizawa and Zbib [12], Gurtin [13], and Mesarovic [14], introduced GND density, quantified by the Nye's tensor, into the free energy expression along with a configurational stress as its work conjugate. Yet a different approach is to invoke crystallographic dislocations densities as internal variables with their own evolution laws, *e.g*., Arsenlis *et al*.[15], Yefimov *et al*. [16], Groma[17], Zaiser and Hochrainer[18], Aifantis [101], and El-Azab[19], with the latter four works being based on statistical mechanics approach to describe the collective behavior of discrete dislocations. The second general approach, DD [26, 102-105], starts form the microscale level where dislocations are explicitly represented as line defects in an elastic medium and the dynamics of their motion and interactions fundamentally determined.

The aforementioned two approaches have their own advantage and drawbacks. While the continuum approach is computationally more efficient and more versatile, it

remains phenomenological in nature and captures the physics of deformation only in an approximate way. Many basic relations in this framework include experimental fitting of constants and parameters whose physical meaning is not clear. Real experiments to estimate such parameters rarely match the corresponding theoretical setup and hence such relations can be problem and boundary conditions-dependent. The DD approach, on the other hand, is argued for to naturally capture the physics of deformation with minimal assumptions and more physical clarity. Nevertheless, it is computationally expensive and, as such, is not expected to be able to handle the variety of problems and sizes of interest for real life engineering applications in the foreseen future.

From the above discussion, it seems natural to consider a multiscale framework combining the strengths of both approaches and bridging the gap between them. This implies the development of computationally efficient dislocation-based continuum models through a process that is closely guided and informed by the more physical DD model. Moreover, DD can also be thought of as a "virtual" clean experiment against which such models can be verified and their parameters fine-tuned. Several researchers have adopted this approach. Fivel, *et al.*,[106] used DD simulations to identify the coefficients of the slip systems interaction matrix identifying the relative strength of latent and self-hardening in FCC crystals. In turn, the interaction matrix was used to determine the threshold stress for slip activation. Arsenlis and Tang[107] studied Stage 0 deformation in BCC metals using a multiscale approach. The evolution of dislocation densities and their fluxes for a single slip orientation were captured by DD simulations and used to determine the form and to fit the parameters of the constitutive relations used

in a continuum density based model. The derived model was then applied for a different orientation and produced good predictions as well. Lemarchand *et al*. [108] presented a homogenization technique where DD analysis is substituted for the constitutive law used in continuum FE calculations. Needleman and Van der Giessen [109] compared results from two-dimensional DD and classical size-independent crystal plasticity models for two boundary value problems, one involving simple shear and the other metal-matrix composites. They showed that size effect was captured by DD analysis in both problem but, expectedly, not in the continuum model. Grujicic and Columbus [110] made a comparative study, using two-dimensional DD model and a small strain classical crystal plasticity model, aimed at predicting strain localization in microbeam bending. Their DD simulations showed continued accumulation of GNDs and plastic flow localization into bands. With the proper selection of the crystal plasticity model parameters, the global response of the beam, including localization, was comparable to that predicted by their DD analysis. This was not the case for the fine details of the deformation and stress fields. Two-dimensional DD and non-local crystal plasticity based on statistical mechanics were also used to study bending of microbeams by Yefimov *et al.* [111]. The study showed that the non-local continuum model, fit with the necessary parameters from the DD analysis of a different boundary value problem, was able to predict the effect of size and crystal orientation on the bending moment-bending angle response.

In this work, we demonstrate how connections between the two scales can be made within the context of example problem, bending of thin beams. In the following sections, we describe our three-dimensional DD model and the scale-dependent crystal

plasticity model used in this study. The setup for the bending problem is then described followed by the results and discussion.

A.2. Three-dimensional DD

In three-dimensional DD analysis, dislocations are represented as general curved lines in an elastic medium and are restricted to move on particular slip planes and directions under the influence of stresses resolved along these slip systems[102-105]. The lines are discretized into a number of segments each identified by a corresponding node. Each segment can be of any character depending on its line sense relative to its Burgers vector. Dislocation motion is governed by a Newtonian type equation of motion of the form [28, 112]

$$m_s \dot{\boldsymbol{v}} + \frac{1}{M_s}\boldsymbol{v} = \boldsymbol{F}_s \tag{A.1}$$

where $\boldsymbol{v}$ is the velocity of a dislocation segment s, m_s is defined as the effective dislocation mass density, M_s is the dislocation mobility, and $\boldsymbol{F_s}$ is effective glide force per unit length of the segment. In our model, $\boldsymbol{F_s}$ has several contributions, which include the dislocation self-force, dislocation-dislocation interaction forces, drag force, lattice friction, force due to external loading, image forces due to free surfaces, and a stochastic contribution resulting from thermal fluctuations. The above equation is integrated through time in small time increments. At each increment the total force per unit length at each dislocation node is estimated. The resulting velocity is then used to move dislocations accordingly. The new resulting configuration is used in the subsequent time step to estimate the new forces, velocities, positions of nodes and so on. Besides the long-range interactions of dislocations through their stress fields, dislocations can interact in the short range upon dislocation-dislocation encounters. The following major interactions

are considered in our model: cross slip, dipole formation, annihilation, and jog and junction formation. As far as the boundaries are concerned, three types of dislocation boundaries are included: free, rigid and periodic. At free boundaries, impinging dislocations leave the simulation cell breaking dislocation loops and resulting in dislocation lines ending on the surface while rigid boundaries are impenetrable and result in dislocation pile-up. Periodic boundaries are used to simulate infinite domains by allowing the simulation cell to be "seen" as repeating itself in the periodic direction of interest. For details, the reader is referred to the review article by Zbib and de la Rubia [35] and the comprehensive list of references there.

Another main feature of our model is highlighted here due to its direct relevance to the multiscale approach and that is the coupling of DD and FE analyses allowing general boundary value problems to be studied [35]. This implies the capacity to rigorously treat finite domains and apply general boundary and loading conditions. Since the stress field of a dislocation is known for the case of infinite, homogenous media, the key for the treatment of the general boundary value problem with internal long range stress field sources is to use the principle of superposition to sum up two solutions: one from the stress field of dislocation as if they existed in an infinite medium and the solution for the problem consisting of the actual finite domain with arbitrary boundary conditions and loads, to which is added the negative of the tractions at the domain boundary resulting from the truncation of internal stress fields. From the above discussion, it can be seen that this feature is essential for the multiscale approach because it allows matching problems to be solved and compared in at both the continuum scale

and the DD microscale. A final point to emphasize here is that the size effect we seek to model is naturally included in our coupled DD-FE model in the sense that both the direct long range interactions as well as the indirect ones due to the finiteness of the medium and effect of surfaces and interfaces are explicitly accounted for.

A.3 Gradient crystal plasticity model

The scale-dependent crystal plasticity model used in this work, developed by Ohashi [113], is based on the classical small deformation, small rotation rate independent model developed by Hill[4]. In this model, deformation is the result of slip on particular slip systems. For FCC materials, those are the commonly known 12 slip systems made form the combinations of the {111} planes and the <110> directions. The main features of this model include the condition that slip on any slip system *s* is initiated when the resolved shear stress $\tau^{(s)}$ reaches a critical threshold level, $\tau_{cr}^{(s)}$. The critical resolved shear strength is given by the modified Bailey-Hirsch model [113],

$$\tau_{cr}^{(s)} = \tau_o + a\,\mu\,b\sum_m \Omega^{sm}\sqrt{\rho_{ssd}^m} \tag{A.2}$$

where τ_o is the lattice friction, *a* is an emperical factor on the order of 0.1, μ is the shear modulus, *b* is the magnitude of the Burgers vector, and dimensionless Ω^{sm} is the interaction matrix of slip systems relating the hardening effect slip system *m* has on slip system *s* based on the strength of possible interactions between dislocations belonging to *s* and *m*. ρ_{ssd}^m represents the statistically stored dislocation (SSD) density on slip system *m*, also referred to as redundant dislocation density [114] because the net Burgers vector of such dislocation densities is zero. SSD densities are distinguished from GND densities, which have a non-zero net Burgers vector and are necessary to accommodate any

incompatibilities resulting from inhomogeneous deformation. The evolution law for the dislocation density is based on the Orowan relation for plastic shear strain, $\dot{\gamma}^{(s)} = b\rho_{mob}^{(s)} v_m^{(s)}$, with $\rho_{mob}^{(s)}$ being the density of mobile dislocations and $v_m^{(s)}$ their mean velocity on slip system *s*, and the simple model that SSD density increases inasmuch as mobile dislocations get arrested due to dislocation-dislocation interactions [113], *i.e.,*

$$\dot{\rho}_{ssd}^{(s)} = \frac{c\,\rho_{mob}^{(s)}}{\tilde{t}_m^{(s)}} \tag{A.3}$$

where *c* is a numerical factor, and $\tilde{t}_m^{(s)}$ is a mean lifetime during which mobile dislocations can move freely before getting arrested. $\tilde{t}_m^{(s)}$ can be equivalently related to the mean free path length of mobile dislocations $L^{(s)}$ as follows,

$$L^{(s)} = \tilde{t}_m^{(s)} v_m^{(s)} \tag{A.4}$$

Combining Eq.(A.3) and Eq.(A.4) leads to the following evolution law for SSD density,

$$\dot{\rho}_{ssd}^{(s)} = \frac{c\dot{\gamma}^{(s)}}{bL^{(s)}} \tag{A.5}$$

Using Eq. (A.2) and Eq. (A.5), the evolution of the strength of a slip system is related to the increment of slip $\dot{\gamma}$ on all slip systems as follows,

$$\dot{\tau}_{cr}^{(s)} = \sum_m h^{sm}\dot{\gamma}^{(m)}, \text{ with } h^{sm} = \frac{0.5\,a\,c\,\mu\Omega^{sm}}{L^{(m)}\sqrt{\rho_{ssd}^{(m)}}} \tag{A.6a,b}$$

where h^{sm} is the strain hardening coefficients matrix quantifying the contribution of a dislocation density on system *m* to the strength of system *s*. Eq.(A.6a) is the commonly

used multiple-slip hardening law suggested by Hill[4] and in arriving at the expression for h^{sm}, Eq.(A.6b), the variation of the critical slip system strength, Eq.(A.2), and the Orowan relation for plastic shear strain were used. Notice that h^{sm} is a function of both ρ_{SSD} and ρ_{GND}, *i.e.*, of slip and slip gradients as argued for in that case of gradient theory, e.g. [20]. The mean free path is inversely related to the dislocation density and is classically expressed in terms of the statistically stored dislocations only,

$$L^{(s)} = \frac{c^*}{\sqrt{\sum_m \omega^{sm} \rho_{ssd}^{(m)}}} \tag{A.7}$$

where c^* is a constant on the order of 10-100 and ω^{sm} is the weight matrix quantifying the contribution of dislocation density on system m to the mean free path length for system s. To introduce scale dependence to the model, Ohashi [21] argues for introducing the GND density measure, as calculated from the strain gradients [115], into the hardening matrix through the dependence of the mean free path length not only on the SSD density but also on the GND density,

$$L^{(s)} = \frac{c^*}{\sqrt{\sum_m \omega^{sm} \left(s \,.\, \rho_{ssd}^{(m)} + g \,.\, \rho_{gnd}^{(m)} \right)}} \tag{A.8}$$

where s and g are controlling coefficients with values ranging 0-1. Thus, in this modified framework, the size effect can only be controlled by the value of factor g in with g=0 implying no size effect and g=1 maximum effect. Eq.(A.8) is substituted in Eq.(A.6b) to obtain the final form of the hardening coefficients h^{sm}.

Finally, the GND density is calculated from the gradients of slip as,

$$\rho_{\text{gnd,edge}}^{(s)} = -\frac{1}{b}\frac{\partial \gamma^{(s)}}{\partial \xi^{(s)}}; \quad \rho_{\text{gnd,screw}}^{(s)} = \frac{1}{b}\frac{\partial \gamma^{(s)}}{\partial \zeta^{(s)}} \tag{A.9}$$

where $\xi^{(s)}$ and $\zeta^{(s)}$ are the parallel direction and the in-slip plane perpendicular direction to the slip direction of slip system ***s***, respectively[115]. The global Nye tensor $\boldsymbol{\alpha}$ is calculated from the GND density by the appropriate coordinate transformation from the local slip system coordinate systems to the global coordinate system and then using the relation,

$$\alpha_{ij} = \sum_{s} \rho_{gnd,edge}^{(s)} b_i^{(s)} t_j^{(s)} + \rho_{gnd,screw}^{(s)} b_i^{(s)} m_j^{(s)} \tag{A.10}$$

where $\vec{b}^{(s)}$ is the Burgers vector, $\vec{m}^{(s)}$ is the slip direction, and $\vec{n}^{(s)}$ is and slip plane normal of slip system *s*, respectively and $\vec{t}^{(s)} = \vec{m}^{(s)} \times \vec{n}^{(s)}$. The Nye tensor components can be understood as a physical basis for representing any arbitrary net dislocations density. For example, $\boldsymbol{\alpha_{11}}, \boldsymbol{\alpha_{22}}$, and $\boldsymbol{\alpha_{33}}$ represent net screw dislocation densities along the 1, 2, and 3 axes, respectively, while all other component with non-similar indices represent edge dislocation densities. For example, $\boldsymbol{\alpha_{12}}$ represent the net density of those edge dislocations which have their line sense parallel the 2-axis and their Burgers vector aligned with the 1-axis.

A.4 Connection between the scales

The scale bridging approach involves using the more physical DD analysis to guide the development and/or the parameter fitting process of the gradient crystal plasticity model to enhance their ability to capture size effects observed experimentally. In this process, it is also desirable that a connection between parameters of the macroscale model and the underlying physics be established. In our case, the specific question at hand is to evaluate

the capacity of our gradient crystal plasticity as formulated to capture size effects. Once the adequacy of the framework is established, the question of fitting the parameters of the model comes next. In our case, these parameters include the density independent part of the relation of the threshold stress for slip, Eq.(A.2), the coefficients of the interaction matrix Ω^{sm}, *c*, s, g***,** and the coefficients of matrix ω^{sm} in Eq.(A.8). Our intention here is to demonstrate the multiscale approach to this question and not to present an exhaustive numerical fitting of the CLP model parameters.

A specific boundary value problem is chosen to conduct this exercise, however, the macroscale model arrived at should be validated for different problems before it is generalized As a simple, yet well-suited, problem to demonstrate the paradigm of multiscale bridging, bending of micro-sized single crystal beams is considered. Strain gradients are inherent in the bending problem, hence the size effect as well. Microbeam bending has been addressed by several researchers. Experimental evidence for the size-dependence of both the initial yield and subsequent flow stress in bending of micro- and nano-sized beams came from the work of Stolken and Evans[1], Shrotriya et al.[116], and Haque and Saif [117]. Several analytical studies using one form or another of gradient plasticity applied to simplified two-dimensional bending problems also proved the scale-dependence on both initial yield and hardening [1, 99, 116, 118-120]. Using two-dimensional DD analysis, Cleveringa *et al*.[121] studied the evolution of dislocations densities and the mechanical response of micro-sized beams and were able to detect size effect in both cases. Yefimov *et al*. employed multiscale approach combining two-dimensional DD and gradient plasticity[111] to analyze size effect in bending. [111].

Their continuum model results, fit with the necessary parameters from the DD analysis of a different boundary value problem, showed good correspondence to their DD results predicting the mechanical response and density evolution dependence on specimen size. The last two works comes closest to out our investigation here with the main difference of using three-dimensional analysis for both the DD and the gradient plasticity. Three-dimensional DD analysis is more realistic and becomes particularly important in the case of the freestanding micro-sized beam bending problem considered here due to the significance of surface effects and the small volume of the specimen. For example, our results show that in spite the idealized single slip system configuration and loading, where the slip plane normal, Burgers vector, and loading are all coplanar, the resulting deformation involves generalized twisting and bending about all axes. Clearly, this observation has important consequences on the GND density evolution, the work done, and the size effect.

In our work using three-dimensional DD, the problem is set up in both models to be as equivalent as possible given the scale difference and hence the level of details by which the problem is described in each case. The sample size, elastic properties, initial dislocation density, loading and boundary conditions can be made identical. In the gradient crystal plasticity model, the dislocation content is described as a continuum density, which can be assigned to any desired slip system(s) and whose magnitude can be randomly given by a normal distribution. In DD analysis, dislocations are explicitly introduced by a random distribution of FRSs, both in location and size, such that the density calculated from the total length of the segments making the FRSs and the specimen volume are matching in both models. Although the yield strength in the

continuum model is determined by the slip systems strength, the choice of the mean FRS size and the dislocation boundary conditions is what determines yield in the micro model. In our case, the Orowan relation for the strength of a FRS, $\tau \approx \mu b/\lambda$, where λ is the FRS size, can only be used as a rough guide due to the finiteness of the medium.

In both models the specimen is bent around the z-axis by the application of linearly varying displacement to the *xy* faces, Figure A.1. The dislocation free buffer region beyond the intended specimen length shown in the figure is intended to avoid any ambiguity at the loading surfaces resulting from an otherwise conflict between dislocations leaving through them and as the finite domain tractions applied to them as required by the auxiliary elastic problem as explained earlier. The boundary conditions on the *xz* and *yz* surfaces are chosen to be free, implying the beam is free standing, while dislocations reaching the surface can leave it readily.

Two samples of two different sizes where studied in each model: 12x3x2 μm and 6x1.5x2 μm. The initial dislocation density was chosen to be $1\text{x}10^{11}$ $1/\text{m}^2$. The specimen material is copper with shear modulus of 38 GPa, Poisson ratio of 0.3 and Burgers vector magnitude of 2.5 A^{o}. The baseline parameters of the crystal plasticity model are $c^*=10$, $c=2$, $a=0.1$. All the coefficients of the interactions matrix Ω^{sm} are set to the value (approximately 1.0), implying an equal contribution from all slip systems to the strength $\tau_{cr}^{(s)}$ of any slip system, see Eq.(A.2). As for the matrix ω^{sm}, diagonal complements were set to 0, while all the off-diagonal ones to 1. Due to the fact that the beam is micro-sized and freestanding, a completely random dislocation distribution will in general result in a very complex generalized deformation of the beam, including twisting and bending about the three axes. Although this scenario is realistic, it is far from being treatable by the

continuum model studied here or, to this matter, most crystal plasticity models in existence, due to the absence from these models of a fundamental treatment of dislocation boundary conditions. An exception to this general *status quo* can be found in those models, which include density as an internal variable with physics based evolution laws [15, 16]. For the aforementioned reason and for simplicity, the crystal orientation and initial dislocation content are chosen so that dislocation exist only on a plane whose normal is lies in the *xy* plane and inclined at 45^{o} to the *x* axis and whose slip direction also lies in the *xy* plane as shown in Figure A.1. The initial density is statistical in nature and hence, if any GND density evolves upon loading, it will be the result of the induced deformation.

Since the GND density is at the heart of the effort to model size effect, the evolution of the Nye dislocation tensor will be evaluated in both models and compared. Within the continuum framework of gradient crystal plasticity, the Nye tensor is found from the gradients of slip as previously mentioned. As for the DD model, the Nye tensor is explicitly estimated from the following relationship[35],

$$\alpha_{ij} = \frac{1}{V}\sum_{k} l^{k}\, b_{i}^{k} v_{j}^{k} \tag{A.11}$$

where l^{k}, $\vec{v}^{k}$, and $\vec{b}^{k}$ are the scalar length, dislocation line sense vector, and the Burgers vector of dislocation segment *k*. Notice the difference between this explicit calculation of $\boldsymbol{\alpha}$ and the continuum density-based calculation in Eq.(A.10). While a dislocation line can have any arbitrary line sense $\vec{v}^{k}$, a density basis consisting of a pure edge density and a pure screw density for each slip system is used to discretize the dislocation density space, hence the use of two specific line senses, $\vec{m}^{(s)}$ (parallel to the Burgers vector) and $\vec{t}^{(s)}$

(perpendicular to the Burgers vector and in the slip plane) for each slip system *s*. *V* is a reference volume over which α is calculated and as such is a fundamental quantity for the homogenization of the discrete dislocation content into continuous dislocation fields. The choice of *V* is not a trivial matter and should be tied to the resolution needed for the details of the dislocation structure.

A.5 Results and discussion

We start by showing an example of the initial distribution of dislocations and FE mesh, Figure A.2, as well as the dislocation structure and the corresponding deformed beam at the yield point, Figure A.3. To examine the sensitivity of the yield strength to the initial random of the dislocation sources, multiple initial random distributions are tested and compared, Figure A.4. The bending moment is normalized as $\widetilde{M} = M\ w/I$, (*M* is the bending moment, and *I* the moment of inertia of the beam) so that it takes stress units and the slope of the linear part of the curve corresponds to Young's modulus of the material, in our case 100GPa. Results show that the obtained yield point obtained from any of the initial distributions is statistically representative of the behavior.

Figure A.5 shows DD simulation results for the mechanical response of the 12x3x2 μm beam measured by the bending moment-bending angle curve for different FRS sizes. As expected, the smaller the FRS size the higher the yield point. For the 50 nm FRS case, the DD simulations indicates that yielding occurs at a normalized bending moment of approximately 4.0 GPa, which corresponds to a resolved shear stress of 250 MPa for the outer most fiber of the beam. An estimate of the strength of a FRS of size 50 nm in an infinite medium is approximately equal to 200 MPa. The existence of free surfaces results in additional image forces felt by the sources, hence a lower applied

stress maybe be needed to activate them. Another contributor to such discrepancy is the fact that the sources are not isolated, as the analytical model assumes, and a long-range effect from neighboring source is expected if they are close enough.

Figure A.6 demonstrates the size effect naturally captured in DD. The reference sample is the large beam and the small sample was obtained in two different ways that would still preserve the initial dislocation content in both cases as that of the reference sample. In the first case the sample is scaled down including the FRS size, while in the second case the FRS source sized in kept constant but their number adjusted to maintain the same dislocation density. In both cases the common trend of size effect, "smaller-stronger", is evident although more pronounced in the case where the FRS size was also scaled down.

Figure A.7 shows the crystal plasticity (CLP) model prediction of the yield strength for different values of τ_o, Eq.(A.2). Notice that the results of the 12x3x2 μm and the 6x1.5x1 μm beams overlap, indicating that the model does not capture size-dependence in the initial yield nor in the early stage of plastic deformation where the SSD density dominates, even when the size effect is maximized by setting g in Eq.(A.8) to 1.0. A recent study on bending of mircobeams using the same CLP model [120] with s and g , Eq(A.8), set to 0 and 1 to further augment the size effect, size effect was detected early on in the plastic stage but not in the initial yield. The physical interpretation inherent to Eq.(A.2), that its density-independent part τ_o represents the lattice friction and depends solely on temperature[113, 122], does not allow a good initial yield prediction, compared to DD results, for any of the specimens studied. A higher value of 50 MPa had to be used for a reasonable match in the case of 12x3x2μm sample with the larger FRS.

This leads to the conclusion that the density-independent part of Eq.(A.2) must have an additional contribution(s) apart from the lattice friction. Furthermore, based on the formulation of the CLP model, this same additional contribution(s) must also contain the missing size-dependency of the initial yield captured by DD, Figure A.6. In fact this point has recently been made in the context of the study of size effect on initial yield in the case tensile loading of micro-sized polycrystals [95]. In this latter work, Ohashi used the same DD model presented here to study the activation condition of a FRS in a single grain modeled as having rigid grain boundaries and found a strong dependence not only on the FRS size but also on the relative size of the source to the size of the grain and also on the location of the source within the grain. When the source is small compared to the grain size and/or relatively far from the boundaries, the activation stress needed to nucleate at least one complete loop can be considered equal to that of the infinite medium case. However, as the source becomes large relative to the grain size and/or closely situated to the boundary, a significant increase in the activation stress is experienced, which is inversely proportional to the grain size. This effect can indeed be attributed to dislocation-surface interaction. The significance of this finding is that there is another length scale affecting the yield point, which needs to be included in a size-dependent crystal plasticity framework. This observation was modeled as another density-independent contribution to the slip system strength, Eq.(A.2), as follows, [95] (d_g is the grain size)

$$\tau_{cr}^{(s)} = \tau_o + 3\beta\frac{\mu b}{d_g} + a\,\mu b\sum_m \Omega^{sm}\sqrt{\rho_{ssd}^m} \tag{A.12}$$

In principle, a similar kind of argument, dislocations-boundaries interactions, can be used to support the observation that came out from our DD analysis about the need to have an

additional contribution to the density-independent term in Eq.(A.2). A simple rough calculation of the magnitude of the term $3\beta\frac{\mu b}{d_g}$ taking β to be equal to 1, d_g half the height h of the beam, Figure A.1, and μ and b 40 GPa and 2.5A^o respectively (same as used in both models), one gets a value of 30 MPa. This value is on the same order of the value mentioned above, 50 MPa, needed to get a good match between the models regarding the yield point. Although the modeled beam is made of single crystal with free boundaries, the presence of a neutral zone with low stresses act as a trap for dislocations and hence can impose a significant back stress and hence significant resistance to source activation. The presence of other neighboring sources can also affect on the nucleation threshold. Finally the image forces from the free surfaces can provide a significant attractive effect, toward the surfaces, on the dislocation segments stimulating the source activation at possibly lower stress level than expected otherwise if the boundary conditions are different.

Figure A.8 shows DD predictions for the evolution of SSD for the same cases detailed above. The point at which density spikes correspond to the sudden macroscopic yield point observed in the corresponding bending moment versus bending angle curves (Figures A.5 and A.7). This point marks an avalanche activity of dislocation motion, thus the sudden drop of measured bending moment. The crystal plasticity predictions for the evolution of SSD are shown in Figure A.9. As can seen, the general trend is only qualitatively match. The continuum model cannot capture sudden avalanches of dislocations because they are already expressed as averaged fields. The sensitivity of the DD model to the initial distribution of sources, location wise and size wise, should first

be studied before making a conclusion about the quantitative discrepancy in the behavior of the two models

The evolution of the Nye tensor (averaged over all the sample volume) obtained from DD is shown in Figure A.10 and that from CLP in Figure A.11. The 1, 2, and 3 indices refer to directions x, y and z respectively. In the case of pure bending about the z-axis (3-axis), the expected non-trivial Nye tensor components are those of edge nature, in particular those representing edge dislocations whose line sense is parallel to the z-axis, hence components 13 and 23. If the slip plane normal were to lie along the y-axis then we would only expect the 13 component to be non trivial. As can be seen from Figures A.10 and A.11, this expectation is met by both models. The existence of smaller nontrivial components in the DD results, indicates the inevitable occurrence of some twisting (indicated by the screw components 11 and 22) and some out-of-plane bending (indicated by the screw components 21 and 13) as dislocations leave the free surface (also can be seen in Figure A.3b showing the final distorted structure of the beam). Quantitative comparison of both model predictions quantitatively, indicates that the GND content is significantly higher and its evolution is much smoother in the CLP model than it is in the DD model. One reason for the magnitude difference is in the actual volume where the GNDs exist in the DD case (see Figure A.3). This volume is considerably smaller (concentrated around the intense dislocation activity region) than that in the case CLP where the distribution is homogenous all over the specimen volume. However this still does not close the difference gap. One expects that at this volume scale the free surfaces effect, which is considered in DD but not in CLP, is a major factor and although we do not have it quantified at this point, might provide the answer to this difference.

Continuum crystal models generally do not provide a rigorous treatment of dislocation-surface interactions and this remains an area where more contribution is needed. A point to make on the CLP result is that although Figure A.11 indicates an obvious size effect in the estimation of the Nye tensor, this effect does not propagate in the systems of equations to make a tangible difference for the bending moment response. This indicates that the method in which the GND density is included in our model, to modify the mean glide path length, is not sufficient to predict the size effect in bending.

A.6 Conclusion

A multiscale approach to model size effect in crystals was demonstrated using as an example the plastic bending of single crystal micro-sized beams. The more physical microscale DD model was used to evaluate capacity of the continuum gradient crystal plasticity model to capture size effect. Through this process, a missing size effect related to initial yield was identified. This effect can be rationalized in the larger context of dislocation-interface interactions. Results indicate that a rigorous treatment of dislocation boundary conditions in the crystal plasticity framework is necessary for meaningful comparisons. Due to the fundamental difference in which a certain problem is described in each model, a statistical approach aimed at averaging DD simulation results is necessary.

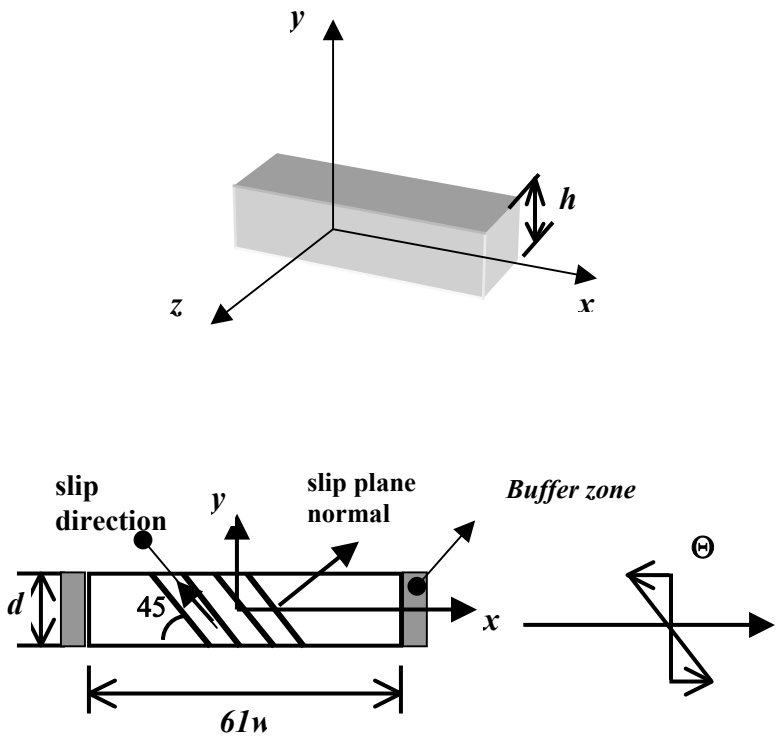

Figure A.1 Bending problem setup.

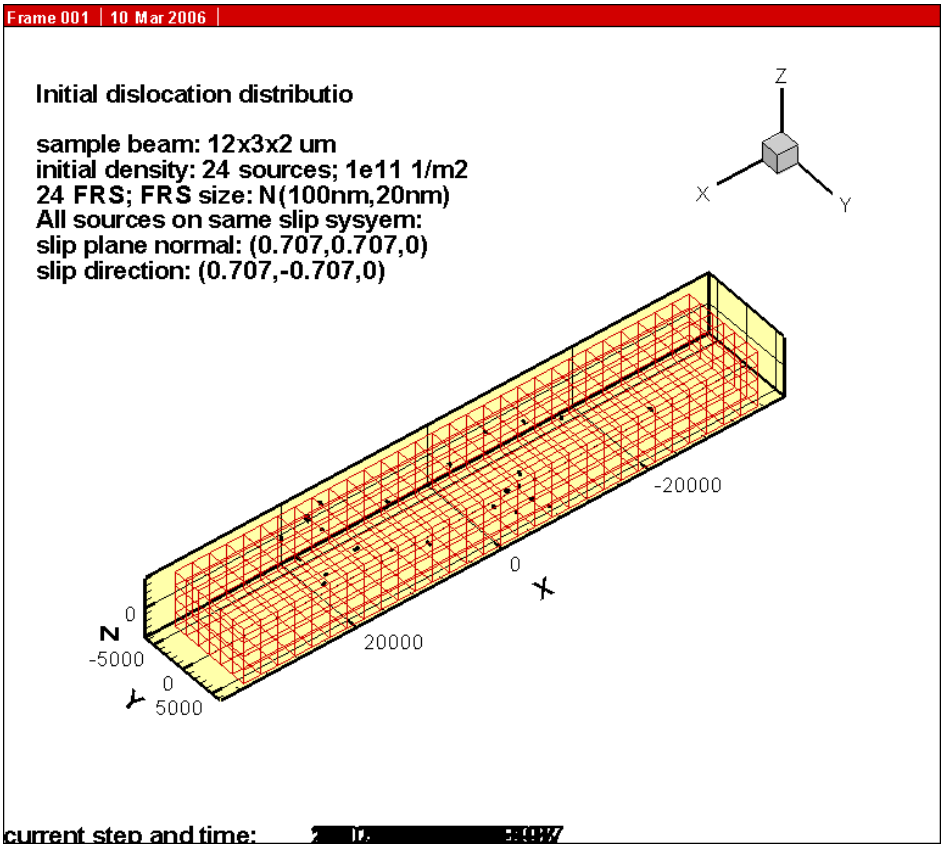

Figure A.2 Sample initial dislocation distribution and FE mesh

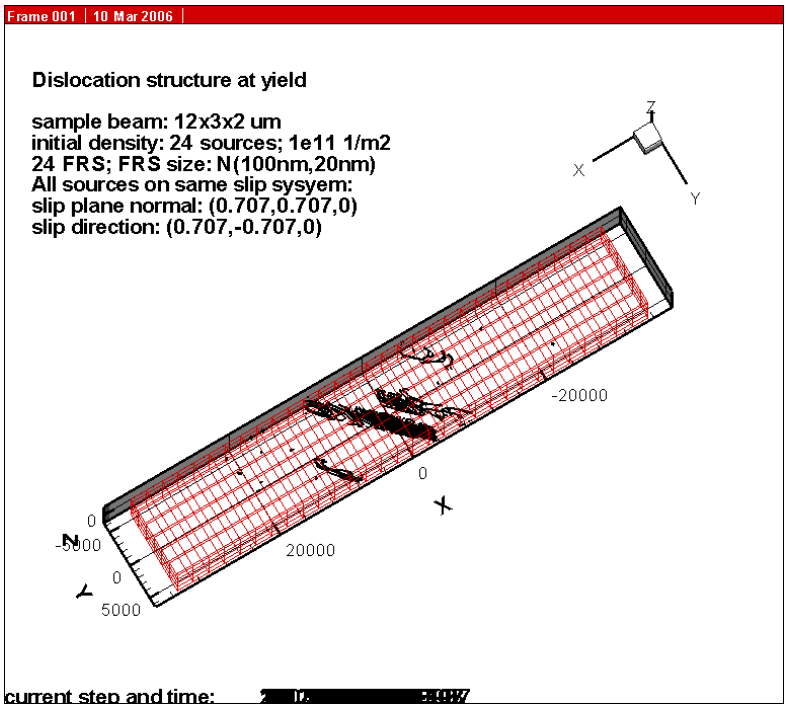

(a)

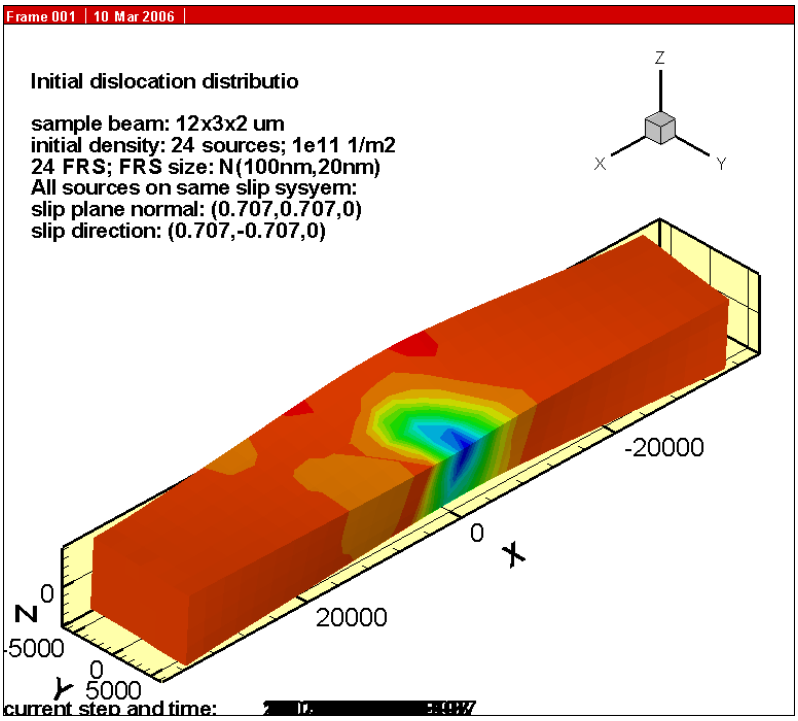

(b)

Figure A.3 (a) Dislocation distribution at yield (the superimposed FE mesh is that of the undeformed structure and included just to show the specimen domain). (b) actual deformed structure shown along with plastic strain ε_{xx}^{p} contour(deflections x5)

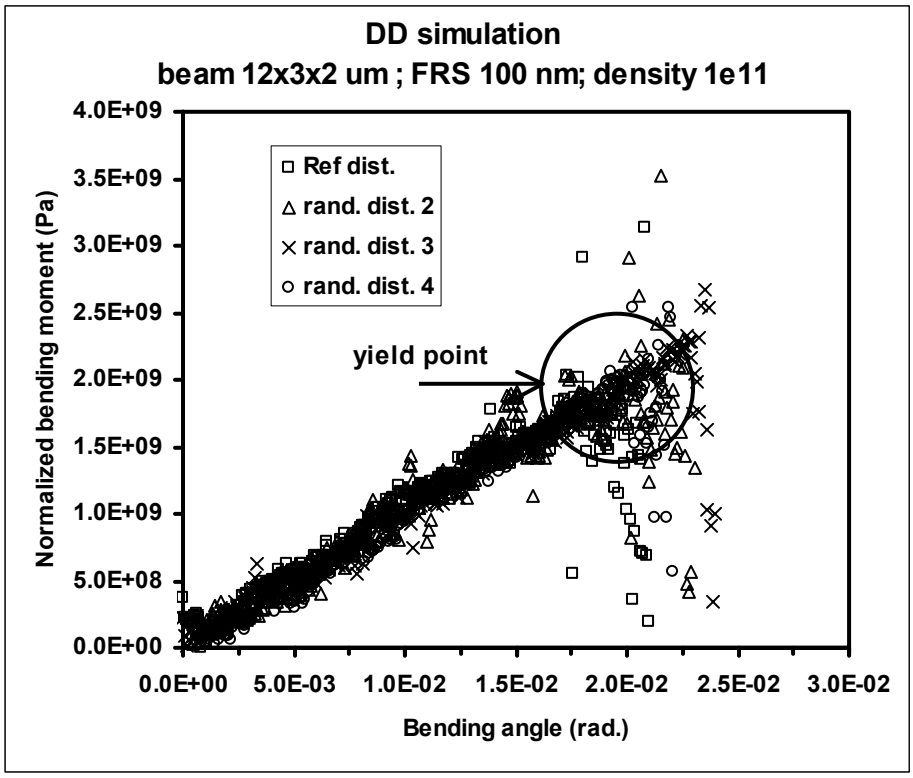

Figure A.4 DD simulation results: effect of initial random distribution on the mechanical response. (*Rand. dist. 1,2,3*: random distribution 1, 2, 3. "*Ref dist.*" denotes the reference distribution otherwise used in this graph and all other DD simulation results in the paper)

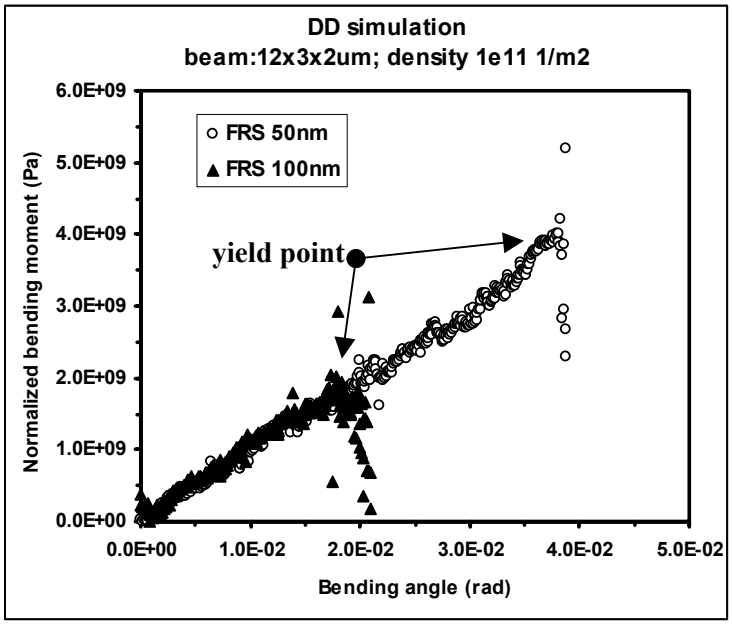

Figure A.5 DD simulation results: effect of FRS size on the response of a freestanding 12x3x2 μm beam with same initial density.

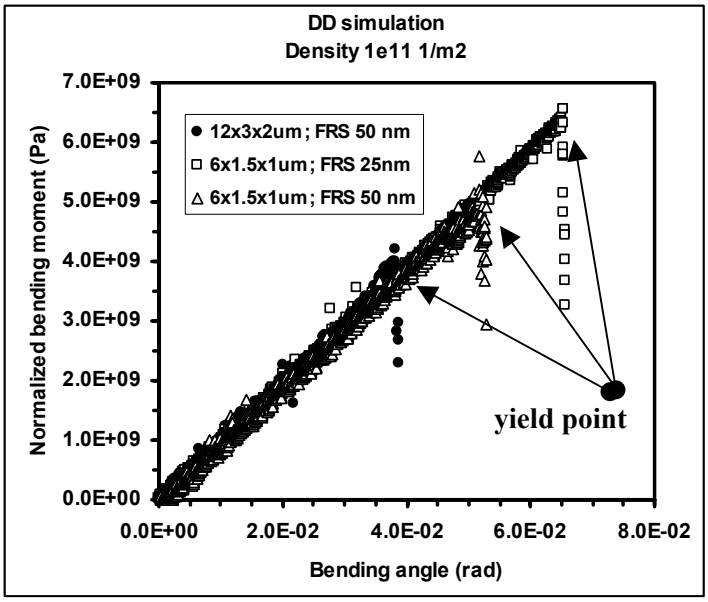

Figure A.6 DD simulation results: effect of sample size on the response of different freestanding beams with same initial density.

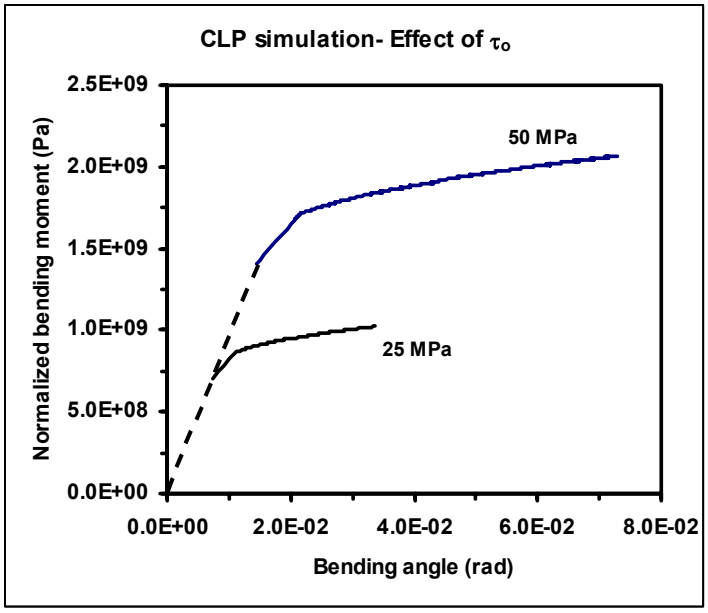

Figure A.7 CLP simulation results: effect of τ_o on the response of a freestanding 12x3x2μm and 6x1.5x1mm beams (results of both beams overlap).

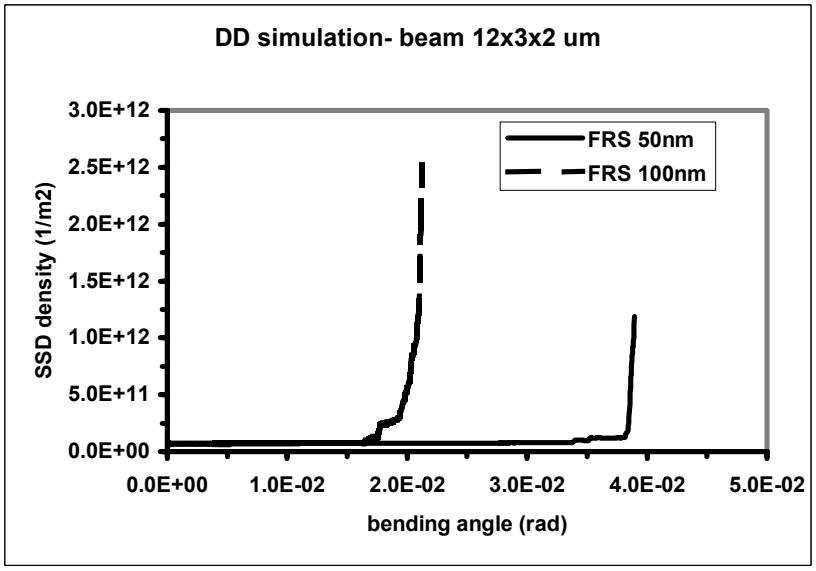

(a)

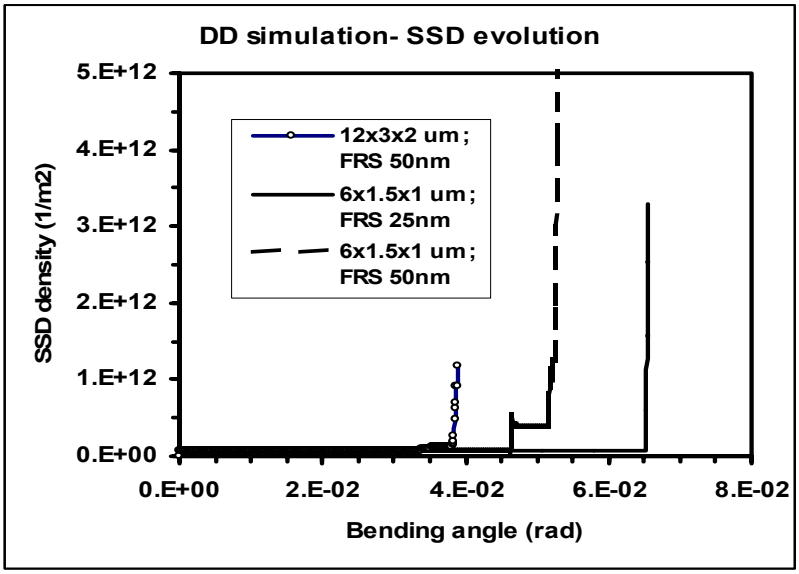

(b)

Figure A.8 DD simulation results: evolution of SSD, (a) effect of FRS size, (b) effect of sample size. In all cases, sample had the same initial density.

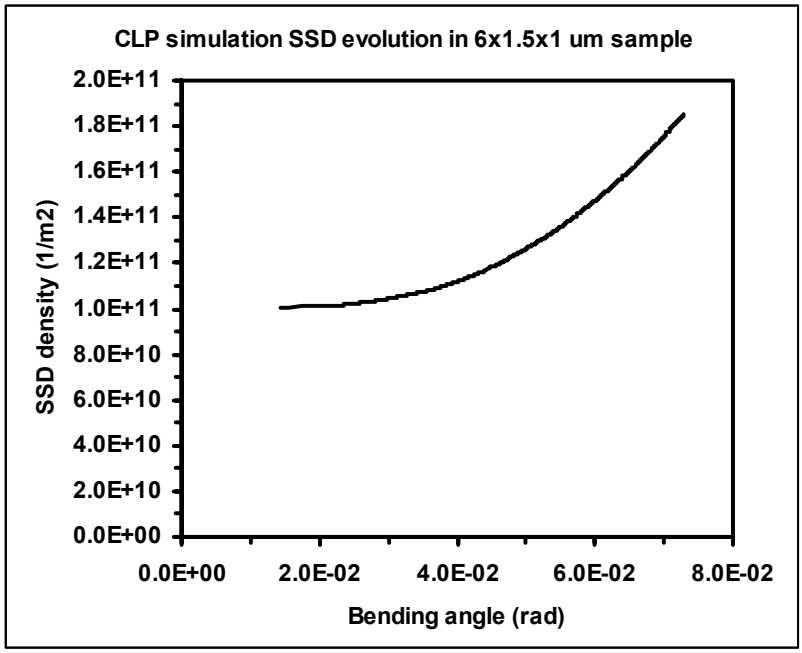

Figure A.9 CLP simulation results: evolution of SSD for 6x1.5x1 μm sample.

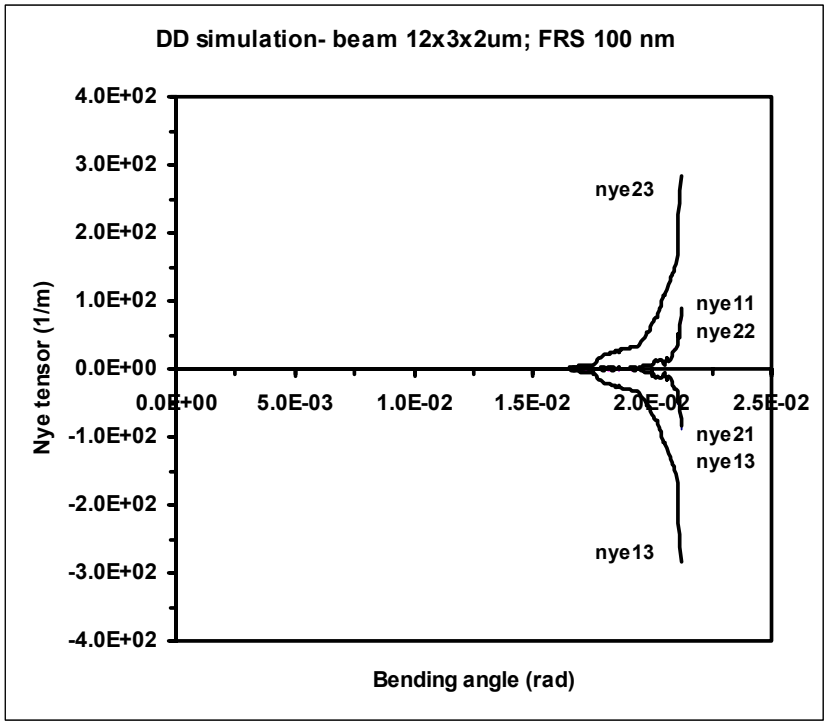

(a)

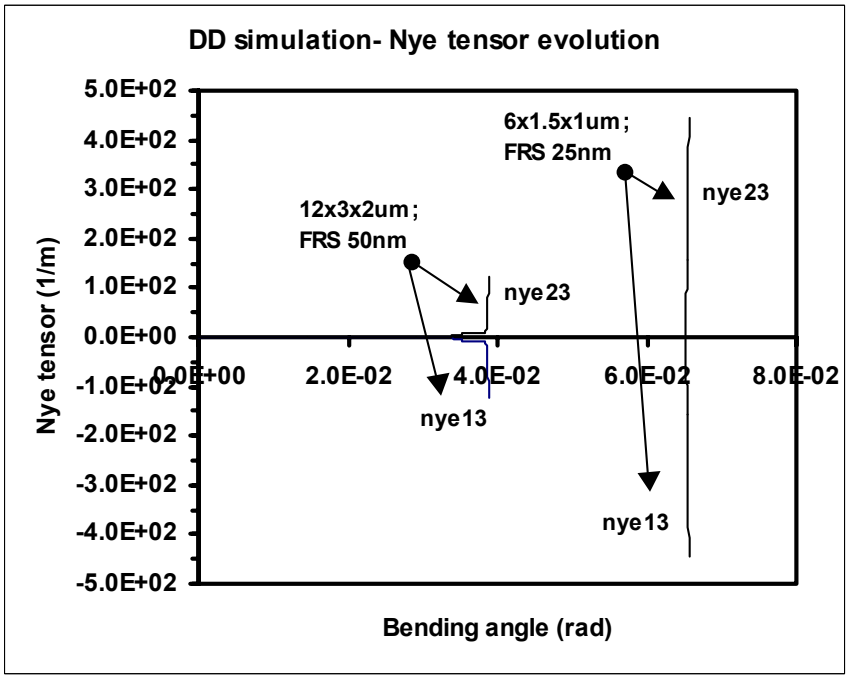

(b)

Figure A.10. DD simulation results: (a) the evolution of Nye tensor, (b) effect of sample size. In all cases, sample had the same initial density.

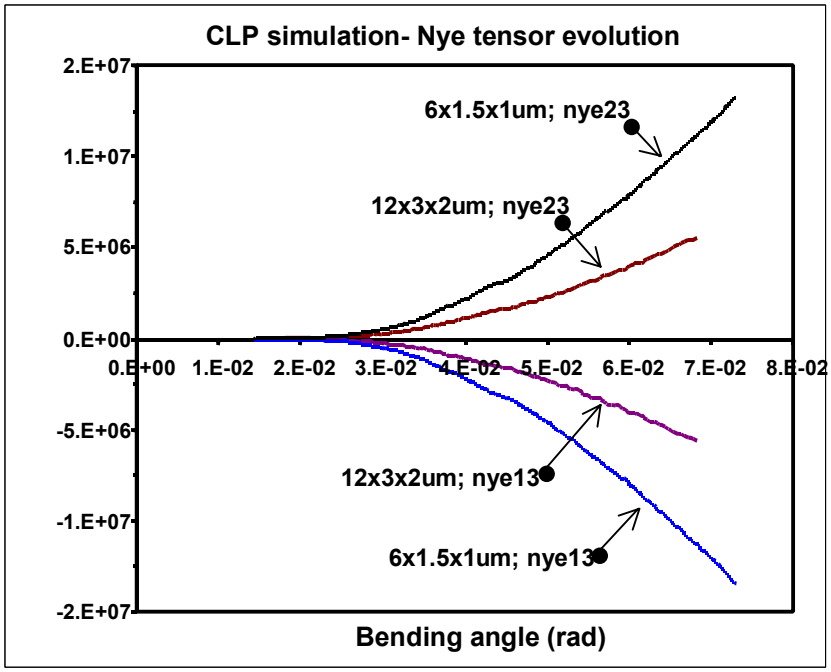

Figure A.11. CLP simulation results: effect of size on the evolution of Nye tensor. Only components 13 and 23 are shown. All other components are insignificant in magnitude.

References

[1] J. Stolken and A. G. Evans, "A Microbend Test Method for Measuring the Plasticity Length Scale," *Acta Mater.*, vol. 46, pp. 5109-5115, 1998.

[2] N. A. Fleck, G. M. Muller, M. F. Ashby, and J. W. Hutchinson, "Strain Gradient Plasticity: Theory and Experiment," *Acta Metall. Mater.*, vol. 42, pp. 475-487, 1994.

[3] W. D. Nix and H. Gao, "Indentation Size Effects in Crystalline Materials: A Law for Strain Gradient
Plasticity," *Journal of Mechanics and Physics of Solids*, vol. 46, pp. 411-425, 1998.

[4] R. Hill, "Generalized constitutive relations for incremental deformation," *Journal of the Mechanics and Physics of Solids*, vol. 14, pp. 95-102, 1966.

[5] R. J. Asaro, "Geometrical effects in the inhomogeneous deformation of ductile single crystals," *Acta Metall.*, vol. 27, pp. 445-453, 1979.

[6] J. F. Nye, *Acta Metall. Mater.*, vol. 1, pp. 153, 1953.

[7] M. F. Ashby, *The Deformation of Plastically Non-Homogeneous Alloys*. Amsterdam: Elsevier, 1971.

[8] E. C. Aifantis, "On the Microstructural Origin of Certain Inelastic Models," *ASME J. Eng. Mat. Tech.*, vol. 106, pp. 326-330, 1984.

[9] H. M. Zbib and E. C. Aifantis, "A Gradient-Dependent Model for the Portevin-Le Chatelier Effect," *Scripta Metall*, vol. 22, pp. 1331-1336, 1988.

[10] H. M. Zbib and E. C. Aifantis, "On the Structure and Width of Shear Bands," *Scripta Metall*, vol. 22, pp. 703, 1988.

[11] N. A. Fleck and J. W. Hutchinson, "A reformulation of strain gradient plasticity," *Journal of the Mechanics and Physics of Solids*, vol. 49, pp. 2245-2271, 2001.

[12] K. Shizawa and H. M. Zbib, "Thermodynamical Theory of Strain Gradient Elastoplasticity with Dislocation Density: Part I - Fundamentals," *Int. J. Plasticity*, vol. 15, pp. 899-938, 1999.

[13] M. E. Gurtin, "A gradient theory of single-crystal viscoplasticity that accounts for geometrically necessary dislocations.," *J. Mech. Phys. Solids*, vol. 50, pp. 5-32., 2002.

[14] S. D. Mesarovic, "Energy, configurational forces and characteristic lengths associated with the continuum description of geometrically necessary dislocation.," *Int. J. Plasticity.*, vol. **21**, pp. 1855-89., 2005.

[15] A. Arsenlis, D. M. Parks, R. Becker, and V. V. Bulatov, "On the evolution of crystallographic dislocation density in non-homogeneously deforming crystals," *Journal of the Mechanics and Physics of Solids*, vol. 52, pp. 1213-1246, 2004.

[16] S. Yefimov, I. Groma, and E. Van der Giessen, "A comparison of a statistical-mechanics based plasticity model with discrete dislocation plasticity calculations," *Journal of the Mechanics and Physics of Solids*, vol. 52, pp. 279-300, 2004.

[17] I. Groma, "Link between the microscopic and mesoscopic length scale description of the collective behavior of dislocation," *Physical Review B*, vol. 56, 1997.

[18] M. Zaiser and T. Hochrainer, "Some steps towards a continuum representation of 3D dislocation systems," *Scripta Materialia*, vol. 54, pp. 717-721, 2006.

[19] A. El-Azab, "Boundary value problem of dislocation dynamics," *Modelling and Simulation in Materials Science and Engineering*, vol. 8, pp. 37-54, 2000.

[20] A. Acharya and J. L. Bassani, *Journal of the Mechanics and Physics of Solids*, vol. 48, pp. 1565, 2000.
[21] T. Ohashi, "A new model of scale dependent crystal plasticity anaysis," *Proc. IUTAM Symposium, Osaka, Japan, July, 2003*, 2003.
[22] N. M. Ghoniem and R. J. Amodeo, *Numerical Simulation of Dislocation Patterns During Plastic Deformation*: Kluwer Academic Publishers, 1990.
[23] H. M. Zbib and E. C. Aifantis, "On the Stability of Inelastic Deformations, [IUTAM Keynote Lecture]," *in: Finite Inelastic Deformations, Eds. Stein, E. and Besdo, D Springer Verlag, Heidleberg*, pp. pp. 15-25, 1992.
[24] H. M. Zbib, T. Diaz de la Rubia, and V. A. Bulatov, "A Multiscale Model of Plasticity Based on Discrete Dislocation Dynamics," *ASME J. Enger. Mater, Tech.*, vol. 124, pp. 78-87, 2002.
[25] G. Canova, Y. Brechet, L. P. Kubin, B. Devincre, V. Pontikis, and M. Condat, "3D Simulation of Dislocation Motion on a Lattice: Application to the Yield Surface of Single Crystals," *Microstructures and Physical Properties (ed. J. Rabiet), CH-Transtech*, 1993.
[26] A. Needleman, "Computational Mechanics at the Mesoscale," *Acta Mater.*, vol. 48, pp. 105-124, 2000.
[27] K. W. Schwarz, "Simulation of dislocations on the mesoscopic scale.I. Methods and examples," *J. Appl. Phys.*, vol. 85, pp. 108-119, 1999.
[28] M. Rhee, H. M. Zbib, J. P. Hirth, H. Huang, and T. D. d. L. Rubia, "Models for Long/Short Range Interactions in 3D Dislocatoin Simulation," *Modeling & Simulations in Maters. Sci. & Enger*, vol. 6, pp. 467-492, 1998.
[29] H. Yasin, H. M. Zbib, and M. A. Khaleel, "Size and Boundary Effects in Discrete Dislocation Dynamics: Coupling with Continuum Finite Element," *Materials Science and Engineering*, vol. A309-310, pp. 294-299, 2001.
[30] M. Rhee, J. P. Hirth, and H. M. Zbib, "A Superdislocation Model for the Strengthening of Metal Matrix Composites and the Initiation and Propagation of Shear Bands," *Acta Metall. Mater.*, vol. 42, pp. 2645-2655, 1994.
[31] M. Hiratani and H. M. Zbib, "On dislocation-defect interactions and patterning: Stochastic discrete dislocation dynamics (SDD)," *Journal of Nuclear Materials*, vol. 323, pp. 290-303, 2003.
[32] E. Van der Giessen and A. Needleman, "Discrete Dislocation Plasticity: A Simple Planar Model.," *Mater. Sci. Eng.*, vol. 3, pp. 689-735, 1995.
[33] M. Rhee, J. P. Hirth, and H. M. Zbib, "On the Bowed Out Tilt Wall Model of Flow Stress and Size Effects in Metal Matrix Composites," *Scripta Metall. et Materialia*, vol. 31, pp. 1321-1324, 1994.
[34] R. W. Leger, T. A. Khraishi, and Y.-L. Shen, "A dilsocation dynamics study of strength differential in particle-containing metals during cyclic loading," *Journal of Materials Science*, vol. 39, pp. 3593-3604, 2004.
[35] H. M. Zbib and T. Diaz de la Rubia, "A Multiscale Model of Plasticity," *Int. J. Plasticity*, vol. 18, pp. 1133-1163, 2002.
[36] A. Khan, H. M. Zbib, and D. A. Hughes, "Modeling Planar Dislocation Boundaries using Multi-scale Dislocation Dynamics Plasticity," *Int. J. Plasticity*, vol. submitted, 2002.

[37] M. Shehadeh and H. M. Zbib, "Dislocation Dynamics unber Extreme Conditions," *in preparation*, 2002.
[38] T. Khraishi, H. M. Zbib, T. Diaz de la Rubia, and M. Victoria, "Localized Deformation and Hardening In Irradiated Metals: Three-Dimensional Discrete Dislocation Dynamics Simulations," *Metall. Mater. Trans.*, vol. 33B, pp. 285-296, 2002.
[39] T. Diaz de la Rubia, H. M. Zbib, M. Victoria, A. Wright, T. Khraishi, and M. Caturla, "Flow Localization in Irradiated Materials: A Multiscale Modeling Approach," *Nature*, vol. 406, pp. 871-874, 2000.
[40] A. Misra and H. Kung, "Deformation behavior of nanostructured metallic multilayers," *Advanced Engineering Materials*, vol. 3, 2001.
[41] A. Misra, J. P. Hirth, R. G. Hoagland, J. D. Embury, and H. Kung, "Disloaction mechanisms and symmetric slip in rolled nano-scaled metallic multilayers," *Acta Materialia*, vol. 52, pp. 2387-2394, 2004.
[42] N. Mara, A. Sergueeva, A. Misra, and A. K. Mukherjee, "Structure and high-temperature mechanical behavior relationship in nano-scaled multilayered materials," *Scripta Materialia*, vol. 50, pp. 803-806, 2004.
[43] Y. C. Wang, A. Misra, and R. G. Hoagland, "Fatigue properties of nanoscale Cu/Nb multilayers," *Scripta Materialia*, vol. 54, pp. 1593-1598, 2006.
[44] M. R. Stoudt, R. E. Ricker, and R. C. Cammarata, "The influence of a multilayered metallic coating on fatigue crack nucleation," *International Journal of Fatigue*, vol. 23, pp. S215-S223, 2001.
[45] T. Hochbauer, A. Misra, K. Hattar, and R. G. Hoagland, "Influence of interfaces on the strorage of ion-implanted He in multilayered matallic composites," *J. Appl. Phys.*, vol. 98, pp. 123516, 2005.
[46] A. Misra, X. Zhang, D. Hammon, and R. G. Hoagland, "Work hardening in rolled nanolayered metallic composites," *Acta Materialia*, vol. 53, pp. 221-226, 2005.
[47] Y. C. Wang, A. Misra, and R. G. Hoagland, "Fatigue properties of nanoscale Cu/Nb multilayers," *Scripta Materialia*, vol. 54, pp. 1593-1598, 2006.
[48] F. C. Frank and J. H. van der Merwe, "One-dimensional dislocations. I. Static Theory," *Proceedings of the Royal Society of London, Series A*, vol. 198, pp. 205-216, 1949.
[49] J. W. Matthews and A. E. Blakeslee, "Defects in epitaxial multilayers, I. Misfit Dislocations," *Journal of Crystal Growth*, vol. 27, pp. 118-125, 1974.
[50] J. W. Matthews, "Misfit Dislocations," in *Dislocations in Solids*, vol. 2, F. R. N. Nabarro, Ed.: North-Holland publishing company, 1979, pp. 461-545.
[51] W. D. Nix, "Mechanical Properties of thin films," *Metallurgical Transactions A*, vol. 20 A, pp. 2217-2245, 1989.
[52] L. B. Freund, "The stability of a dislocation threading a strained layer on a substrate," *Journal of Applied Mechanics*, vol. 54, pp. 553-557, 1987.
[53] B. W. Dodson and J. Y. Tsao, "Relaxation of strained-layer semiconductor structures via plastic flow," *Applied Physics Letters*, vol. 51, 1987.
[54] J. W. Matthews, S. Mader, and T. B. Light, "Accomodation of misfit across the interface between crystals of semiconducting elements or compounds," *J. Appl. Phys.*, vol. 41, pp. 3800-3804, 1970.

[55] R. G. Hoagland, R. J. Kurtz, and C. H. Henager Jr, "Slip resistance of interfaces and the strength of metallic multilayer composites," *Scripta Materialia*, vol. 50, pp. 775-779, 2004.
[56] A. Misra, J. P. Hirth, and H. Kung, "Single-dislocation-based strengthening mechanisms in nanoscale metalic multilayers," *Philosophical Magazine A*, vol. 82, pp. 2935-2951, 2002.
[57] X. Feng and J. P. Hirth, "Critical layer thickness for inclined dislocation stability in multilayer structures," *J. Appl. Phys.*, vol. 72, pp. 1386-1393, 1992.
[58] J. P. Hirth and X. Feng, "Critical layer thickness for misfit dislocation stability in multilayer structures," *J. Appl. Phys.*, vol. 67, pp. 3343-3349, 1990.
[59] T. J. Gosling, J. R. Willis, R. Bullough, and S. C. Jain, "The energetics of dislocation array stability in strained epitaxial layers," *J. Appl. Phys.*, vol. 73, pp. 8297-8303, 1993.
[60] T. J. Gosling, R. Bullough, S. C. Jain, and J. R. Willis, "Misfit dislocation distributions in capped (buried) strained semiconductor layers," *J. Appl. Phys.*, vol. 73, 1993.
[61] A. Atkinson and S. C. Jain, "The energy of finite systems of misfit dislocations in epitaxial strained layers," *J. Appl. Phys.*, vol. 72, pp. 2242-2248, 1992.
[62] A. Atkinson and S. C. Jain, "Energetics of dislocation dipoles in capped epitaxially strained layers," *J. Appl. Phys.*, vol. 76, pp. 1598-1603, 1994.
[63] J. R. Willis, S. C. Jain, and R. Bullough, "The energy of an array of dislocations: implictions for strain relaxation in semiconductor heterostructures," *Philosophical Magazine A*, vol. 62, pp. 115-129, 1990.
[64] L. B. Freund, "A criterion for arrest of a threading dislocation in a strained epitaxial layer due to an interface misfit dislocation in its path," *J. Appl. Phys.*, vol. 68, pp. 2073-2080, 1990.
[65] W. D. Nix, "Yielding and strain hardening of thin metal films on substrates," *Scripta Materialia*, vol. 39, pp. 545-554, 1998.
[66] H. M. Zbib and T. D. de la Rubia, "A multiscale model of plasticity," *International Journal of Plasticity*, vol. 18, pp. 1133-1163, 2002.
[67] H. M. Zbib, M. Rhee, and J. P. Hirth, "3D simulation of curved dislocations: discretization and long range interactions," presented at Advances in Engineering Plasticity and its Applications, 1996.
[68] P. Pant, K. W. Schwarz, and S. P. Baker, "Dislocation interactions in thin FCC metal films," *Acta Materialia*, vol. 51, pp. 3243-3258, 2003.
[69] K. W. Schwarz and J. Tersoff, "Interaction of threading and misfit dislocations in a strained epitaxial layer," *Applied Physics Letters*, vol. 69, pp. 1220-1222, 1996.
[70] K. W. Schwarz, "Simulation of dislocations on the mesoscopic scale.II. Application to strained-layer relaxation," *J. Appl. Phys.*, vol. 85, pp. 120-129, 1999.
[71] H. M. Zbib, M. Rhee, and J. P. Hirth, "On plastic deformation and the dynamics of 3D dislocations," *Int. J. Mech. Sci.*, vol. 40, pp. 113-127, 1998.
[72] J. P. Hirth and J. Lothe, *Theory of Dislocations*, second ed: Krieger Publishing Company, 1982.

[73] D. Mitlin, A. Misra, V. Radmilovic, M. Nastasi, R. G. Hoagland, D. J. Embury, J. P. Hirth, and T. E. Mitchell, "Formation of misfit dislocations in nanoscale Ni-Cu bilayer films," *Philosophical Magazine*, vol. 84, pp. 719-736, 2004.
[74] R. Madec, B. Devincre, L. Kubin, T. Hoc, and D. Rodney, "The role of collinear interaction in dislocation-induced hardening," *Science*, vol. 301, pp. 1879-1881, 2003.
[75] F. Akasheh, H. M. Zbib, J. P. Hirth, R. G. Hoagland, and A. Misra, *in preperation*.
[76] J. D. Embury and J. P. Hirth, "On dislocation storage and the mechanical response of fine scale microstructures," *Acta Metallurgica et Materialia*, vol. 42, pp. 2051-2056, 1994.
[77] D. J. Srolovitz, S. M. Yalisove, and J. C. Bilello, "Design of multiscalar metallic multilayer composites for high strength, high toughness, and low CTE mismatch," *Metallurgical and Materials Transactions A*, vol. 26A, pp. 1085-1813, 1995.
[78] R. Schwaiger, G. Dehm, and O. Kraft, "Cyclic deformation of polycrystalline Cu films," *Philosophical Magazine*, vol. 83, pp. 693-710, 2003.
[79] G. P. Zhang, C. A. Volkert, R. Schwaiger, E. Arzt, and O. Kraft, "Damage behavior of 200-nm thin copper films under cyclic loading," *Journal of Materials research*, vol. 20, pp. 201-207, 2005.
[80] A. Misra, H. Kung, D. Hammon, R. G. Hoagland, and M. Nastasi, "Damage Mechanisms in Nanolayered Metallic Composites," *International Journal of Damage Mechanics*, vol. 12, pp. 365, 2003.
[81] F. Akasheh, H. M. Zbib, J. P. Hirth, R. G. Hoagland, and A. Misra, "DD analysis of dislocation intersections in nanoscale metallic multilayered composites," *Journal of Applied Physics*, vol. in press, 2006.
[82] R. G. Hoagland, J. P. Hirth, A. Misra, and D. Mitlin, "Influence of surface steps on glide of threading dislocations during layer growth," *Applied Physics Letters*, vol. 84, pp. 5136-5138, 2004.
[83] J. P. Hirth, R. G. Hoagland, and A. Misra, "The effect of surface steps on the critical thickness for spreading of threading dislocations in thin epitaxial films," *Philosophical Magazine*, vol. 85, pp. 3019-3028, 2005.
[84] V. Weihnacht and W. Bruckner, "Dislocation accummulation and strengthening in Cu thin films," *Acta Materialia*, vol. 49, pp. 2365-2372, 2001.
[85] E. R. Kreidler and P. M. Anderson, "Orowan-based deformation model for a layered metallic material," presented at Mat. Res. Soc. Symp. Proc, 1996.
[86] P. M. Anderson and E. R. Kreidler, "Dislocation-based models of stress-strain behavior in multilayered thin films," presented at Mat. Res. Soc. Symp. Proc., 1998.
[87] D. Mitlin, A. Misra, T. E. Mitchell, J. P. Hirth, and R. G. Hoagland, "Interface dislocation structures at the onset of coherency loss in nanoscale Ni-Cu bilayer films," *Philosophical Magazine*, vol. 85, pp. 3379-3392, 2005.
[88] D. Mitlin, A. Misra, T. E. Mitchell, R. G. Hoagland, and J. P. Hirth, "Influence of overlayer thickness on the density of Lomer dislocations in nanoscale Ni-Cu bilayer thin films," *Applied Physics Letters*, vol. 85, pp. 1686-1688, 2004.
[89] J. P. Hirth and J. Lothe, *Theory of Dislocations*, 2nd ed. New York: Wiley, 1982.

[90] G. MacPherson, R. Beanland, and P. J. Goodhew, "On the development of misfit dislocation distributions in strained epitaxial layer interfaces," *Scripta Metallurgica et Materialia*, vol. 33, pp. 123-128, 1995.
[91] A. Misra, J. P. Hirth, and R. G. Hoagland, "Length-scale-dependent deformation mechanisms in incoherent metallic multilayered composites," *Acta Materialia*, vol. 53, pp. 4817-4824, 2005.
[92] K. W. Schwarz, J. Cai, and P. M. Mooney, "Comparison of large-scale layer-relaxation simulations with experiments," *Applied Physics Letters*, vol. 85, pp. 2238-2240, 2004.
[93] K. W. Schwarz, "Discrete dislocation dynamics study of strained-layer relaxation," *Physical Review Letters*, vol. 91, pp. 145503-1-145503-4, 2003.
[94] R. G. Hoagland, T. E. Mitchell, J. P. Hirth, and H. Kung, "On the strengthening effects of interfaces in multilayer fcc metallic composites," *Philosophical Magazine A*, vol. 82, pp. 643-664, 2002.
[95] T. Ohashi, "A multiscale approach for modeling scale-dependent yield stress in polycrystalline metal crystals," *International Journal of Plasticity*, vol. accepted for publication, 2006.
[96] G. I. Taylor, "The Mechanism of Plastic Deformation of Crystals Parts I, II," *Proc. Roy. Soc*, vol. A145, pp. 362, 1934.
[97] H. B. Muhlaus and E. C. Aifantis, "A Variational Principle for Gradient Plasticity," *Int. J. Solids Structures*, vol. 28, pp. 845, 1991.
[98] H. M. Zbib, "Strain Gradients and Size Effects in Nonuniform Plastic Deformations," *Scripta Metallurgica et Materialia*, vol. 30, pp. 1223-1226, 1994.
[99] M. Zaiser and E. C. Aifantis, "Geometrically necessay dislocations and strain gradient plasticity-a dislocation dynamics point of view," *Scripta Materialia*, vol. 48, pp. 133-139, 2003.
[100] H. Gao, Y. Huang, W. D. Nix, and J. W. Hutchinson, "Mechanism-based strain gradient plasticity- I. Theory," *Journal of the Mechanics and Physics of Solids*, vol. 47, pp. 1239-1263, 1999.
[101] E. C. Aifantis, "The Physics of Plastic Deformation," *Int. J. Plasticity*, vol. 3, pp. 211-247, 1987.
[102] L. P. Kubin and G. Canova, "The Modelling of Dislocation Patterns," *Scripta Metall*, vol. 27, pp. 957?962, 1992.
[103] H. M. Zbib, M. Rhee, and J. P. Hirth, "3D Simulation of Curved Dislocations: Discretization and Long Range Interactions," *Advances in Engineering Plasticity and its Applications, eds. T. Abe and T. Tsuta. Pergamon, NY*, pp. 15-20, 1996.
[104] K. W. Schwarz, "Interaction of dislocations on crossed glide planes in a strained epitaxial layer," *Physical Review Letters*, vol. 78, pp. 4785-4788, 1997.
[105] N. M. Ghoniem and L. Sun, "A Fast Sum Method for the Elastic Field of 3-D Dislocation Ensembles," *Phys. Rev. B*, vol. 60, pp. 128-140, 1999.
[106] M. Fivel, L. Tabourot, E. Rauch, and G. Canova, "Identification through mesoscopic simulations of macroscopic parameters of physically based constitutive equations for the plastic behaviour of FCC single crystals," *J. Phys. IV France*, vol. 8, pp. Pr8-151-Pr8-158, 1998.

[107] A. Arsenlis and M. Tang, "Simulations on teh growth of dislocation density during Stage 0 deformation in BCC metals," *Modelling and Simulation in Materials Science and Engineering*, vol. 11, pp. 251-264, 2003.
[108] C. Lemarchand, B. Devincre, and L. P. Kubin, "Homogenization method for a discrete-continuum simulation of dislocation dynamics," *Journal of the Mechanics and Physics of Solids*, vol. 49, pp. 1969-1982, 2001.
[109] A. Needleman and E. Van der Giessen, "Discrete dislocation and continuum descriptions of plastic flow," *Materials Science and Engineering A*, vol. 309-310, pp. 1-13, 2001.
[110] M. Grujicic and D. Columbus, "A comparative discrete-dislocation/crystal-plasticity analysis of bending of a single-crystalline microbeam," *Journal of Materials Science*, vol. 36, pp. 2179-2188, 2001.
[111] S. Yefimov, E. Van der Giessen, and I. Groma, "Bending of a single crystal: discrete dislocation and nonlocal crystal plasticity simulations," *Modelling and Simulation in Materials Science and Engineering*, vol. 12, pp. 1069-1086, 2004.
[112] J. P. Hirth, H. M. Zbib, and J. Lothe, " Forces on High Velocity Dislocations," *Modeling & Simulations in Maters. Sci. & Enger.*, vol. 6, pp. 165-169, 1998.
[113] T. Ohashi, "Numerical modelling of plastic multislip in metal crystals of FCC type," *Philosophical Magazine A*, vol. 70, pp. 793-803, 1994.
[114] J. Weertman, "Anomalous work hardening, non-redundant screw dislocations in a circular bar deformed in torsion, and non-redundant edge dislocations in a bent foil," *Acta Materialia*, vol. 50, pp. 673-689, 2002.
[115] T. Ohashi, "Finite element analysis of plastic slip and evolution of geometrically necessary dilsocations in FCC crystals," *Philosophical Magazine Letters*, vol. 75, pp. 51-57, 1997.
[116] P. Shrotriya, S. M. Allameh, J. Lou, T. Buchheit, and W. O. Soboyejo, "On the measurement of the plasticity length scale parameter in LIGA nickel foils," *Mechanics of Materials*, vol. 35, pp. 233-243, 2003.
[117] M. A. Haque and M. T. A. Saif, "Strain gradient effect in nanoscale thin films," *Acta Materialia*, vol. 51, pp. 3053-3061, 2003.
[118] W. Wang, Y. Huang, K. J. Hsia, K. X. Hu, and A. Chandra, "A study of microbend test by strain gradient plasticity," *International Journal of Plasticity*, vol. 19, pp. 365-382, 2003.
[119] E. C. Aifantis, "Strain Gradient Interpretation of Size Effect," *Int. J. Fract*, vol. 95, pp. 299-314, 1999.
[120] M. Kuroda, V. Tvergaard, and T. Ohashi, "Simulations of micro-bending of thin foils using a scale dependent crystal plasticity model," *Modelling and Simulation in Materials Science and Engineering*, vol. accepted for publication, 2006.
[121] H. H. M. Cleveringa, E. Van der Giessen, and A. Needleman, "A discrete dislocation analysis of bending," *International Journal of Plasticity*, vol. 15, pp. 837-868, 1999.
[122] T. Ohashi, "Crystal plasticity analysis of dislocation emission from micro voids," *International Journal of Plasticity*, vol. 21, pp. 2071-2088, 2005.